ABSTRACT

Title of Document: AN OPTICAL DENSITY DETECTION PLATFORM WITH INTEGRATED MICROFLUIDICS FOR *IN SITU* GROWTH, MONITORING, AND TREATMENT OF BACTERIAL BIOFILMS

Matthew P. Mosteller, Master of Science, 2012

Directed By: Dr. Reza Ghodssi
Department of Electrical and Computer Engineering
Institute for Systems Research

Systems engineering strategies utilizing platform-based design methodologies are implemented to achieve the integration of biological and physical system components in a biomedical system. An application of this platform explored, in which an integrated microsystem is developed capable of the on-chip growth, monitoring, and treatment of bacterial biofilms for drug development and fundamental study applications. In this work, the developed systems engineering paradigm is utilized to develop a device system implementing linear array charge-coupled devices to enable real-time, non-invasive, label-free monitoring of bacterial biofilms. A novel biofilm treatment method is demonstrated within the developed microsystem showing drastic increases in treatment efficacy by decreasing both bacterial biomass and cell viability within treated biofilms. Demonstration of this treatment at the microscale enables future applications of this method for the *in vivo* treatment of biofilm-associated infections.

AN OPTICAL DENSITY DETECTION PLATFORM WITH INTEGRATED MICROFLUIDICS FOR *IN SITU* GROWTH, MONITORING, AND TREATMENT OF BACTERIAL BIOFILMS

By

Matthew Philip Mosteller

Thesis submitted to the faculty of the Graduate School of the
University of Maryland, College Park in partial fulfillment
of the requirements for the degree of
Master of Science
2012

Advisory Committee:
Professor Reza Ghodssi, Chair
Professor William Bentley
Associate Professor Mark Austin

Dedication

To my mom and dad, without whom none of this would be possible.

Acknowledgements

I would like to acknowledge the help and contributions of my advisor, Dr. Reza Ghodssi, for his continued dedication throughout this research and degree process. Additionally, I would like to thank my co-advisor in systems engineering, Dr. Mark Austin, for his support and useful discussions with respect to this work and his instruction throughout the Masters of Science in Systems Engineering program. I would also like to offer thanks to my committee member, Dr. William Bentley, for his useful input and to Mr. Steve Sutton and Mrs. Sue Frazier in the Institute for Systems Research for their guidance and input.

The author would also like extend thanks to his colleagues in the MEMS Sensors and Actuators Lab (MSAL) for all of their help, advice, and useful discussion over the past years. He would like to offer special thanks to the members of the BioMEMS group and specifically to Ms. Mariana Meyer, Mr. Young Wook Kim, and Dr. Peter Dykstra for their instruction, guidance, and collaborative efforts throughout this work.

Last, but not least, special thanks are given to the members of the Maryland BioChip Collaborative led by principles Dr. Gregory Payne, Dr. Gary Rubloff, Dr. William Bentley, and Dr. Reza Ghodssi for their interdisciplinary insight, to Mr. Jeremy Feldman for his useful work, and to the staff of the Maryland Nanocenter Fablab facility, Mr. Jonathan Hummel, Mr. John Abrahams, Mr. Tom Loughran, and Mr. Jim O'Connor for their assistance during the fabrication process.

Table of Contents

List of Tables

List of Commonly Used Abbreviations

(Listed Alphabetically)

AC: Alternating current, characterized in this work by a sinusoidal voltage potential signal and thus a sinusoidal time-varying electric effect

ANOVA: Analysis of variance, a standard method of statistical significance evaluation in experimental studies

AU_{CCD}: Unitless measure of optical density (arbitrary units or absorption units) for the developed Micro-BOAT system. These values can also be converted to other AU_{SOD} and OD_{600} values

AU_{SOD}: Unitless measure of optical density (arbitrary units or absorption units) for commercial Beckman-Coulter spectrophotometer, synonymous with OD_{600} measurements. These values can also be converted to AU_{CCD} values

BE: Bioelectric effect, an enhanced biofilm treatment utilizing AC and/or DC electric fields in the presence of traditional antibiotic therapies

BioMEMS: micro-electro-mechanical systems (MEMS) specifically designed and used for biological and biomedical applications

CAD: Computer-aided design, the use of computer software to assist in the creation, modeling, specification, and optimization of engineering designs

CCD: Charge-coupled device, a linear-array photopixel component used as the sensor for the developed system

CLK: The square wave signal clock used to drive the charge-coupled device components

COTS: Commercial off-the-shelf, a term used to describe components that are commercially available, typically in an IC package form

DAQ: Data acquisition card, a commercially produced piece of equipment for the connection of electrical signals to a computer for processing

DC: Direct current, characterized by a constant voltage potential and thus constant electric field

ECM: Extracellular matrix, the encasing structure of bacterial biofilms composed of polysaccharides, adhesins, and exoproteins excreted by bacteria upon reaching a threshold population

IC: Integrated circuit, an electronic circuit formed on a small piece of semiconducting material, performing the same function as a larger circuit made from discrete components.

LB: Lysogeny broth, an aqueous media used in this work for the culturing and growth of bacterial samples and biofilms

LED: Light emitting diode, an optical light source used in this work to illuminate the Micro-BOAT system to perform optical density measurements

MBSE: Model-based systems engineering, the use of system modeling languages to formally design, analyze, and optimize engineering systems

MEMS: Micro-electro-mechanical systems, a technology of very small devices in the micro/nano range manufactured using IC fabrication techniques to create sensors and/or actuators

MIC: Minimal inhibitory concentration, the lowest concentration of an antimicrobial that will inhibit the visible growth of a microorganism after incubation. Minimum inhibitory concentrations are important diagnostic measurements to determine the resistance of microorganisms to an antimicrobial agent

Micro-BOAT: The microfluidic biofilm observation, analysis, and treatment system developed as the principle focus of this research

OD: Optical density, a measurement of light absorbance of a material or structure, in this case a bacterial biofilm

PBS: Phosphate buffered saline, or phosphate buffer solution, a commonly used buffer solution in biological studies. It is a water-based salt solution containing sodium chloride, sodium phosphate, and, in some formulations, potassium chloride and potassium phosphate demonstrating a steady pH value

PCB: Printed circuit board, a commercially produced epoxy-resin substrate with embedded electrical circuits customized for on-chip components

PDMS: Polydimethylsiloxane, a silcone-based polymer, is a transparent, biocompatible, chemically inert material used in this work for the molding of microfluidic channels

SE: Systems engineering, the field of engineering aimed at the design and integration of complex systems

SI: Serial input bit, a single square wave pulse used to trigger CCD data output and light integration

SP: Superpositioned, typically to refer to the superpositioned electric fields utilized for the superpositioned bioelectric effect

SP BE: Superpositioned bioelectric effect, the novel biofilm treatment technique demonstrated as a major result of this work

VI: Name given by National Instruments for logical subcomponents in their LabVIEW software environment, used in LabVIEW programming

VLSI: Very-large-scale integration, the process of creating integrated circuits by building large networks of transistors on a single chip

List of Figures

Chapter 1: Introduction

1.1 Motivation and Outlook

In the human body and the other natural environments, bacteria aggregate to form living communities of microbes, called biofilms, composed of interacting bacteria and an extracellular matrix (ECM) of adhesins and polysaccharides [1]. Once formed, biofilms produce harmful toxins that have been linked to as many as 65% of all microbial infections within the human body, making them of considerable relevance in clinical fields [2]. The treatment of biofilms is a medical challenge, often requiring 500-5000 times the concentration of antibiotics for effective treatment compared to bacteria in planktonic suspension [3]. The presence of the ECM limits molecular diffusion within the biofilm, making antibiotics less effective by limiting the number of bacterial cells they encounter and thus decreasing the overall efficacy of these drugs [1]. A second factor complicating treatment arises due to the ability of bacteria in close proximity to readily exchange genes such as those that promote antibiotic resistance, thereby developing advanced levels of drug resistance and requiring more aggressive antibiotic therapies for effective treatment [4]. The frequent use of high antibiotic doses is problematic as it increases the risk of harmful side effects and promotes the proliferation of multidrug resistant bacteria. The extent to which bacterial biofilms are clinically relevant and the difficulties associated with treating infections of this type provide strong motivation for the development of new methods for the early detection and treatment of bacterial biofilms. As a result, current medical research displays a strong focus in this area, thus providing a need for new systems capable of *in vitro* bacterial biofilm testing to determine the efficacy of candidate pharmaceutical treatments.

With the current market for antimicrobial treatments totaling well over US $25 billion, there is considerable interest and investment in the field aimed at the development of these new antibiotics [5]. In addition to these financial incentives, the emergence of antibiotic resistance to most common treatments is problematic and therefore motivates a need for new drugs that can treat infections within the human body, such as those caused by bacterial biofilms. The development of new methods to perform efficient drug screening processes can reduce the cost and time-to-market of these new treatments, thereby having far-reaching effects including increased treatment efficacy and patient survival rates, and increased access to medications through reductions in cost.

Current methods of antibiotic evaluation typically employ macroscale reactors for biofilm growth, with fluorescence labeling and microscopy constituting the primary means of determining candidate drug efficacy [6, 7]. The high cost, low throughput, and large sample volumes required for these techniques limits the pace of current drug discovery efforts. This, in turn, points to a strong need for novel drug screening methods that utilize low-cost parallel testing and microscale sample-volumes in order to increase the economic and time-to-market efficiency of drug development.

A factor currently limiting the development of new biomedical systems is founded in the complex nature of biological systems. Such complexity often hinders the development of new technologies, as biologists, clinicians, and engineers exhibit a disconnect in expertise that inhibits the effective design of new systems [8, 9]. Recent advancements in the field of systems engineering have begun to suggest possible solutions to this dichotomy by offering strategies to integrate the separate realms of biology and engineering [8]. Visual and mathematical modeling methods that

incorporate abstraction, standardization, and decoupling allow for engineering and biological concerns to be understood by both domains, thus facilitating a transition to unified system design [8, 10]. As a case in point, the field of microbiology has already begun to benefit from this union by adapting various microtechnologies to address the specific needs of biological applications that are not traditionally addressable by macroscale systems [11]. Emerging clinical drug screening methods have begun to utilize microfabrication techniques that were initially developed for use in the integrated circuits (IC) industry in order to benefit from the capabilities of devices on the microscale [11]. Specifically, recent work has suggested that the use of soft lithography and microfluidic systems, those utilizing microliter-scale fluid volumes as opposed to the milliliter-scale volumes of macroscale systems, have numerous advantages over current methods. The low fabrication cost, highly parallel throughput, and precise environmental control capabilities of these devices gives strong support for their use in drug screening applications and is a principle demonstration of the ways in which systems engineering approaches are currently finding new ways of integrating engineering and biological domains to more effectively meet the needs of the clinical world [11].

Future advances in the field of microbiology will involve the integration of these microscale techniques in order to address the sensing and monitoring needs of the field. To date, the majority of microfluidic-based drug screening systems continue to utilize the same complex external instrumentation often used in macroscale methods, such as confocal microscopy, for the evaluation of biofilms [6]. Recent advancements in microfabrication techniques, specifically those relating to soft lithography and bioengineered micro-electro-mechanical systems (BioMEMS) have begun to allow for

the integration of biocompatible microfluidic systems with sensors and actuators capable of bacterial growth monitoring [11, 12]. A major focus of this work is in the integration of such methods through a systematic approach that enables novel functionality not currently achievable using established drug discovery methods.

Looking forward, a more detailed understanding of bacterial biofilms as biological systems and more efficient ways of developing antibacterial treatments are needed if the current efficacy of drugs is to be maintained or improved in coming years. The collaboration of microfabrication and IC technologies with the fields of microbiology and biopharmaceuticals enables this transition due to the complimentary length scales shared between the two domains and the high-throughput, low-volume advantages of batch-fabricated micro/nano systems [11-13]. The use of systems engineering principles to bridge the gap between these two regimes facilitates a synergistic effort that can result in a unified approach to treating and studying bacterial biofilms and related infections [10, 11].

1.2 Thesis Accomplishments

The primary objective of this research is the design, fabrication, and characterization of a microfluidics based system for the *in situ* monitoring of bacterial biofilms. Systems engineering principles are used to drive a unified device design supporting both the engineering and biological requirements of the system. MEMS fabrication technologies are used to structure microfluidic chambers for the controlled growth and treatment of biofilms for drug screening applications. The integration of the microfluidic structures with linear array charge-coupled devices (CCD) enables temporal tracking of biofilm development via the optical density (OD) properties of the film as its

cell density increases [14]. Such an optical method has been explored previously within our group and demonstrates an ability to perform real-time monitoring of changes in biofilm biomass due to growth and treatment [6]. The added spatial resolution of the photopixel array allows for biofilm monitoring with respect to both average biofilm optical density as well as localized morphology, an enhanced capability over previous work. This sensing method provides a non-invasive, label-free method of continuous bacterial biofilm growth and treatment monitoring that is currently unachievable using established methods. To enable parallel throughput of biofilm experiments in a full microsystem, multiple devices are integrated in parallel with the capability of providing independent treatments to each biofilm sample. The realized microsystem achieves high-throughput, minimally invasive biofilm testing for the screening of multiple candidate drugs in a single device.

A second objective of this work focuses on the demonstration of a novel on-chip bacterial biofilm treatment method utilizing an enhanced bioelectric effect to achieve improved antibiotic efficacy. In order to validate the superpositioned bioelectric effect (SP BE) treatment method for microscale environments, microfabricated electrodes are integrated with the microfluidic device to supply superpositioned (SP) AC and DC electric fields to the biofilms in the presence of antibiotics. This combinatorial biofilm treatment method expresses improved efficacy over antibiotics alone, while demonstration at the microscale in a lab-on-a-chip device encourages the use of this method for potential clinical applications. Importantly, the use of the microfluidic biofilm monitoring platform for such diverse drug screening applications verifies its flexibility as a tool for the evaluation of prospective antimicrobial treatments.

1.3 System Overview

The crux of this work focuses on the design, fabrication, and testing of the microsystem presented in figure 1.1, termed the microfluidic biofilm observation, analysis, and treatment (Micro-BOAT) system, to achieve continuous biofilm monitoring and simultaneous on-chip treatment using the SP BE.

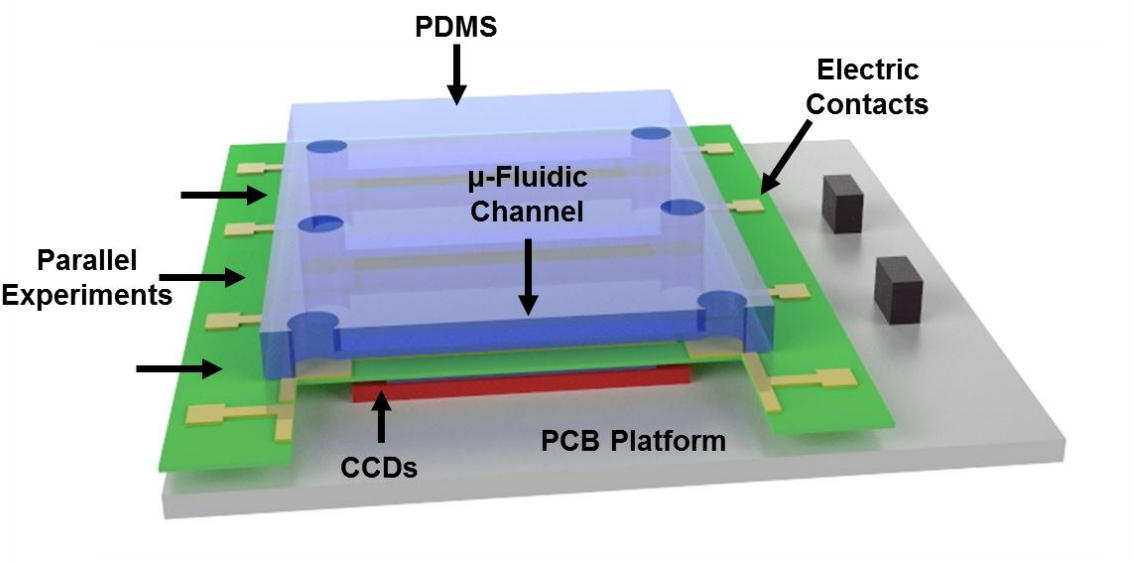

Figure 1.1: Three-dimensional schematic of the developed microsystem.

The developed system addresses many of the shortcomings of current biofilm monitoring techniques by offering real-time, non-invasive, and label-free measurements of biofilms through an optical density approach. Additionally, the use of microfluidic reactors to grow, maintain, and treat experimental biofilms provides a major advantage of this system over macroscale methods by reducing assay times as well as the necessary volumes of high-cost reagents. Implementation of the novel SP BE treatment method on-chip demonstrates the flexibility of this microfluidic microsystem for various biological and drug screening applications, establishing it as a new tool for a variety of biofilm studies.

Systems engineering principles realized through the use of a unique biomedical device design paradigm, referred to as a design "platform" in this work, enable the efficient and flexible system design architecture achieved in the Micro-BOAT system [15]. This platform provides a conceptual framework for the development of many classes of biomedical devices that is readily adapted to the biofilm analysis application addressed in this work. The platform allows for the segmentation of various modules of the biomedical system and hence a system-level analysis linking device requirements to device functionality and structure. The Micro-BOAT tool resulting from this systems-driven design process features an optical sensing mechanism, a microfluidic growth module, supporting software, on-chip supporting electronics, and integrated electrodes enabling the novel SP BE therapy, thereby representing a full system for biofilm investigations and the testing of novel treatment methods.

The system itself utilizes commercial off-the-shelf (COTS) components integrated on a printed circuit board (PCB) with a biocompatible microfluidic device module to realize the full system architecture. CCD and supporting electronic components are integrated in parallel on a single PCB to enable six experiments on a single chip. Microfluidic growth chambers formed in polydimethylsiloxane (PDMS) and gold electrode structures for applying the enhanced bioelectric effect (SP BE) are constructed using microfabrication techniques on a transparent Pyrex^{TM} substrate. CCD components are aligned to their corresponding microfluidic chambers to enable spatiotemporal optical density measurement. Diffused light provided by a panel of light emitting diodes (LED) is absorbed by biofilms formed in the microfluidic chambers and transmitted to each CCD, where changes in CCD output signal correspond to changes in biofilm optical

density, a proven indicator of biofilm biomass. Bacterial cultures, biofilm growth media, and antibiotics are supplied to the device's microfluidic channels via inlets in the PDMS bulk, with an external syringe pump providing control of sample fluid flow. An external power supply and function generators drive the device operation and application of the electric field for the enhanced bioelectric effect. Device readout is achieved via PCB-mounted connectors, shown in black in Figure 1.1, with an accompanying data acquisition card and supporting software uniquely designed for this application.

A fully fabricated and assembled system is capable of running parallel biofilm experiments featuring six unique biofilms, each with their own accompanying treatment, for long experimental periods in excess of several days. Treatment experiments are conducted by initially forming bacterial biofilms within the microfluidic chambers before providing the various treatments. Optical density measurements are obtained in real-time in order to characterize localized and average changes in biofilm optical density, thereby enabling full imaging of the highly variant biofilm structures. Comparisons between multiple treatments can determine the relative efficacy of each in removing bacterial biofilms and hence bacterial biofilm infections.

1.4 Review of Related Work

This section provides background relevant to bacterial biofilms and the current state-of-the-art with respect to biofilm growth and monitoring techniques. A review of relevant MEMS microfabrication techniques is provided with a concentration on microfluidic and lab-on-a-chip devices for biomedical applications. The section concludes with information relevant to the SP BE utilized as an on-chip biofilm treatment

in this work, as well as insight into the methods by which systems engineering can benefit the development of biomedical microsystems. Cumulatively, this review establishes a starting point and motivation for the system development presented in this work, which is addressed by the design considerations and system-level development presented in Chapter 2.

1.4.1. Bacterial Biofilms

Bacterial biofilms have displayed a remarkable propensity to form under nearly any set of environmental conditions and preferentially attach to any number of surfaces in the natural world, with early fossil records indicating the growth of biofilms as far as ~3.25 billion years ago [16]. While much of the work to date has been concerned with the development of bacterial biofilms with regards to macroscopic applications, where biocorrosion and biofouling are of interest, recent work in the field of microbiology has revealed a number of clinical applications in which bacterial biofilms are of particular relevance due to their ability to cause dangerous infections in the human body [2, 16-20]. Their prevalence in infections related to biomedical implants and intravenous tubing including heart valves, artificial hips, and catheters has been well documented [2, 4, 21, 22]. Additionally, they have been shown to attack body tissues and organs through various mechanisms, including the lungs, teeth, gums, ears, and urogenital tract [2]. Advances in technology have enabled the study of these microorganisms at the cellular and sub cellular levels, allowing for a greater understanding of biofilms as complex biological systems whose level of intricacy are often compared to the tissues and organs of higher organisms [1, 23].

Biofilms are generally defined as a heterogeneous community of bacterial cells that attach to a substrate and, upon achieving a certain cell density, begin to form a polymeric matrix of polysaccharides, adhesins, and bacterial cells as a means of protective growth against hostile environmental conditions [4, 6, 23]. A model of development for bacterial biofilms is presented in Figure 1.2, where biofilm growth initiates with the attachment of planktonic cells to a surface.

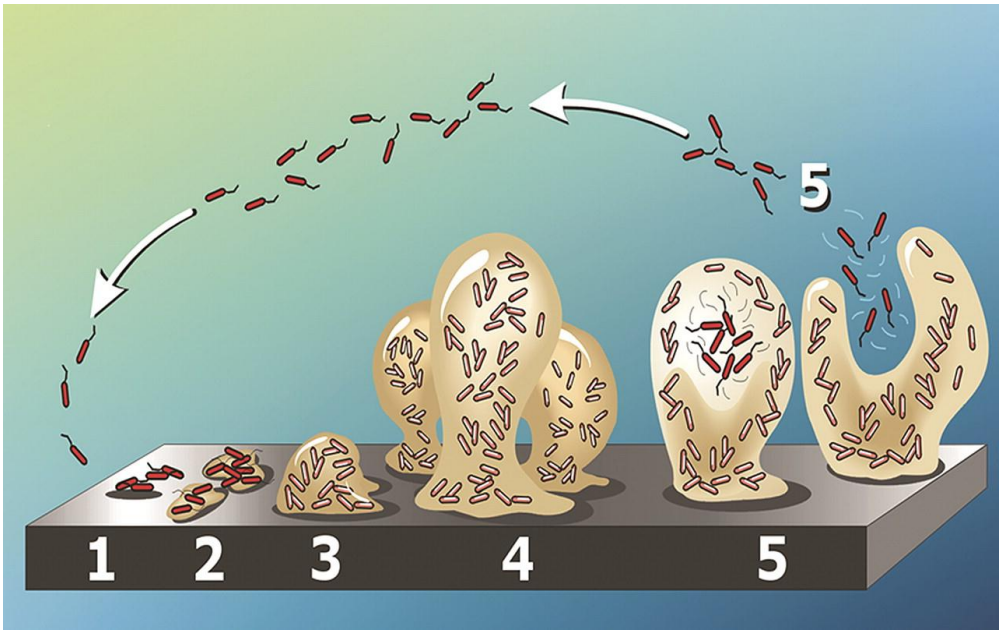

Figure 1.2: Flow diagram illustrating the development cycle of bacterial biofilms [24](1) Planktonic bacteria reversibly adhere to a surface, (2) Bacteria begin to produce ECM and become irreversibly attached to the substrate, (3) and (4) Separate colonies of bacteria develop into mature biofilms, and (5) Biofilms propagate and spread.

As bacteria cells accumulate and attach to the surface, individual cells are capable of determining their localized density by monitoring the uptake and release of autoinducer communication molecules in a process known as quorum sensing [18, 25]. Once the bacteria have reached a threshold population, or quorum, the immature biofilm begins to produce a matrix of exoproteins and sister cells that are bound within the biofilm ECM. The development of biofilm microcolonies continues until a robust and mature biofilm

has been realized consisting of single bacterial cells and microcolonies of sister cells encased in a hydrated matrix of bacteria, exopolysaccharides, and extraneous macromolecules [23, 26-28]. As the biofilm reaches this mature state, it continues to proliferate through the shearing and spread of individual biofilm clumps (clumping and surface dispersal) as well as the release of individual bacterial cells from the biofilm mass through seeding (swarming/seeding dispersal) [16]. The development cycle repeats, thereby increasing the overall biofilm mass, and in clinical applications, the spread of the bacterial infection.

As biofilms mature, they begin to express specific genes that allow for increased protection against harsh environments as well as the continued development of a robust biofilm structure [29]. In order to facilitate the movement of nutrients, oxygen, and water throughout the biofilm, transport channels are formed to maintain the vitality of biofilm microcolonies that would otherwise die due to nutrient depletion [16]. In response to external environmental conditions such as fluid shear stress and available nutrient concentration, bacterial films develop a colony structure that facilitates a healthy and vigorous biofilm. Biofilms formed in regions of high fluid shear stress tend to form thin, dense colony striations, while those formed in regions of slower flows demonstrate fingerlike formations [16]. For both thin-film and fingerlike structures, most biofilms are supported by the mechanics shown in Figure 1.3, where advection, diffusion, and attachment/detachment processes determine overall biofilm viability and structure [30]. Diffusion and advection maintain the necessary levels of oxygen and nutrient concentrations within the biofilm in order to support embedded bacterial cells, while the attachment, detachment, and growth/decay of individual cells determines the overall mass

and maturity of the biofilm as a whole. Additional gene exchange within the biofilm further promotes the specialized function of individual bacterium to enhance the benefits of colony formation [25].

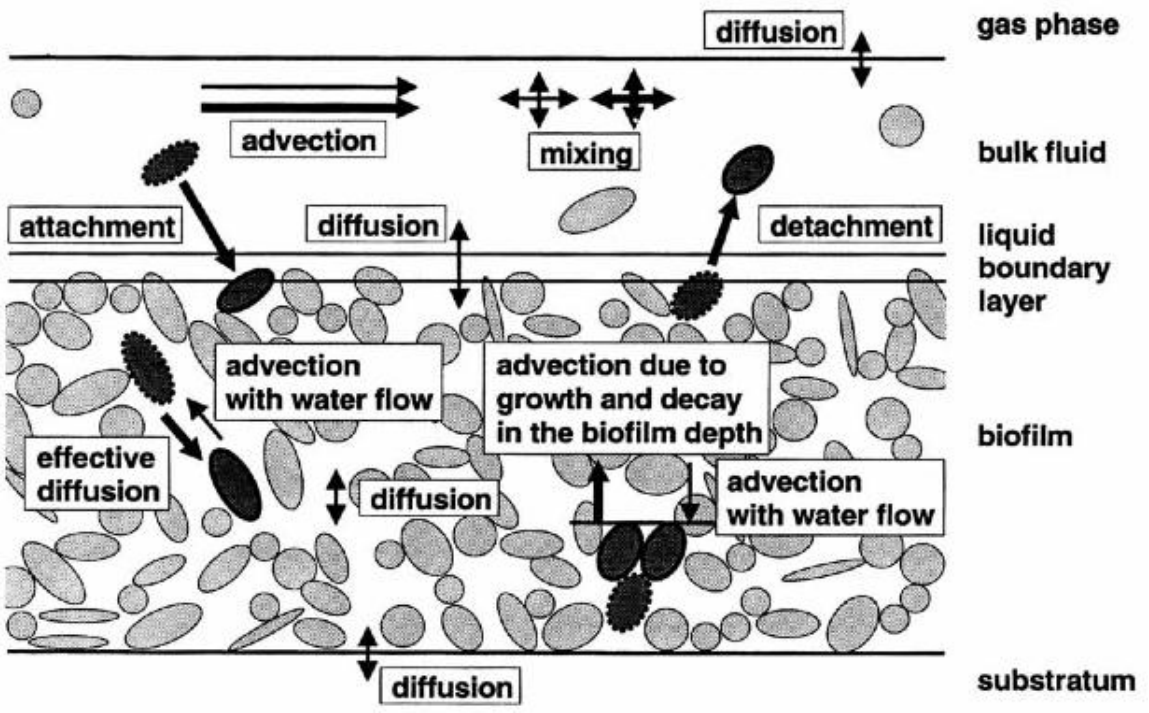

Figure 1.3: Various mechanisms determine growth and nutrient transfer in biofilms [30]. A close-up view of a biofilm structure, shown with level liquid-film boundary for simplicity, reveals that advection and diffusion mechanisms at the molecular level are vital to biofilm growth.

The complexity and diversity of biofilm-associated infections makes the use of traditional approaches to new treatment development exceedingly difficult and time consuming. In order to increase knowledge of the biological system as well as streamline the development process for new bactericidal therapies, efforts in the areas of bioengineering, systems biology, and systems engineering are focusing on the development of new mathematical models and device systems in order to advance the current state-of-the-art. These works directly address the major factors outlined here with

respect to biofilm growth and treatment: surface attachment, quorum sensing and gene expression, fluid flow shear stress, and nutrient/toxin concentrations and diffusion. Utilizing the Micro-BOAT system developed in this work, many of these factors can be controlled to a high level of precision, thereby enabling others to be examined for applications in both biological science and biofilm treatment development.

1.4.2 Antibiotic Treatments and Biofilm Antibiotic Resistance

In this work, the developed microsystem is employed for the evaluation of a novel bacterial biofilm treatment mechanism and its level of efficacy with respect to other antibiotic therapies. Traditional antibiotic therapies are well-founded and engineered to affect specific bacteria in effective ways to either halt their ability to reproduce and function or to be eradicated. Since the new method explored in this work utilizes such antibiotics in conjunction with external electric fields, an understanding of the mechanism of these drugs is useful for understanding how the proposed mechanism can aid antibiotic efficacy.

From a high level, antibiotics function by either stopping bacterial reproduction (bacteriostatic) or by interrupting vital bacterium functions, thus resulting in bacteria death (bactericidal) [31]. Within these groups, the vast majority creates either bactericidal or bacteriostatic effects by affecting one of three aspects of the bacteria: (1) the cell wall or membrane, (2) the synthesis and use of essential enzymes, or (3) the synthesis of necessary proteins within bacteria [31]. Each antibiotic is specifically designed to affect bacteria in one of these three ways by entering the cell (or in some

cases binding to its exterior wall or membrane) and binding to specific receptors or producers within the bacterium, thereby hindering normal bacterium functions.

While the mechanisms of antibiotics are highly effective in planktonic bacteria, the emergent properties of bacterial colonies form a basis for numerous clinical challenges with respect to bacterial infection treatment [32, 33]. Bacterial biofilms preferentially adhere to inert surfaces within the human body, such as dead tissue and medical implants. Once established, biofilms demonstrate enhanced antibiotic resistance by various mechanisms [34]. The presence of the polysaccharide matrix reduces antibiotic diffusion rates by a factor of two to three within the biofilm and even limits the ability of the antibiotic molecules to enter the biofilm structure, thereby diminishing biocidal effects. Additionally, bacteria within the extracellular matrix coordinate responses to the environmental stresses of antibiotic treatment by slowing or altering metabolic processes, altering gene expression, and developing increased populations of persister cells, all with the purpose of defending against antimicrobial treatments [34]. Biofilms developing within the human body tend to grow slowly, with overt signs of infection often not being visible until the biofilm has reached relative maturity. The production of toxic antigens by sessile bacteria cells stimulates the production of antibodies by the host's immune system, however, this response is often insufficient for reduction of the bacterial infection [35].

As a result, antibiotic therapy is typically used to augment the antimicrobial effect of these antibodies by exploiting various weaknesses in bacterial cell functionality. While such treatments are effective in removing the majority of bacteria, small populations of antibiotic resistant bacteria frequently remain after the treatment has ended

and the production of antibodies has subsided, allowing bacterial infections to redevelop in the host organism. Such recursions often require surgical removal of the infection for decisive treatment, procedures that incur their own risk and cost and thus drive progress in novel treatment methods for bacterial infections [36].

1.4.3 Bioelectric Effect for Enhanced Antibiotic Efficacy

In order to increase the effectiveness of antibiotic treatment, much work has been performed both in the development of new antibiotic types as well as in developing methods of increasing the efficacy of currently available drugs. Previous studies have shown that the biocidal effects of antibiotics can be increased if they are used in the presence of an electric field, commonly referred to as the "bioelectric effect" [37-43]. While the mechanism behind this level of increased treatment is not yet fully understood, it is currently believed that the application of alternating currents (AC) and direct currents (DC) have different effects upon bacteria under antibiotic treatment, both of which show an increase in efficacy of supplied drugs. The application of AC electric fields to bacterial cells results in molecular vibrations at the bacterial cell wall. Such vibration increases the permeability of the cells themselves, allowing for antibiotics to more readily penetrate and affect cells [44]. DC electric fields applied to bacterial cells in the presence of antibiotics have also shown increases in treatment efficacy, which is currently attributed to the ability of the induced electric field to apply a force upon antibiotic molecules and bacteria and thus increase the rate at which the cells are exposed to the biocides [44]. Many bacteria (both gram-negative and gram-positive) display a net negative charge at their surface, while antibiotic molecules and other molecules within

bacterial growth solutions often display a slight positive charge. The electrophoretic forces of the DC electric field on these molecules create gradients of antibiotic molecules and pH, which results in an increase in the efficacy of the applied drugs. Recent work in our group by Kim et al. utilizes a superposition of these two electric fields in macroscale systems showing a 400 times increase in treatment efficacy versus standard antibiotic treatments while maintaining electric fields below those that would induce hydrolysis of the aqueous growth media (Figure 1.4) [45].

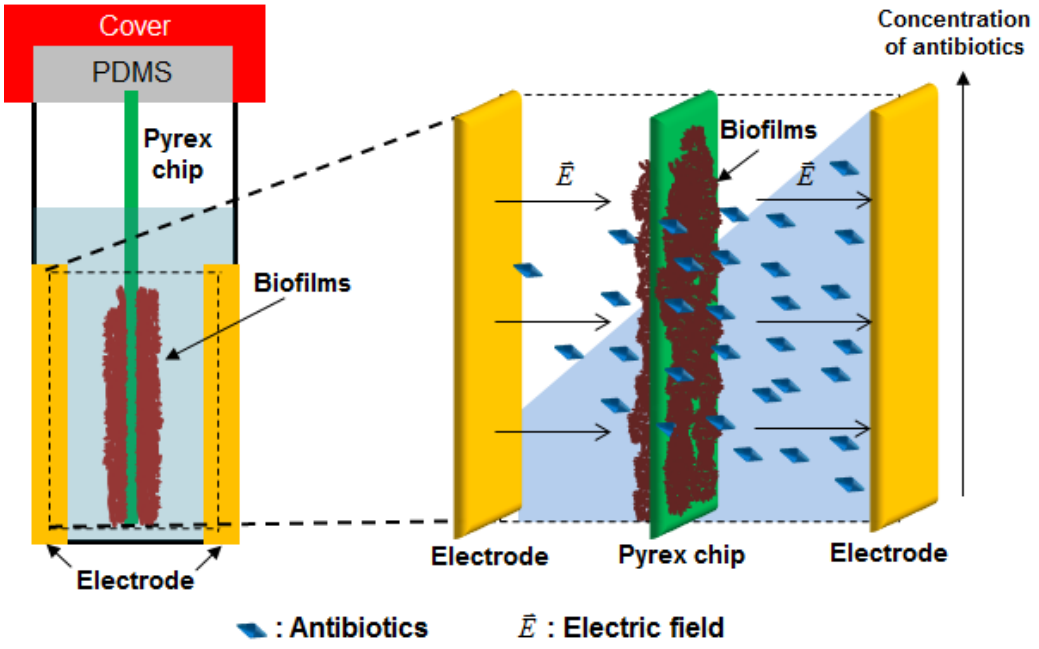

Figure 1.4: Schematic of the macroscale experimental set up for the testing of the SP BE. Electric fields applied across the two electrodes have been shown to increase biofilm treatment efficacy as well as create a gradient of antibiotics within the experimental cuvette [8, 45].

The development of this potential treatment method using SP electric fields in conjunction with antibiotics is a focus of this work, where principle objectives include demonstrating this method at the microscale for potential clinical applications, while also reducing the voltages required for these electric fields to biocompatible limits, a

necessary step for the future use of this treatment method in patients. Further discussion of this method, including its implementation, is discussed in Section 2.4 of this thesis.

1.4.4 MEMS and Microfabrication

Micro-electro-mechanical systems (MEMS) have been traditionally defined as the integration of mechanical microsystems with on-chip or external electronics for both sensing and actuating applications. These technologies rely heavily upon the mature integrated circuit (IC) industry and the advantages of batch microfabrication in order to produce systems that are capable of diverse functions in ideally small, low power, and highly sensitive system architectures. In recent decades, the field of MEMS has expanded beyond the realm of microscale mechanical systems to include the integration of biological, chemical, and optical components in order to increase the breadth of possibilities for these technologies [46].

The small size and batch fabrication capabilities of MEMS makes them ideal for a number of application areas. Due to the capability of MEMS to be fabricated using techniques from the IC industry such as photolithography, thin-film deposition, etching, etc., these systems can often be produced more quickly and at a fraction of the cost of their macroscale counterparts [47]. As a result, numerous MEMS devices have reached production and are now fully integrated into larger electronic systems or exist as stand-alone sensing devices. Some of the most common include accelerometers, gyroscopes, micro-mirror arrays, microphones, microfluidics, and various sensors, with more devices reaching commercialization every year [48].

The success and rapid growth of the MEMS field is largely attributable to the maturity of present IC fabrication capabilities, since many of the materials and processes implemented for the semiconductor industry are also used in the development and production of MEMS [48]. The majority of devices are constructed using materials native to the semiconductor field such as silicon and silicon compounds, other III-V group materials, and some metals, with bulk and surface micromachining enabling the realization of small-scale, three-dimensional features. Bulk micromachining techniques, in which holes or trenches can be formed in an existing substrate, enable the full or partial release of MEMS devices, thereby allowing for physical movement of the device. Similarly, surface micromachining enables the creation of physical structures by first depositing materials onto a bulk substrate followed by patterning and etching of the material to create MEMS structures. In addition to the use of CMOS-compatible materials, the development of new polymers and composites that are well-suited to these fabrication techniques enables the expansion of MEMS to other fields, where the requirements of specific applications have driven a need for materials that are biocompatible, flexible, or otherwise unique [48].

The advantages of using MEMS in lieu of macroscale devices extends beyond ease-of-fabrication and cost reduction, since many applications can benefit from the performance of devices manufactured at this scale. While these benefits are broad and often specific to a particular use, they typically involve leveraging physical mechanics that scale well for various applications including: (1) the development of laminar flow at low Reynolds numbers, (2) increased surface-to-volume ratio for thermal transfer and surface reaction area, and (3) the non-linear scaling of mechanical strength compared to

generated inertial force [46]. Additionally, the ability of MEMS to integrate with present-day electronics and at a similar scale makes these systems preferable in many instances by providing simpler, more reliable, and more cost effective full-system packaging and assembly [49].

With these considerations in mind, MEMS and integrated microfluidics are ideal technologies for the biofilm growth, treatment, and monitoring system pursued in this work. Microfluidics produced using high-throughput soft-lithography processes provide cost-effective, biocompatible alternatives to macroscale flow reactors that can provide enhanced control over assay parameters and conditions [12]. Furthermore, the materials used for microfluidic fabrication are chemically inert and therefore ideal for biofilm studies, where surfaces must serve as an attachment point for biofilm growth while avoiding extraneous chemical reactions that can affect the results of biofilm studies. Finally, the ease of integration of microfabricated structures and materials, such as the gold used for the electrodes integrated in the Micro-BOAT system, makes devices developed using such microtechnologies easily adaptable to different applications within a single system architecture. This component approach to microfluidic system design, in which individual functionality is contained in subsystems such as micropumps, valves, mixers, channels, and detectors provides high system agility for adaptation to related applications in microbiology [12, 13].

1.4.5 Bacterial Biofilm Measurement Methods

The following section provides a brief review of the literature with respect to methods for the measurement and characterization of bacterial biofilms in clinical and

biomedical applications. While this summary is not intended to be all-inclusive, it provides a sufficient background and motivation for the development of the novel optical density method implemented through the Micro-BOAT platform presented here.

1.4.5.1 Present-Day Industry Methods

The system developed in this work for the growth, treatment, and monitoring of bacterial biofilms represents a new method of conducting studies related to bacteria and their infections, including those studies aimed at drug screening and development. Currently, the majority of drug screening methods utilize macroscale devices and systems to perform assays that determine the effectiveness of prospective treatments on inhibiting or eradicating microbial growths. Advanced industry methods utilize primarily automated systems to perform common screening techniques such as broth microdilution, antibiotic gradient, and disk diffusion studies on mature microbial cultures to determine the efficacy of various treatments as well as the minimal inhibitory concentration (MIC) of these drugs (Figure 1.5 and 1.6) [50, 51]. In addition to these microbiological methods, other immunoassays are frequently used to perform highly selective and sensitive studies by integrating methods such as ELISA (discussed subsequently in Section 1.4.5.2), fluoroimmunoassay (FIA) and time-resolved fluoroimmunoassay (TRFIA) with large-scale capabilities, however, these methods are also limited in the types of molecules they can detect and therefore are not currently an all-encompassing method for antimicrobial drug screening [52, 53].

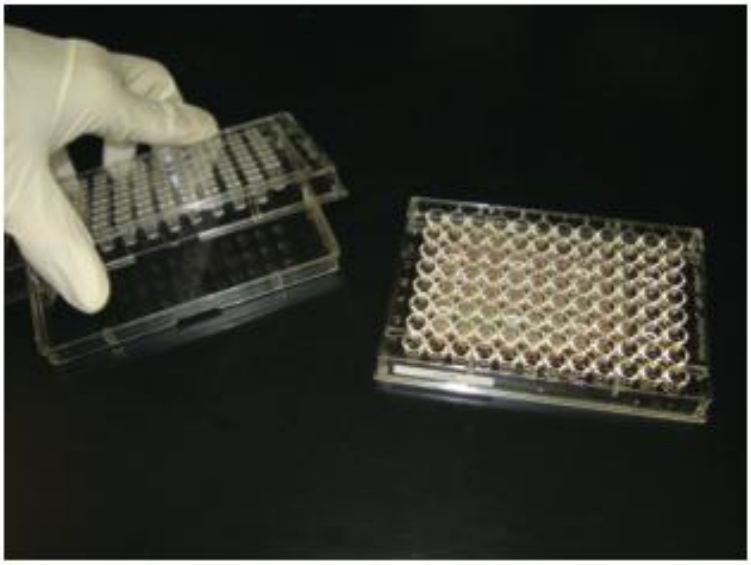

Figure 1.5: A broth microdilution susceptibility panel (microtiter plate) containing 98 reagent wells and a disposable tray inoculator [51]. Bacteria samples in suspension are treated with various concentrations of candidate drugs and each suspension tested using colony counting or spectroscopy to determine therapeutic efficacy.

Figure 1.6: An Eclipse gradient diffusion testing plate featuring three candidate drugs on a single agar substrate. The MIC of each agent is determined by the intersection of the organism growth with the measuring scale strip [51].

While these various methods perform a similar function by enabling screening to determine a lead compound for a candidate drug, most current methods are limited by

their high cost, large size, and low throughput capabilities. Moving forward, new methods of drug screening must utilize emerging technologies such as the micro/nano methods presented previously in order to take advantage of the benefits provided by devices at this scale [52].

1.4.5.2 Macroscale Methods

The majority of previous biofilm study mechanisms have utilized macroscale methods to determine biofilm viability, biomass, and overall structure for various biomedical, industrial, and environmental applications. The majority of these studies were performed using macroscale flow reactors to culture biofilm samples with integrated, external detection methods [6].

One of the most basic methods of biofilm quantification involves the counting of bacterial colonies, where bacteria are cultured on an agar plate and subsequently enumerated using microscopy and image analysis to determine their average density [54]. Polymerase chain reaction (PCR) techniques are another standard method, which use the amplification of DNA segments to quantify the presence of target biological elements [55]. Fluorescence techniques provide an extremely accurate and simple method of biofilm detection by applying a fluorescent stain to a sample or, for greater precision, genetically engineering a bacteria strain to selectively express a fluorescent protein [56-58]. Heyduk, et al. demonstrated the representative fluorescent immunosensor technique shown in Figure 1.7, in which nanometer length linkers modified with fluorochromes could participate in fluorescence resonance energy transfer (FRET) to increase sensitivity. However, since this and similar approaches require a labeling method and

external microscopy equipment such as a confocal or fluorescence microscope for biofilm detection, it does not represent a high throughput or cost effective method of sensing, thus presenting a barrier to drug screening applications [7].

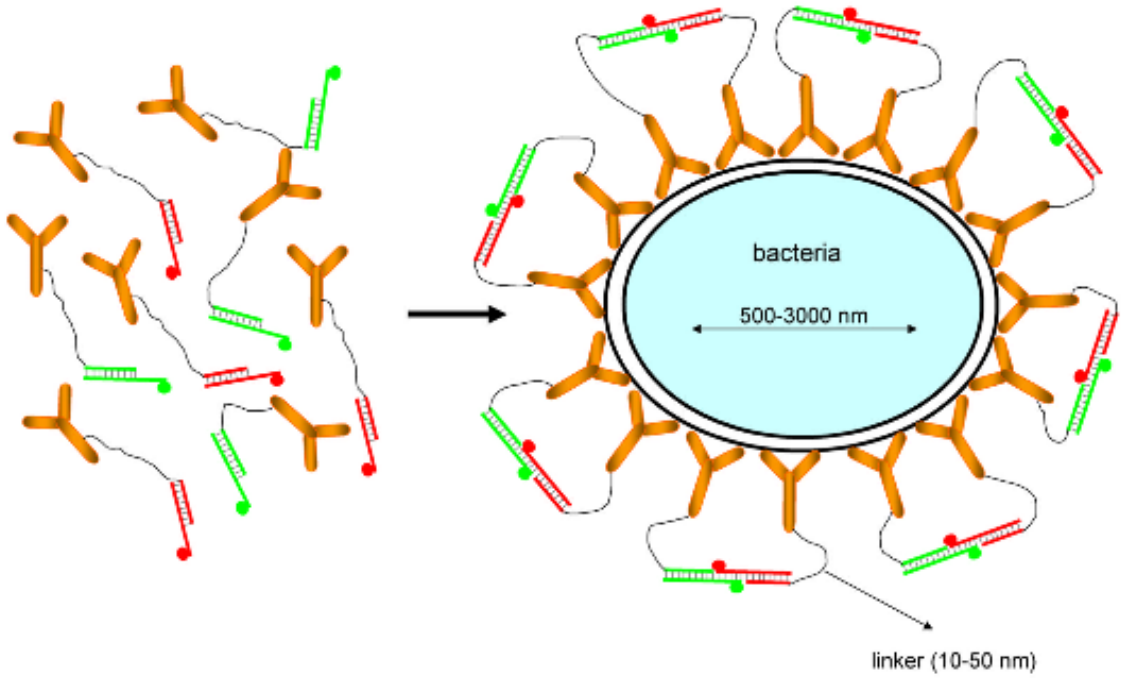

Figure 1.7: Design of homogeneous biological immunosensors for pathogenic bacteria detection [57].

Similar to the FRET approach, considerable research has been directed towards the use of the Enzyme-Linked Immunosorbent Assay (ELISA) in laboratories to perform detection analyses on mixed cultures [59]. ELISA utilizes the specific binding of particular antibodies and antigens in combination with a fluorescent label to enable a specific and highly sensitive method for quantitative measurement of target antibodies or analytes in solution. The method has seen vast use as a diagnostic tool in medical and other industrial fields and is also useful for chemical quality assurance due to its high sensitivity and selectivity [55]. A typical procedure for performing an ELISA analysis in a laboratory setting is provided in Figure 1.8 below.

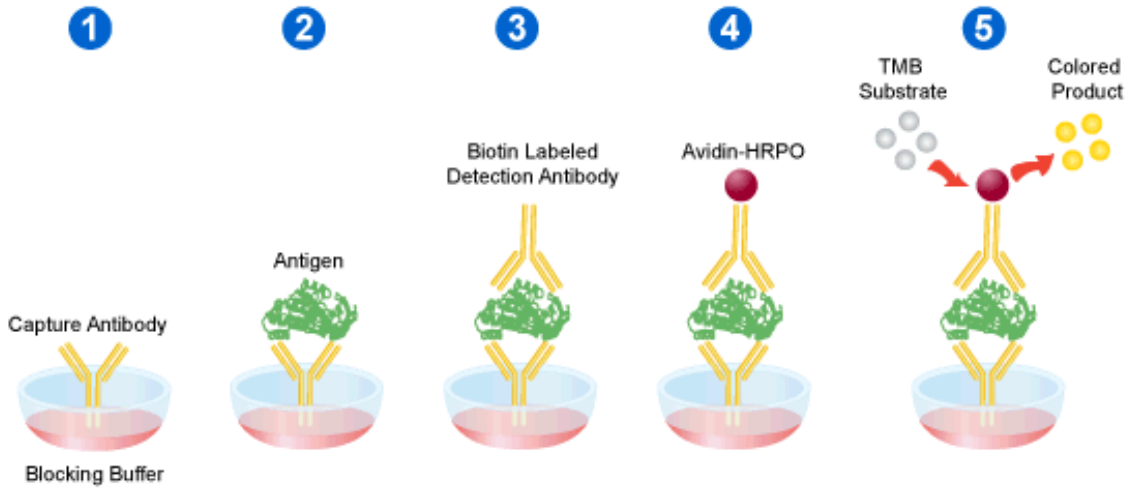

Figure 1.8: Typical ELISA procedure: (1) A plate is coated with a suitable capture antibody (2) as sample is added any matching antigen is captured by the antibody (3) a suitable biotin labeled detection antibody binds to the antigen (4) a second conjugate antibody binds to the biotin labeled detection antibody (5) add a fluorescent label and read out [60].

Despite the highly selective and precise results provided by ELISA, it is rather arduous to perform, often requiring up to a full week for analysis, and often difficult to perform in lab-on-a-chip devices [57]. As a result, it has limited usefulness for high-throughput drug screening applications, lending to the development of new techniques for biofilm detection.

PCR, FRET, and ELISA techniques are commonly used in microbiology studies due to their high level of accuracy and precision, as well as their robustness as reliable quantification mechanisms. The high cost, slow assay rates, large sample volumes, and expensive, labor intensive properties that define macroscale biofilm detection methods, however, motivates the development of similar techniques at the microscale in order to address the shortcomings of these technologies.

1.4.5.3 Microscale Methods

Microscale methods leverage the technologies available for larger systems while taking advantage of capabilities only available in microscale and microfabricated devices. Some of these methods enable on-chip biofilm detection that is not possible in macroscale systems, while others adapt existing macroscale technologies to smaller environments. By adapting macroscale technologies to microscale regimes, key advantages of micro/nano detection are leveraged including the use of small sample sizes, highly parallel throughput, tight control over environmental conditions, and inexpensive production through batch fabrication [11].

Recently, the development of small-scale devices and microsystems for drug screening applications has received attention [52, 53]. These 'lab-on-a-chip' devices typically rely upon optical methods such as surface Plasmon resonance (SPR) and fluorescence or electrochemical reactions on the sensor surface to detect microbial growth and treatment, which allows many measurements to be taken *in situ*. In addition, the relatively low cost of these devices enabled by batch fabrication allows for microsystems that are specific to particular assay types and applications.

Fluorescence imaging methods have been adapted to integrate with microfluidic systems in a number of cases, allowing for increased control over the growth conditions of bacterial biofilms while taking advantage of a highly accurate and easily implemented optical detection method [61, 62]. Fluorescence microscopy systems of this type utilize fluorescent protein expression or cell staining methods to perform bacteria imaging and quantification of biofilm growth via cell colony counting or bacterial density. Similarly, laser confocal microscopy systems enable in-depth analysis of localized biofilm

structures with respect to cell viability, surface roughness and morphology, and cell colony distribution within the polymeric ECM matrix.

The device produced by Kim et al enables the testing of different bacterial signal concentrations on biofilms formed in microchambers by integrating a gradient mixer into a microfluidic flow cell [63].

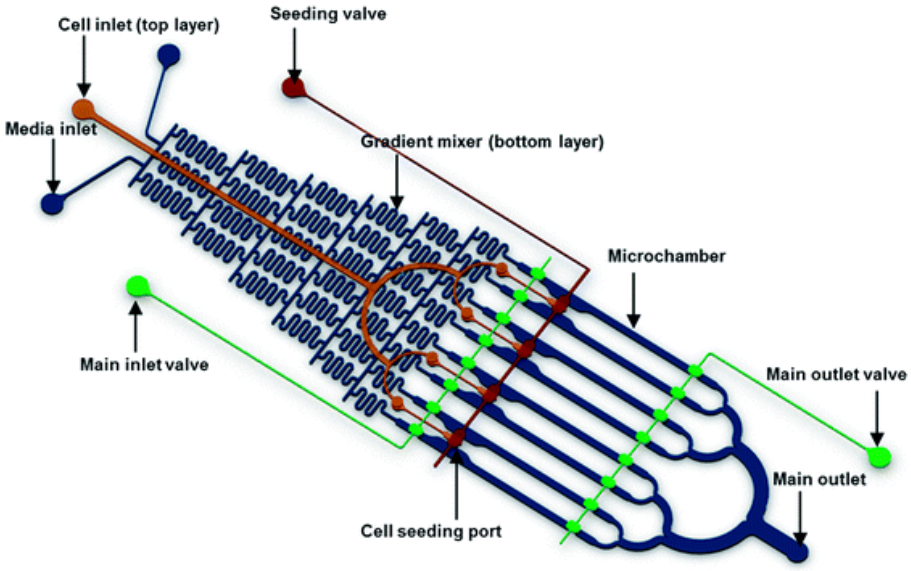

Figure 1.9: A microfluidic flow cell enabling gradient efficacy testing of eight concentrations of antibiotic simultaneously in a single device [63].

The device produces results similar to those that could be obtained through traditional macroscale methods using lower reagent volumes and more paralleled experimentation, with analysis of biofilm growth being performed via confocal microscopy at select points in time.

In order to address the limitations of fluorescence detection methods at the microscale, the work conducted by Meyer et al utilizes a label-free method of detection based on the optical density properties of bacterial biofilms [6]. The system utilized microfluidic growth reactors on glass coverslip substrates such as those utilized in

fluorescence-based methods, with optical measurement performed by measuring changes in light transmittance through biofilms using COTS photodiodes. The measurement technique provides an *in situ* method of overall biomass quantification that does not require a permanent fixture on the external equipment used in confocal and fluorescence methods, thereby allowing for highly paralleled biofilm testing at reduced cost. While the use of discrete photodiodes in the microsystem limits the number of measurement points to a few select areas, a shortcoming considering the high variability of bacterial biofilm structures, the system can achieve real-time monitoring of changes in biofilm mass due to growth and treatment.

For extensive analysis and detection at the molecular level, microscopic systems have also been integrated with ELISA methods in order to utilize specific fluorescent labels to detect the presence of target antibodies within a solution, such as bacterial biofilm cells. While this and similar fluorescent microscopy-based methods are extremely accurate and provide precise information with regards to the development of bacterial biofilms, they require expensive and complex equipment for biofilm measurement and, without a permanent fixture upon the microscope stage to perform continuous *in situ* measurement, are limited explicitly to end-point measurements [6].

In order to enable continuous measurement of bacterial biofilm development without the use of optical measurement, electrochemical sensors have been developed that are able to detect biofilm growth with respect to both time and position within a microfluidic reactor [64-66]. Sensors of this type detect the presence of bacterial biofilms attaching to an exposed or passivated set of electrodes via changes in capacitance or impedance [67, 68]. While electrochemical biosensors provide continuous

detection and a relatively high level of precision, they require extensive characterization and calibration in order to produce reliable and meaningful measurements. Output of the system is highly dependent upon the types of bacteria used and the aqueous media implemented, since each of these factors affects the electrical response of the system to changes in bacterial biofilm mass. Finally, use of electrochemical detection methods requires significant signal processing as well as external equipment such as impedance spectrometers for precise signal analysis, thus adding undesirable complexity and overhead to the system architecture.

A final type of bacterial biofilm detection method utilizes surface acoustic waves (SAW) and shifts in propagating wave resonant frequency in order to determine changes in biofilm mass over a sensor area [69-71]. A set of interdigitated electrodes (IDT) on a planar piezoelectric substrate is fabricated to produce a known resonant frequency when the surface is unloaded. As the mass of the material between the two electrodes changes, it results in a known resonant frequency shift that is detectable using a network analyzer or similar equipment designed to determine changes in signal resonance.

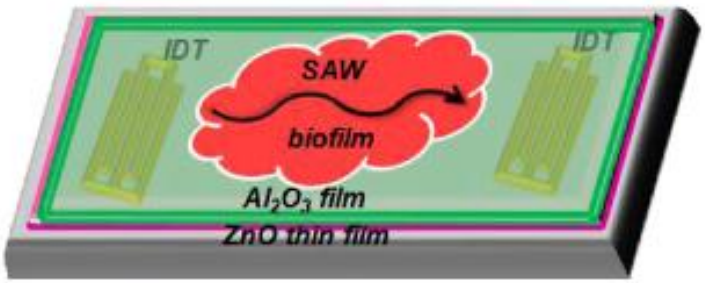

Figure 1.10: A surface acoustic wave sensor passivated using atomic layer deposition (ALD) for bacterial biofilm monitoring and early detection [69].

Surface acoustic wave biosensors such as that produced by Kim et al for early biofilm detection are extremely accurate, with detection limits often below tens of pictograms

[69]. Widespread use of such a mechanism is limited, however, due to the complex nature of SAW sensor microfabrication and difficulties in utilizing SAW sensors for multiple and long-term experiments due to the fouling of sensing surfaces by developing bacterial biofilms. As a result, SAW sensors and similar resonant devices are not typically used for commercial drug screening methods, which typically employ macroscale methods as described in the following section.

1.4.6 Systems Engineering Principles in the Biomedical Field

In recent decades, systems engineering has begun to take hold as a freestanding engineering discipline motivated by a need to manage the design, development, operation, and integration of increasingly complex systems and networks. While originally developed for use within large-scale corporations and projects such as military, government, and large-industry, recent years have made it increasingly evident that systems engineering principles are applicable, if not necessary, in a much broader spectrum of industries and fields [72]. For smaller scale industries and those that operate in less ideal research and development environments, systems engineering aids in the execution of design processes and daily operations that would otherwise face "imminent" failure if managed using less comprehensive methods.

The biomedical and pharmaceutical fields have begun to pursue the use of interdisciplinary research strategies in order to aid the development of new medical devices and antimicrobial treatments, as well as the operation of treatment facilities such as hospitals and clinics [72, 73]. In many of these applications, systems engineering lies at the heart of efforts to control development and system operation to ensure that

requirements are continuously met and safety is maintained. As a case in point, in 2010 the FDA initiated a requirement that infusion pumps for the intravenous delivery of drugs (i.e., insulin) must perform an assurance case in order to ensure patient safety even in the event of device malfunction or operator error [74]. Such assurance cases derive directly from systems engineering principles and are closely linked to the requirements and traceability matrices that guide principle design cycles to ensure proper device functionality. Similarly, medical physicians and treatment facility analysts are now looking at the capabilities of adaptive systems engineering and similar principles to address inefficiencies and streamline medical care with respect to both patient flow and treatment efficacy [72, 75].

Looking forward, considerable encouragement has been set forth for the integration of systems engineering and related fields with microbiology in order to create a unified effort towards the development of new antimicrobial agents [15, 76]. Integration at multiple levels of complexity and in diverse application areas has been suggested, including the fragmentation of microbiological processes to enable model-based system engineering of biological systems and the use of control system theory to direct biological processes and treatments. Overall, these efforts aim to enable biomedical scientists and engineers to develop treatments or devices that directly and acutely address requirements in order to ensure efficacy while limiting potentially negative emergent responses. Thus, the use of systems engineering principles in the design of biomedical devices, such as those developed here for drug screening or bacterial biofilm monitoring applications, can direct system development to achieve a

more effective final product than is achievable by approaching the problem from biology or engineering perspectives alone [15].

1.5 Thesis Organization

This thesis will be organized according to the following outline. Following Chapter 1, which has provided the background and motivation of this work, Chapter 2 discusses design considerations driving the development of the integrated Micro-BOAT system. Specifically, this will present considerations towards the choice of optical detection and growth chamber methods, as well as systems engineering requirement and integration analyses that aid in the full enablement of the integrated microsystem. In addition to providing design concerns pertinent to the development of the device, parameters relevant to the use of the SP BE treatment are also discussed. Chapter 3 will provide the overall system design and fabrication with respect to the microfluidic biofilm growth chambers, optical density detection mechanism, and components required to generate the SP BE. Assembly of the complete Micro-BOAT system will also be explored in this chapter. Chapter 4 will investigate the performance of the Micro-BOAT by providing testing and results. These results will investigate the performance of the system in terms of its ability to accurately and definitively detect the growth and movement of molecules within the microfluidic growth chamber, as well as its capabilities for biofilm treatment screening applications. Finally, the integration of a novel bioelectric effect for biofilm treatment will be presented and its relative efficacy evaluated using the Micro-BOAT as a testing instrument. An extensive discussion of these results will be presented at the conclusion of this chapter, evaluating the overall

performance of the Micro-BOAT as a tool for biofilm monitoring and drug screening applications, as well as determining areas of difficulty and possible improvement in the device design and implementation. Finally, Chapter 5 will provide a summary of the research performed and presented in this thesis. Future work will be presented, followed by an analysis of the potential impacts and benefits of this research, leading to a final conclusion. Supplemental information, including signal acquisition programming and data processing scripts, is provided at the conclusion of the document.

Chapter 2: Systems Engineering of Experimental Biomedical Systems

Recent work in the area of systems engineering has made a discipline-wide thrust in the areas of systems biology and biomedical sciences, presenting the advantages of systems engineering principles and model based systems engineering (MBSE) in the development of biomedical devices and models for biological processes [8, 10, 15, 72, 74]. A similar thrust has occurred in microfabrication fields, including MEMS, where systems engineering and MBSE have earned notoriety through the development of very-large-scale integration (VLSI) design [77]. In both fields, there has been a growing need for the use of systems engineering in order to manage the increasing levels of complexity associated with systems such as that developed in this work [8, 10, 78-80].

System design and validation is performed in this research using the high level descriptive modeling language SysML as well as several application-specific software packages to conduct low-level analysis of system component functionality. System-level design using SysML is performed using activity diagrams, state machine diagrams, sequence diagrams, use-case analysis, case diagrams, and requirements analysis in order to obtain a full understanding of the system functionality, structure, and control prior to the fabrication of system components for the final device.

In order to enable the development of not only the system developed in this work, but the streamlined development of biomedical devices aimed at experimental applications on a broader scale, a principle focus of this work targets the development of a systems-driven design platform for experimental biomedical systems. This platform provides a framework for the design of biomedical devices that is not currently available for devices in this regime, where the integration of biological systems and traditional

engineering device systems poses a number of unique challenges that must be addressed. Specifically, current systems engineering methods for the design of device systems cannot capture the stochastic and complex properties of biological systems, leaving developers in this regime to attempt to approximate these stochastic properties by integrating them into more complex requirements and approximations of potential biological system variance.

Here, a platform architecture is designed and proposed that attempts to bridge the gap between traditional engineering domains and biological domains by providing a method of formal system design that integrates the complexity of biological systems with the design of devices for target biomedical applications. By providing such a means through a systems approach, an interface is created that enables both biologists and engineers to integrate requirements and system functionality in a single paradigm, thus ensuring validation and verification of the resulting system and increasing the efficiency of biomedical device development. In the remainder of this thesis, the presented paradigm is implemented in order to demonstrate its utility for the development biomedical devices, with the microfluidic biofilm observation, analysis, and treatment platform providing a prime example.

2.1 Systems Engineering as an Integration Tool

As described, the design of systems for biomedical applications, and specifically experimental biomedical applications, is complicated by the variant nature of the biological systems that play an integral role in the function of the overall system [8]. The growth of living organisms is dependent upon a large number of factors unique to each

system, typically driving a same set of biological system inputs to produce a stochastic set of system outputs, and making the design, validation, and verification of biomedical devices exceedingly difficult. In designing experimental biomedical devices, the integration of both biological and device engineering domains is a necessity in designing systems that properly address system requirements, posing a current hindrance to the design of these devices, as the complex nature of biological systems limits their extensive understanding solely to biologists and clinicians well-versed in their respective fields.

To address this knowledge discontent, design techniques must implement a method enabling validation and verification of system performance in the context of these highly stochastic biological elements, thereby assimilating biological and engineering domains and enabling efficient device design [8]. Drawing upon the capabilities of systems engineering tools to model systems in the design phase, the development of a platform for engineering experimental biomedical systems is a large step towards producing more effective biomedical systems. Figure 2.1 presents the method by which these platforms allow for the integration of biological and engineering domains, and forms the basis of the systems engineering design paradigm developed in this work. Here, the biological and engineering domains are pictured as separate regimes, i.e., the top and bottom halves of Figure 2.1. The requirements of a specific application, such as functional, performance, interface, and testing requirements, are provided by those operating in the biological domain, in addition to models relevant to the application, such as models of the behavior or structure of the biological system. The existence of mathematical models of biological systems enables the integration of such models within a description of the overall system, providing, from a system perspective, capabilities for

full architecture engineering. Coincidently, the engineering domain proposes libraries of design options and components defining the architecture space. By integrating these two domains within a single platform interface, the entirety of the explorable design space is accessible to enable the concrete design of a biomedical device system addressing the requirements of the biological application.

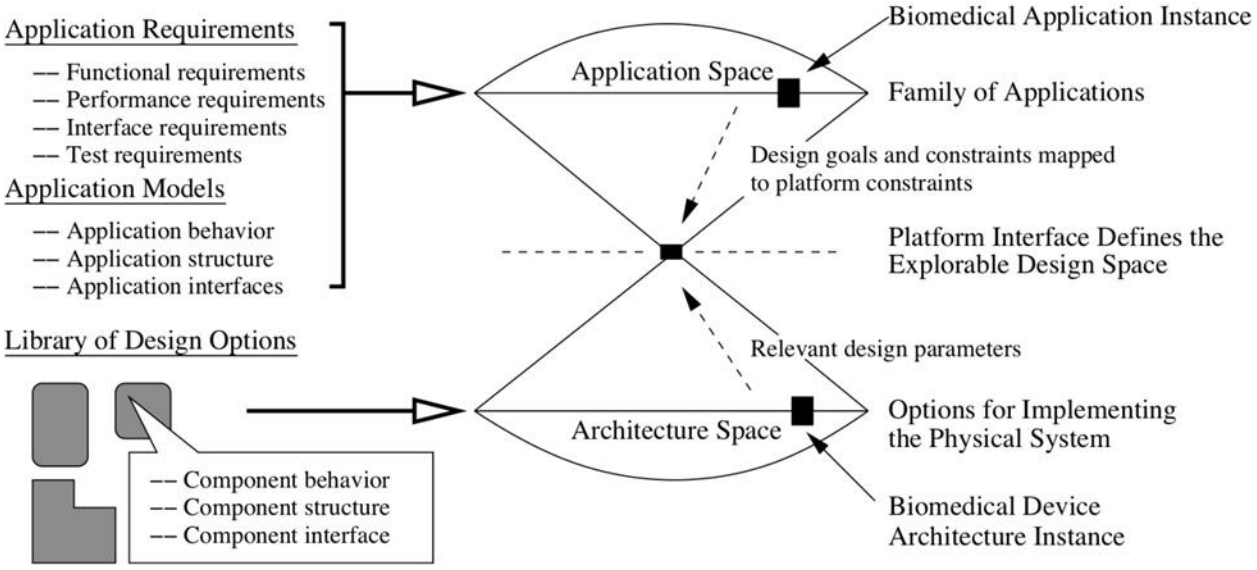

Figure 2.1: Conceptual diagram presenting the integration of biological and engineering domains at a platform level, designed and developed in this work for the acquisition of system architectures that successfully satisfy design requirements unique to the integration of these two domains.

In order to capitalize upon the added capabilities of such a technique, two key tenets of this work are that (1) methods to succinctly model a breadth of biological systems must be developed, and (2) these models must be able to integrate with system-level models capable of describing the performance of the entire engineering system. Recent work in the area of systems engineering has made a discipline-wide thrust in the areas of systems biology and biomedical sciences, presenting the advantages of systems engineering principles and model based systems engineering (MBSE) in the development

of biomedical devices and models for biological processes [8, 10, 15, 72, 74]. A similar thrust has occurred in microfabrication fields, including MEMS, where systems engineering and MBSE have earned notoriety through the development of very-large-scale integration (VLSI) design [77]. In both fields, there has been a growing need for the use of systems engineering in order to manage the increasing levels of complexity associated with systems such as that developed in this work [8, 10, 78-80]. Through these thrusts, both points (1) and (2) mentioned above are satisfied, and the system paradigm is achievable through the interface of these modeling mechanisms.

Functionally, the platform presented in Figure 2.1 can be implemented through hierarchies of modeling paradigms that, overall, enable the integration of the biological and device engineering domains, which is then accessible at a higher level through the use of standardized systems engineering tools, such as the SysML or UML languages. System-level design using SysML is performed using activity diagrams, state machine diagrams, sequence diagrams, use-case analysis, case diagrams, and requirements analysis in order to obtain a full understanding of the system functionality, structure, and control prior to the fabrication of system components for the final device. Using these languages as a framework on which to integrate lower level models of device components and subsystems in addition to biological models, a full-system model is realized that can fully describe the functionality of the experimental biomedical system under development. This implementation can be visualized as in Figure 2.2, presented below, in which the design spaces of Figure 2.1 are mapped to a modeling regime, thereby displaying the integration of different modeling techniques to achieve a complete platform for the engineering of experimental biomedical devices.

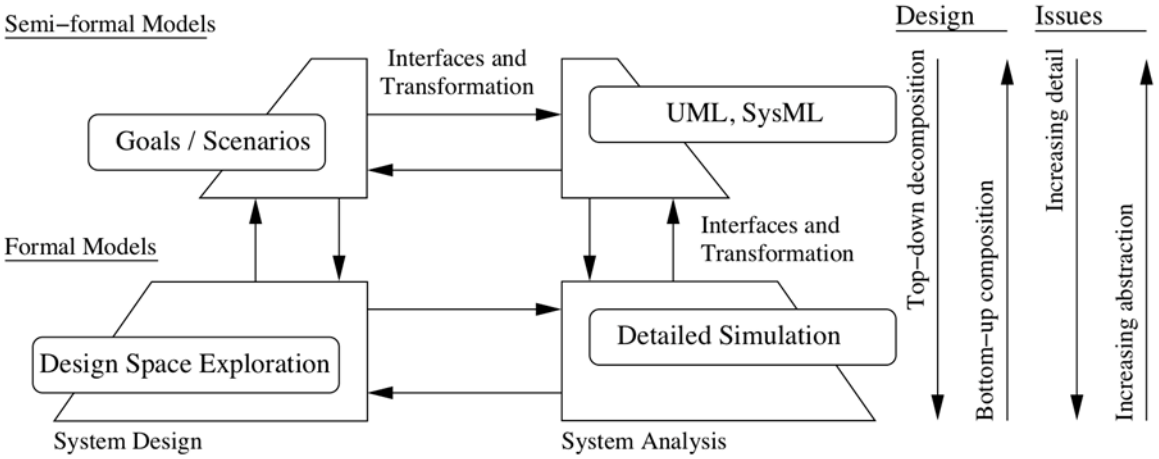

Figure 2.2: Abstraction as a tool for the design of biomedical systems. The design paradigm, or "platform," establishes application goals and scenarios that are modeled at a high level, while the design space is explored through detailed simulations of specific system components [15].

2.2 Platform for Designing Experimental Biomedical Devices

The developed platform for the system-level design of experimental biomedical systems can be divided into two high-level areas of system architecture, namely, an experimental process or functionality related to the device system, and the physical design and implementation of the device system. As implemented, the systems engineering paradigm recognizes a typical experimental process utilizing a device architecture is shown in Figure 2.3. The researcher or clinician begins with a hypothesis about their subject that, for example, may be founded in prior data of biological systems or patient symptoms [81]. For a medical researcher or systems biologist, this hypothesis may involve a parameter or process that the experiment is intended to verify. Examples commonly include a metabolic process, the effects of a compound on a biological system (e.g., candidate drug), or verification of the unique characteristics of a particular

organism. For the clinician, a hypothesis may involve a patient diagnosis or prognosis, or may be geared towards determining an effective treatment for a patient's verified medical condition. With this hypothesis in place, an experiment is begun under ideally controlled conditions. At the conclusion of the established assay, the researcher or clinician inspects the outcome to determine if the test was successful or if alterations or repetition of the experiment is required. Due to the highly stochastic nature of biological systems, such a feedback process is common in order to verify experimental results.

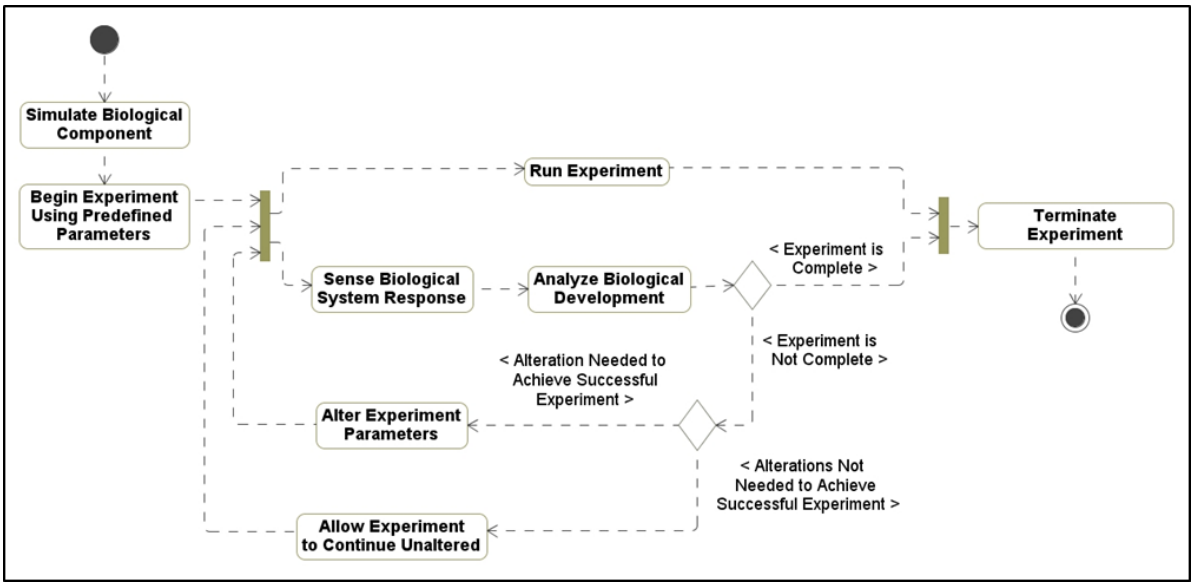

Figure 2.3: Activity diagram presenting the system-level functionality of biomedical devices during experimental procedures. Beginning with a set of predetermined experimental conditions, continuous monitoring of the biological system enables feedback in the system operation that can optimize experiments as well as detect errors occurring in situ [15].

The goal of the design engineer is to develop device systems that can aid in reducing the number of iterations needed to achieve a required level of confidence in the result. This is especially important in clinical applications, due to the patient discomfort often associated with invasive testing (e.g., prick tests to determine skin allergies). Similarly,

current medical research often utilizes high cost, low throughput methods of testing, giving strong motivation for the development of methods to limit the number of iterations needed to verify an experiment.

Coincident with the structure for system performance, the physical structure of biomedical devices can be approximated using a high level architecture that is useful for a variety of applications. While the structure of such devices for experimental applications is diverse and typically suited to the needs of the particular application, most systems can be abstracted to the system architecture shown in Figure 2.4.

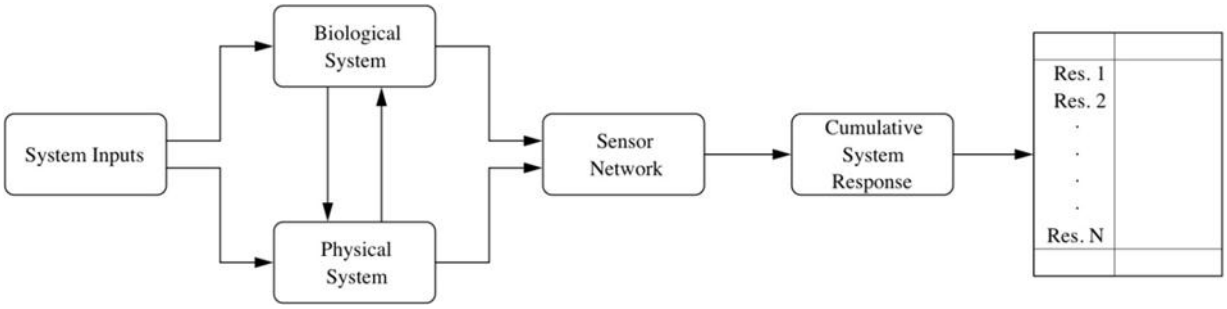

Figure 2.4: Implementation of the platform for experimental biomedical devices, utilizing a device architecture in which system inputs affect integrated biological and physical system modeling structures. The resultant of these interactions is detected by a physically implemented sensory network, which acts as a transducer to detect the biological system output, which can then be recorded as a set of responses (Res. 1-N).

System inputs are typically comprised of a number of different domains, including environmental conditions and actuation or application conditions (i.e., what is done to the biological system during the experiment). Depending upon the requirements of the assay, the physical device system can take any number of forms but will typically have three distinct structural elements including: (1) a way to contain or integrate with the biological system or sample, (2) a way to control experimental conditions, and (3) a way to integrate with a sensor network for detection. The sensing mechanisms utilized for experimental

devices also vary depending upon the application, though they typically aim to optimize a tradeoff between minimal invasiveness and achieving the required detection limit and sensitivity of the application. The cumulative effect of the physical system's interactions with the biological element results in a set of potential experimental results, each having a unique probability of occurrence. These probabilities are dependent upon the stochastic biological system, providing at the simulation level a range of statistically relevant outcomes that can be used to confirm experimental results. Figure 2.5 provides a high-level implementation of the system elements and their interactions at the component and subcomponent levels.

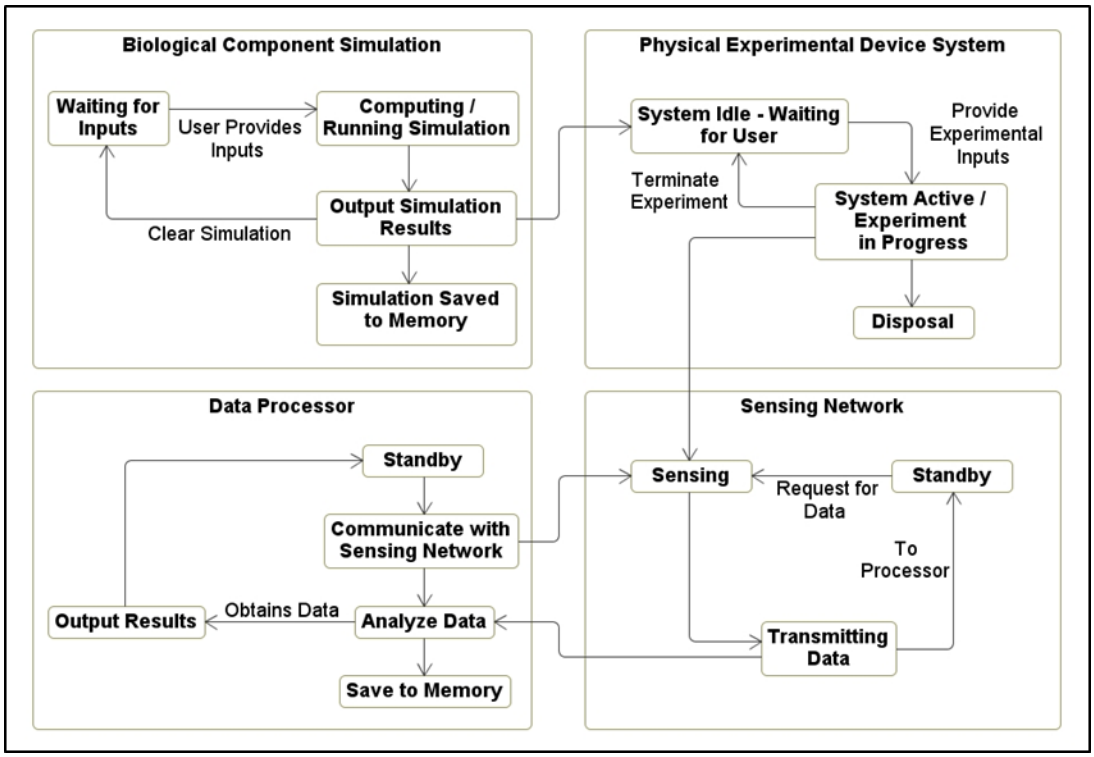

Figure 2.5: State machine diagram presenting the functional dependencies of biomedical testing devices. Based on the set of system interdependencies between simulations/initial conditions, physical device systems, and integrated data processors, an optimized system is realized for this research work [15].

Most biomedical devices are constructed through a similar architecture, providing strong support for the development of the generalized platforms for experimental device engineering presented here. The platform exhibits a flexible structure that can be adapted to numerous applications in the biomedical field, thus expanding the scope of the developed platform. The development of libraries of components to represent physical systems (e.g., through finite element modeling tools, and/or subsystems modeled through SysML or UML) and sensory network elements (e.g., using similar tools as for the physical device systems) aids in the efficient development of new devices and the adaptation of existing devices to new application areas. Additionally, the formal platform of such an implementation is capable of integrating such libraries with models of stochastic biological components, enabling full-system modeling that can effectively aid efficient and proper design, validation, and verification of biomedical systems. The implementation of such a platform using existing systems languages like UML and SysML as presented here, takes advantage of the mature properties of these tools, where implementing extensions to other modeling domains is a well-established practice. As explained in the following section, the use of Markov Chain modeling and Hidden Markov Models is ideal for such an application, and is explored in this work as a preliminary study of the capabilities of the presented paradigm for the design and modeling of biomedical device systems.

2.3 Biological System Modeling via Markov Chains

Markov Chains and Hidden Markov Models provide a method of modeling probabilistic systems with finite states, making them ideal for the modeling of biological

systems, including numerous common biological systems relevant for biomedical devices [82]. While this method has existed for over a century, only recently has it begun to see significant use in engineering applications to understand the development of systems over time. A Markov Chain model can be easily visualized as a set of states, each with a probability of propagation to a future state. Figure 2.6 shows how a simple Markov Chain may be easily visualized.

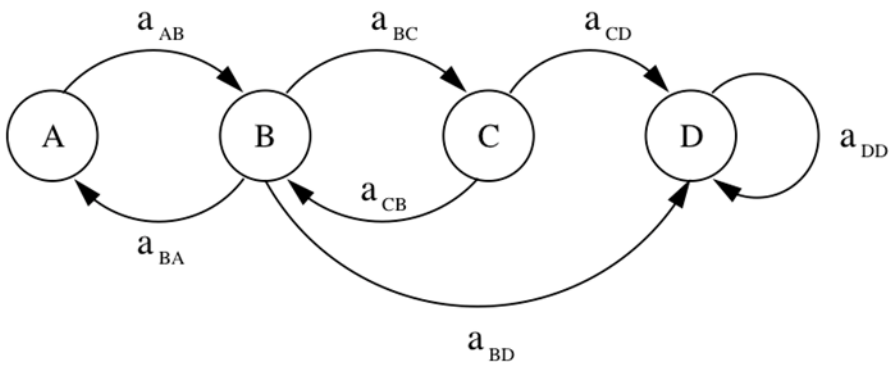

Figure 2.6: An example Markov Chain model featuring four finite system states (A-D), with an example set of propagation paths and respective probabilities (a_{XY}), where the probability is expressed as the probability of propagating from state X to state Y in a given step. For any system state, the sum of the propagation probabilities to other states must be equal to 1.0, including the odds that the system states at the same system state, such as in propagation probability a_{DD}.

Each state of the Markov Chain model represents a physical system state, with arrows showing the probability (a_{XY}) of propagation from state X to state Y in one time step. The sum of all propagation probabilities from each state must sum to 1.0, with feedback or steady-state operation between states also being possible. Additionally, segmentation and hierarchical Markov Chain models are also possible, where the probabilities of a state's propagation may be dependent upon the current state of a separate, but related, Markov Chain. For the application discussed here, this property is leveraged in order to build intrinsic hierarchies of biological system complexity, thus allowing for full system

analysis from both high and low levels. Additionally, Markov Chain models offer an easily scalable method of modeling biological systems (in lieu of traditional systems of partial differential equations) and enable the modeling of highly complex systems in a manner that is intuitive, adaptable, and quick to implement or alter in software [82].

Hidden Markov Models are an extension of the Markov Chain concept, where the Markov Chain or network of interacting Markov Chains are developed based on observed real-world performance. Behavior of a system, be it discrete in nature or a continuous spectrum, is tracked and documented, and then a Markov Model is developed to fit this system performance. This model then enables further analysis or prediction of future system functionality [82]. The emergent properties of these models makes them "hidden" to the model developer, since it is not initially clear how system states may be related or with what probabilities the system may fluctuate between states. With respect to the development of the platform presented here for the systematic design of biomedical devices, Hidden Markov Models play a valuable role by enabling researchers and developers to empirically develop biological models of systems in instances where these models do not initially exist, thus expanding a library of available (i.e., "stock") biological models.

2.4 Implemented Platform for Biomedical Device Development

By combining the modeling mechanisms available for physical engineering systems with the Markov techniques presented for biological systems, this work presents a comprehensive platform realized for the full system design of experimental biomedical devices. Borrowing from the high-level system architecture in Figures 2.4 and 2.5, this

framework platform creates a union of the biological and engineering domains that enables the simulation of a full biomedical system. Figure 2.7 showcases how such a union is achieved in this work, where the biological element is modeled as a component in the system architecture.

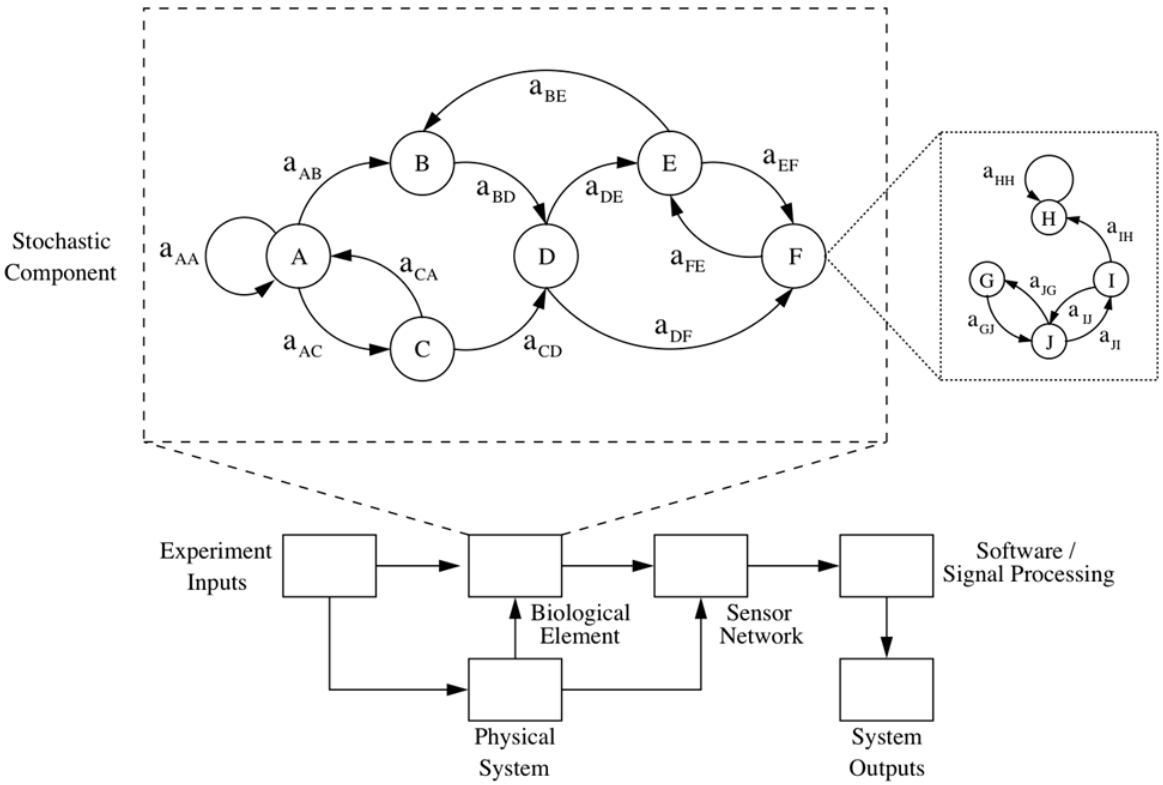

Figure 2.7: Implementation of the developed platform for the engineering of experimental biomedical device systems. The stochastic biological element is inserted into a functional model of the device system, enabling full system modeling. Hierarchical structures of Markov Chains enable varying levels of abstraction to be used when modeling the biological element of the full biomedical device system.

Modeling of the full system architecture is achieved using established systems modeling platforms, such as UML or SysML, as many of these tools have reached a level of maturity to support extensions to other languages and models. In order to utilize the

platform for overall engineering of the biomedical system, the implementation process follows a straightforward path as follows:

1. Gather relevant data of the biological system at a level of abstraction coincident with the application requirements. This data will be used to formulate a Markov model of the biological system component.
2. Formulate a Markov model describing the biological component. An iterative process is often used to achieve convergence of such a model, as well as to define the appropriate segmentation of finite states for continuous systems [82, 83].
3. Represent the validated Markov model using a tool capable of integrating with the physical system model. This biological element will exist as an extension from the modeling platform used to define the larger device system.
4. Design the proposed physical device components and how these components relate using the modeling platform named in (3) (i.e., SysML or UML). An additional component should also be represented in the system model that will extend to the biological component.
5. Perform simulation, validation, and verification of the complete system model. The results of these analyses will provide a means of redesign and device optimization for the particular experimental application.

The outputs generated from this system analysis provide a range of potential experimental outputs based on the operation of the physical system and the development of the stochastic biological system. The value of obtaining such a resultant set is

paramount to the design engineer, as it allows them to directly address real-world concerns that are not otherwise visible in the design phase. In the prototyping phase of device development and beyond, this same analysis can be used to verify proper device operation, to confirm the results of experiments, and to detect and avoid undesirable system performance. Such analyses are currently difficult and exceedingly time-consuming using established methods, giving a platform for experimental biomedical device development considerable value to the field.

Using the established platform for the design of biomedical devices, the Micro-BOAT platform is analyzed in light of both physical system and biological system considerations in order to optimize the system for the proposed application of performing *in situ* growth, monitoring, and treatment of bacterial biofilms in a microfluidic environment. As presented in the following sections, these two areas are pursued independently in order to establish the component functionality of the system, evaluate the efficacy of Markov techniques for the approximation and prediction of biological systems, and determine the readiness with which the two domains integrate for full system modeling.

Chapter 3: Design Considerations and System-Level Engineering

In the design of integrated systems involving multiple component types and interactions between various physical and biological modules, a system-level approach to the design of individual components is needed in order to ensure a properly functioning end product that supports the requirements of the application. For the biomedical Micro-BOAT device in this work, a systems engineering "platform", or design paradigm, is implemented as a flexible methodology that can be applied uniformly to any number of biomedical devices. In the design of the Micro-BOAT, subsystem components and their interactions are taken into consideration as a fundamental step in the development process. The following sections in this chapter outline such considerations and the figures of merit that support the design of each component, as well as how these factors drive not only the design of the system but also use of the system for the demonstration of the SP BE as a potential clinical method for biofilm treatment.

3.1 Design Considerations

The key focus of this work is the development of a device for the growth, monitoring, and on-chip treatment of bacterial biofilms that can be used as a tool for drug screening and development applications. To most effectively address this system functionality, a number of design factors and options for the components were considered. Overall, the areas of consideration for the system design can be placed into two separate, yet interdependent, categories: (1) methods of effectively monitoring biofilms and (2) methods of enabling on-chip biofilm growth and development. Additional consideration is also given to the use and implementation of the SP BE

enhanced biofilm treatment method tested in this work. An analysis of these alternatives resulted in the presented integrated Micro-BOAT system consisting of a microfluidic biofilm growth chamber with an optical density (OD) detection method achieved via linear array charge-coupled devices (CCD).

In determining the monitoring schema that best matches the application presented here, it was established that the preferred method would integrate well with the selected biofilm growth reactor architecture while also satisfying functionality requirements unique to the drug screening tool. In order to address the limitations of current biofilm measurement technologies, the selected sensing method should be capable of continuous, *in situ* monitoring of biofilm growth, development, and treatment with minimal external equipment. Furthermore, in unison with the requirements of the biofilm growth reactor explained subsequently, the ideal monitoring solution should be capable of parallel implementation on a single chip in order to allow for biofilm detection in multiple experiments simultaneously. The sensing mechanism should be non-invasive to the furthest extent possible in order to emulate realistic biofilm growth and treatment in a laboratory setting, while also being cost effective to implement, allowing for large-scale drug screening operations.

In combination with the requirements of the biofilm monitoring mechanism, several factors were of principal importance in regards to the reactors for bacterial biofilm growth and development. Due to the high cost of candidate drugs in low production quantities, it is preferred that the biofilm growth chamber utilize small reagent volumes in order to limit the costs associated with treatment efficacy experiments. Furthermore, the biofilm growth chamber must be biocompatible, meaning it is both non-

toxic to the bacteria and non-reactive with other chemicals that may be used in biofilm experiments, such as chemical stains, growth media, or other biocides. In order to enable realistic *in vitro* biofilm experiments that are representative of *in vivo* applications, the growth chamber must be capable of emulating conditions within the human body, including temperature (37 °C) and pH. Finally, in order to achieve high throughput testing, the developed biofilm growth reactor should be able to accommodate parallel bacterial biofilm growth and *in situ* monitoring by integrating with the chosen detection method.

The designed microsystem addresses device requirements by integrating a microfluidic growth chamber formed in the biocompatible silicone polydimethylsiloxane (PDMS) with CCD integrated circuit (IC) components for optical biofilm sensing [84, 85]. The biofilm growth chamber can be fabricated on other biocompatible materials such as gold and Pyrex^{TM} while utilizing small reagent volumes on the orders of tens of microliters [86, 87]. By placing these microfluidic chambers on a transparent substrate, optical monitoring can be used to determine real-time changes in biofilm OD using CCD components to achieve a non-invasive method of biofilm measurement [14]. Based on these factors, the integration of these two mechanisms represents a system design space that is well suited to drug screening applications featuring bacterial biofilms and a potentially broad spectrum of candidate biofilm treatments.

3.2 Measures of Effectiveness at the Micro-BOAT Device Level

The following sections analyze the various technologies and components utilized in the Micro-BOAT system in order to determine the optimal design parameters and use

of these components to satisfy the design requirements of the presented device. Measures of effectiveness are analyzed at a low level via the performance metrics and governing equations that determine the physical operation of the integrated system. Specifically, these measures of effectiveness include (1) the measurement of biofilm optical density as a means of quantifying changes of biofilm mass, (2) the suitability of implementing CCD components in the Micro-BOAT to achieve biofilm OD measurement, (3) the design of the microfluidic biofilm growth reactor as a component in the Micro-BOAT system, and (4) the implementation of the SP BE within the developed device for the testing of enhanced bioelectric biofilm treatment.

3.2.1 Optical Biofilm Density

Optical density has been shown as a viable metric of biofilm growth and development correlating to overall biofilm mass [88]. As biomass accrues, light incident upon the film is increasingly absorbed by bacterial cells and the extracellular matrix, resulting in a decrease in light intensity transmitted through the film. The Beer-Lambert Law for light absorption in a material provides a method for correlating this absorbance to overall biomass, where the concentration of bacterial cells is proportional to light intensity reduction within fixed ranges of cell size and shape [14, 89]. The governing equations for these physical properties are provided in equations (1) – (3) below, which derive the biofilm optical density measurement.

$$T = \frac{I}{I_o} = 1\,0^{-\alpha l} \qquad (1)$$

$$A = -\log_{10}(T) = -\log_{10}\left(\frac{I}{I_o}\right) = -\log_{10}(10^{-\alpha l}) \qquad (2)$$

$$A = \alpha l = Biofilm\,OD \qquad (3)$$

Here, T represents transmission percentage, α is the absorbance coefficient, l is the path length, A is absorbance in arbitrary absorption units (AU), I is light intensity, and I_o is the initial reference light intensity. While factors such as wavelength, light path type, and detection device are also relevant parameters for this measurement, these are considered in the coefficient values and quantity for the path length and are thus supported by this set of equations.

Investigations into the correlation between optical biofilm density and biofilm characteristics such as biomass, thickness, and morphology have been performed previously (Figure 3.1) [14, 88].

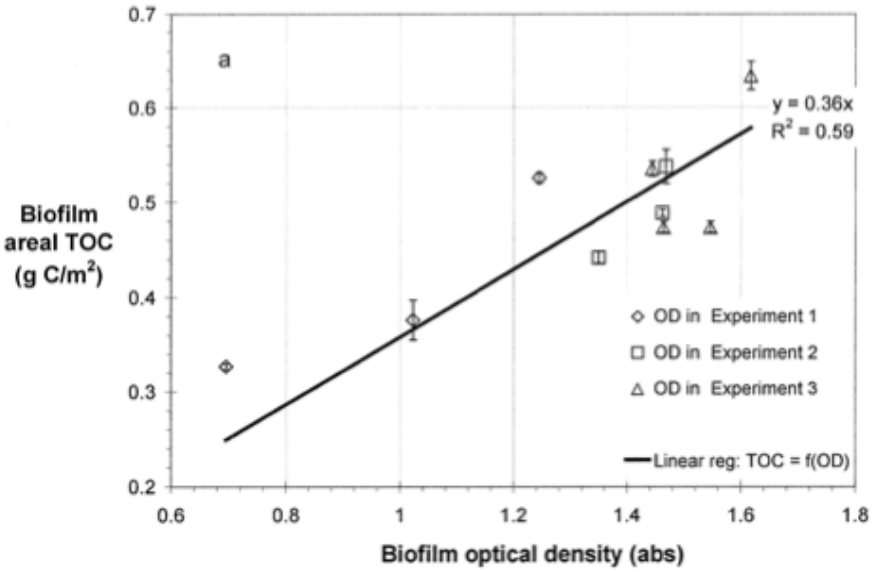

Figure 3.1: Biofilm total organic carbon (TOC) concentrations have a linear correlation to measured biofilm OD [14]. Here, the line represents the best linear fit forced through the origin (R2 = 0.59).

Bakke et al demonstrated a linear relationship between biofilm mass and optical density for thin-film bacterial colonies on the order of 35 μm. While this linear relationship holds for bacterial biomass, the optical density measurement shows only limited correlation to biofilm thickness and morphology. Thus, we can utilize the OD measurement method to quantify biofilms with respect to overall growth, while other measurement techniques may be better suited to investigating other structural characteristics. In figure 3.2, below, biofilm thickness was shown to reach a steady state after approximately 100 hours of growth, while the optical density continued to increase for >200 additional hours. This suggests that the biofilm did not achieve full maturity, signified by reaching a steady-state overall biofilm biomass, until this point in time, despite this suggestion by other measured parameters including biofilm thickness, substrate concentration, effluent TOC, and cell concentrations [14].

The ability of optical density measurement to detect and quantify the development of bacterial biofilms beyond the capabilities of these traditional metrics provides strong support for the use of OD as a biofilm growth valuation. Additionally, optical density measurement is preferential for biofilm studies for several other reasons including: (1) non-invasive biofilm detection (samples are taken without physical contact with the biofilm), (2) real-time, *in situ* measurement with minimal overhead in terms of equipment, complexity, and time required to perform measurements, (3) low internal variability, and (4) flexibility to adapt to various applications.

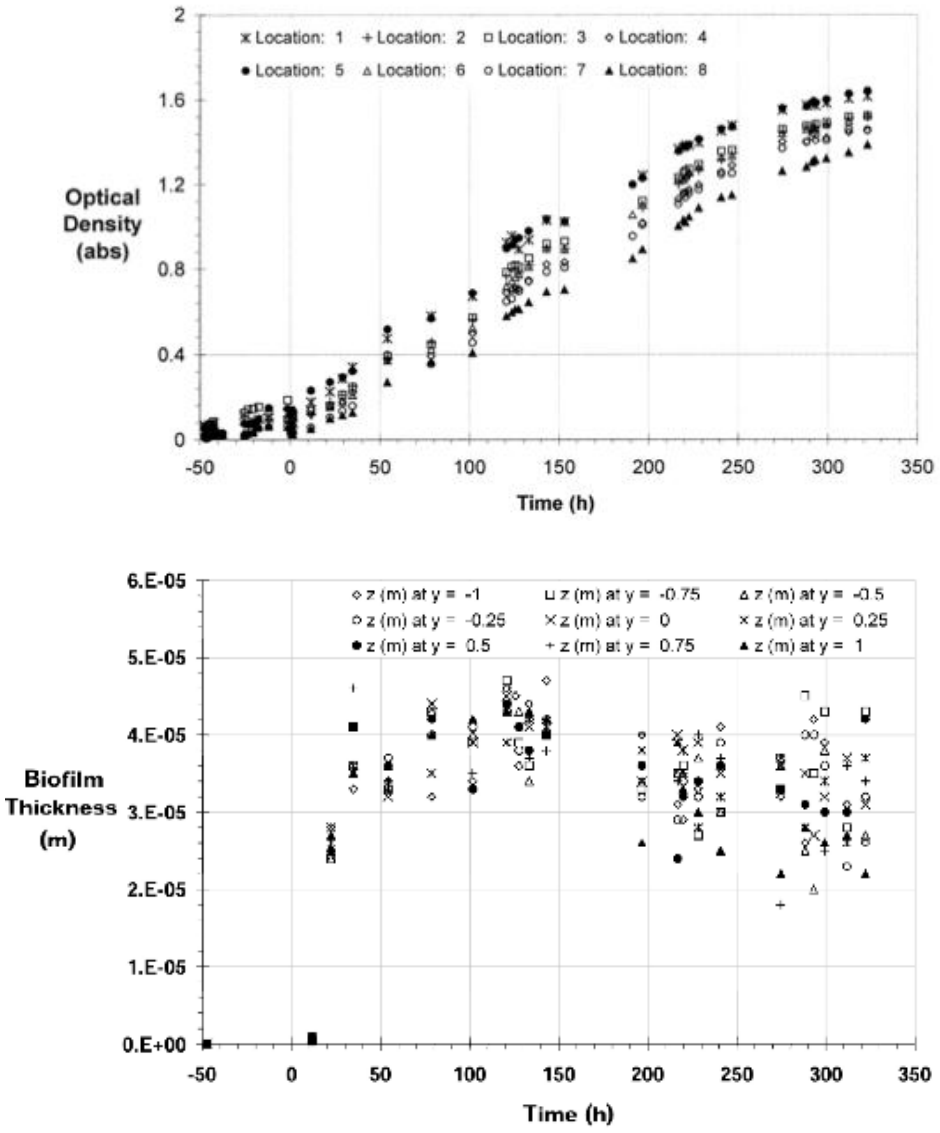

Figure 3.2: Biofilm optical density and relation to average biofilm thickness. (a) Biofilm OD increases for approximately 300 hours before reaching steady state. (b) Steady state biofilm thickness is achieved after only approximately 100 hours of growth [14].

The frequency of light used to measure optical density can be tuned to address the sensitivity of a specific sensor device or to determine absorbance of specific target molecules within materials or cells. For typical OD applications, the selection of a single light frequency to match the specified photodetector can increase measurement sensitivity, while the scanning of multiple frequencies can provide insight with respect to

low-level molecules within material or biological structures. Bacterial biofilms such as those examined in this work typically display broad-spectrum OD changes due to reflection from large components in the biofilm matrix, such as bacterial cells, and therefore do not show preferential absorption or reflection at specific wavelengths. As a result, OD measurements can be taken using many light frequencies while displaying similar biofilm absorbance, therefore motivating the chosen OD measurement frequency to be tuned to the photodetector device in order to optimize the sensitivity of the application.

For these reasons, the use of optical biofilm density measurement is a preferred method of biofilm monitoring and well suited for the prescribed use. The mechanism can be readily adapted to drug screening instruments such as that presented in this work and provides a means of non-invasive, sensitive, and highly scalable biofilm growth detection which is well suited for real-time detection applications.

3.2.2 Optical Density Monitoring via Charge-Coupled Devices

Biofilm optical density monitoring is typically achieved by transmitting light through the biofilm reactor normal to the substratum/biofilm interface (Figure 3.3). When grown on a transparent substrate and in a reactor that can transmit light with little absorption or reflection, biofilm OD is detected using a photodetector placed on the backside of the reactor opposite a light source. A baseline measurement removes background absorbance by the biofilm growth reactor material and fluid within the reactor. Increasing bacterial density on the substrate results in the attenuation of light

intensity transmitted through the device, which can then be converted to a net change in OD according to equation (2).

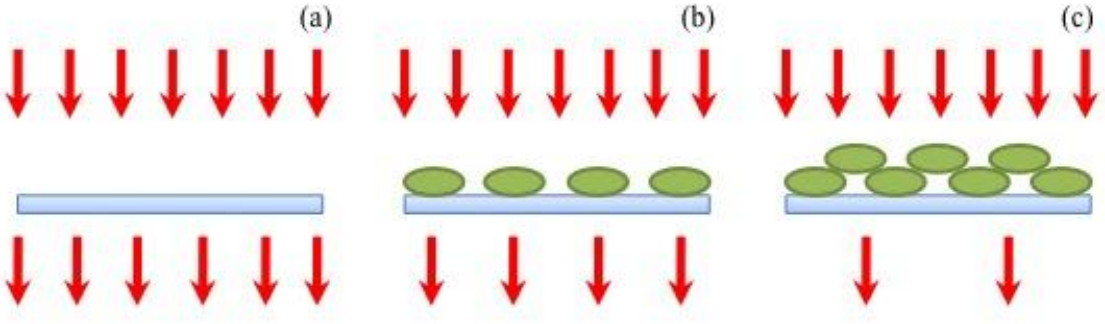

Figure 3.3: Optical density detection of biofilms in fluidic reactors. (a) A baseline measurement removes the absorbance properties of the reactor materials and fluid. (b-c) As bacterial biofilm density increases, optical density also increases according to equations (1-3).

Due to the highly stochastic nature of biofilm growth, in which bacterial density and morphology often vary drastically across a single biofilm or substrate, it is desirable to have localized measurements throughout the biofilm structure in order to determine average and spatiotemporal changes in optical density. An array of photodetectors positioned on the backside of the reactor can enable this detection. While light scattering and reflection due to the irregular biofilm surface limits the spatial resolution of such detection, knowledge of an average biofilm OD can greatly enhance the accuracy of experimental results, while an understanding of spatial biofilm distribution provides further insight into the developments of the film under applied conditions.

In order to leverage the advantages of operating at the microscale, this work implements a compact linear array charge-coupled device (CCD) to enable both average and spatiotemporal biofilm monitoring along the full length of a growth reactor. The device (Texas Advanced Optoelectronic Solutions TAOS-TSL202R) features a 128x1 linear array of photopixels integrated into a sealed IC package [90]. Each pixel measures

120 μm (H) by 70 μm (W) with 55 μm pixel-to-pixel spacing for an overall linear array length of 1.6 cm. The IC package is a standard through-hole component measuring 19 mm (L) by 11 mm (W) and was chosen due to its simplicity of operation and ease-of-implementation on a standard printed circuit board (PCB).

The principle of operation of the device is as follows: as light energy impinges upon the pixels of the CCD, photocurrent is generated which is integrated by the active circuitry located on-chip and stored in a sampling capacitor that corresponds to each pixel. The amount of charge accumulated on each pixel's capacitor is directly proportional to the light intensity and integration time according to equation (4), where V_{out} is the analog voltage output of that pixel, V_{drk} is the analog voltage for the dark condition, R_e is the device responsivity for a particular wavelength of light, E_e is the incident irradiance in $\mu W/cm^2$, and t_{int} is the integration time in seconds. The linear response of this output to irradiance is critical to enable biofilm optical density measurement with limited calibration of the device. Since V_{drk} approaches 0 V while the device responsivity and integration time are constant during operation of the system, we can directly derive the relationship between optical density and CCD pixel output voltage according to the following:

$$a \quad V_d \quad \rightarrow \quad (4)$$

(5)

$$A = -1 \log\left(\frac{V_{out}}{V_{o\_init}}\right) \quad (6)$$

Substituting equation (5) into equation (6), one finds a final representation for the overall relationship between the analog output voltages and absorbance.

$$A = -\log\left(\frac{(R_e)\,E_e()\,t_i()_n}{(R_e)\,E_{e\_i}()\,t_i()}\right) \quad (7)$$

$$A = -\log\left(\frac{E_e}{E_{e\_i}}\right) = -\log\left(\frac{I}{I_o}\right) \quad (8)$$

Thus, optical density measurements can be obtained directly using equation (6). Operation of the device is achieved using only a DC rail voltage, a timing clock and a serial-input (SI) that triggers the discharge of the pixels for signal readout.

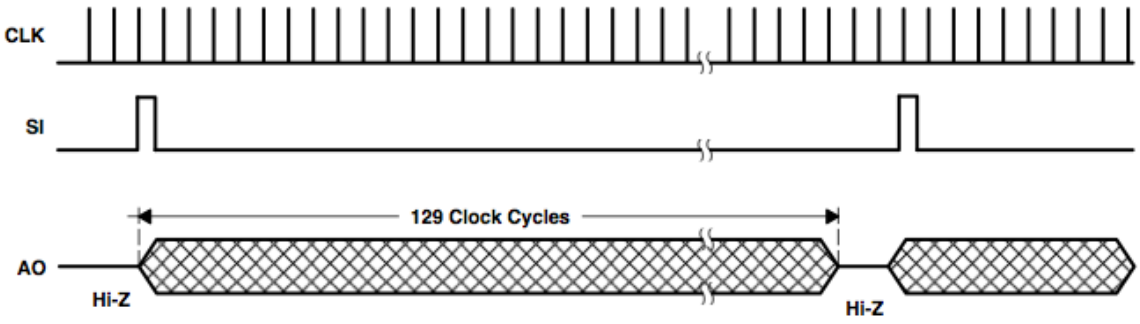

Figure 3.4: Timing diagram of the TSL202R charge-coupled device. A serial-input bit during a rising edge clock pulse (CLK) triggers data readout from the 128 pixels, with each clock pulse shifting the pixel being read. A 129th clock pulse returns the output to a high-impedance state [90].

Maximum device responsivity is achieved at a visible red wavelength of approximately 680 nm, which is the wavelength chosen for optical density measurement since biofilm absorption is broad spectrum and thus non-sensitive to the frequency selected.

The selected device is optimal for the application of drug screening due to its established performance characteristics and steady operation, with reported noise levels of 1 mVrms. Implementation of the device is readily achieved due to the on-chip

circuitry, which supports most data storage and readout functions. The small size of the device is ideal for the adaptation of drug screening processes to the microscale, since the device can integrate easily with a microfluidic or other small-scale growth reactors for biofilm optical density monitoring. Finally, the linear output response of the device makes it ideal for measuring biofilm optical density since recorded voltages can be translated directly to optical density according to equation (6) with limited calibration.

3.2.3 Microfluidic Biofilm Growth Flow Cell

A microfluidic growth reactor has been designed for this work that addresses the needs of the application to provide a chamber for the biocompatible growth, treatment, and monitoring of bacteria biofilms. In order to meet these requirements, several considerations determine the design of the microfluidic channels used in the Micro-BOAT system. The dimensions and materials used to structure the microfluidic channel must meet the needs of OD detection, while being of an adequate size to support the growth and treatment of clinically relevant biofilms. By optimizing the microfluidic component of the overall system, an end product device is achieved that is functional for drug screening and biological studies of bacterial films.

The microfluidic biofilm growth flow cell developed for this work is comprised of a 100µm deep, 2000µm wide, and 1.75cm long microfluidic channel formed in PDMS on a Pyrex^{TM} substrate. PDMS was chosen as a fabrication material due to its biocompatibility for biological experiments, transparency, ease of fabrication and replication (see Chapter 3: Device Fabrication), and low cost as a silicone polymer. A Pyrex^{TM} substate was chosen for many of these same advantages, in addition to its

relative thinness (500µm) in comparison to other viable options, such as a glass microscope slide (>0.8mm). The footprint of the microfluidic chamber was optimized to allow for visual alignment of the channel to the CCD photopixel array. Since misalignment of the pixel array and microchannel would result in unreliable device operation in which changes in biofilm OD are missed or skewed, the microfluidic channel is sized to allow for sufficient overlap of the microfluidic chamber over the linear pixel array. Doing so considerably mitigates the chances that developments in biofilm OD within the channel will proceed undetected by the CCD pixel array. Figure 3.5 below provides a top-down view of the microfluidic channel design used for the Micro-BOAT system. The tapered portions of the channel leading to the 2mm diameter inlet and outlet, used to provide a fluid flow source through the top of the PDMS slab, are not included in the dimensions of the microfluidic chamber.

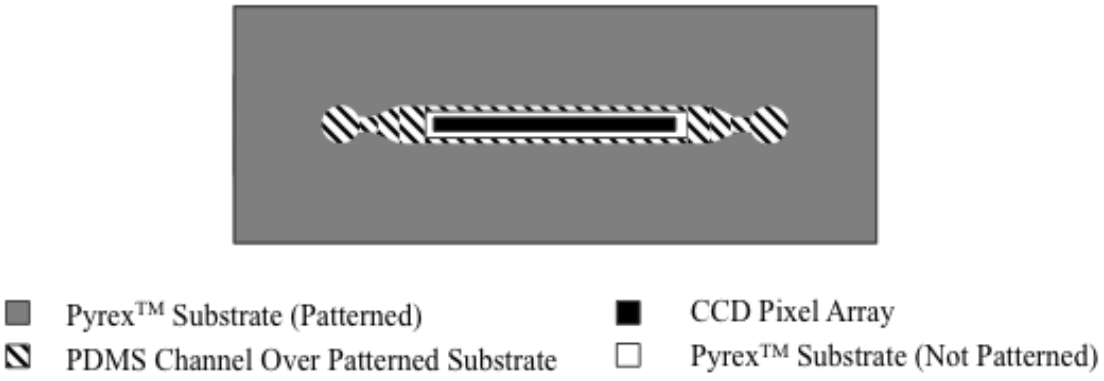

Figure 3.5: Top-down schematic of the microfluidic channel used for biofilm growth and treatment in the Micro-BOAT system, also showing the positioning of the CCD pixel array with respect to the channel. Proper alignment of the channel to the CCD device ensures effective biofilm sensing.

Total chamber volume is designed to support bacterial biofilms and is supported by previous research that utilizes microfluidic channels as biofilm growth reactors. These chambers typically range in depth from 20µm to 250µm, with total growth reactor

volumes typically ranging from several picoliters to several microliters [6, 63, 65, 87, 91, 92]. Dimensions of the channels used in the Micro-BOAT system provide a $200nm^2$ cross-sectional area and a total chamber volume of 3.5µL, placing it on par with other microfluidic growth reactors. At this scale, channel clogging due to biofouling is rarely encountered and the size of the inlets and outlets of the microfluidic devices are large enough to support commercially available fluidic interfaces such as connectors and capillaries.

Fluid flow within the microfluidic device can be characterized using standard equations for rectangular fluidic channels at small scales and low Reynolds numbers [93]. Flows at this scale can be described using the equations below in terms of their average and maximum flow velocities, flow-induced shear stress, and Reynolds number.

$$\overline{U} = \frac{Q}{W} = \frac{2}{3} U_M \qquad (9)$$

$$\tau_w = \frac{6\eta}{Wh^2} Q \qquad (10)$$

$$R_e = \frac{\rho_m \overline{U} D_H}{\eta} \qquad (11)$$

Here, $\overline{U}$ and U_{Max} represent the mean and maximum flow velocities, respectively, Q is the volumetric flow rate, W the width of the channel and h the height of the channel. τ_w represents the flow-induced shear stress in the channel, η the dynamic viscosity of the fluid, ρ_m the density of the fluid, R_e the Reynolds number of the flow, and D_H the hydraulic diameter of the channel. For typical volumetric flow rates used in biofilm growth applications (less than 100µL/h), the fluid characteristics of water at 40ºC (used as an approximation of both growth media and bacterial biofilms), and the channel

geometry used in this device system, we can characterize the microfluidic device performance using the following plots.

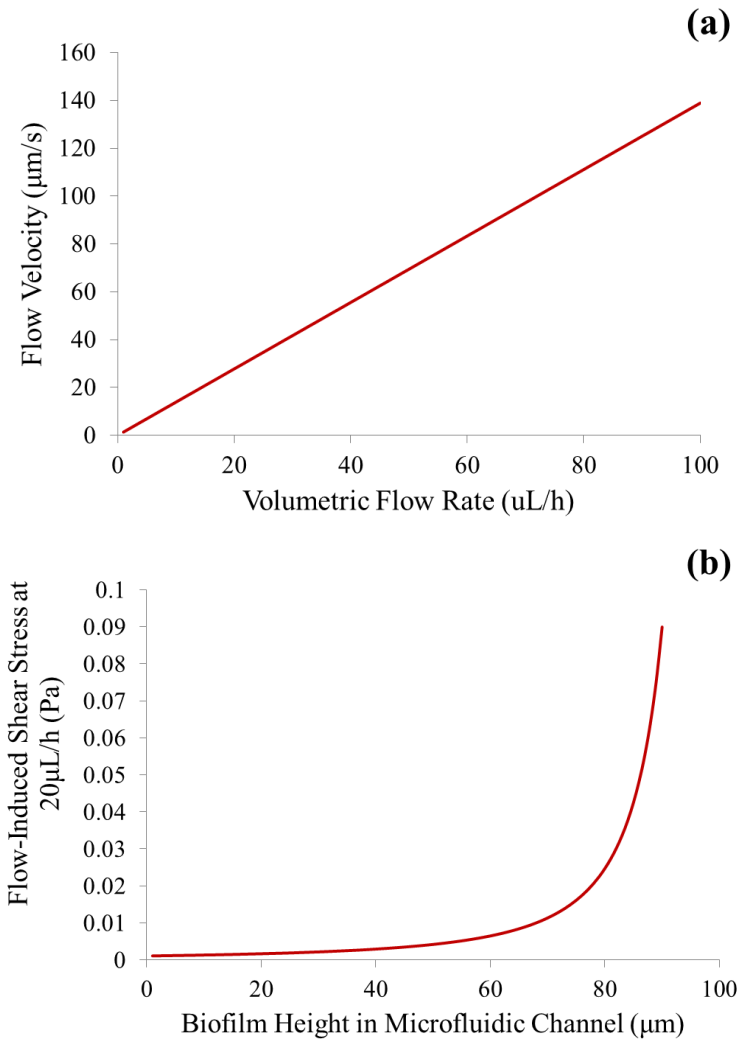

Figure 3.6: (a) Volumetric flow rate versus flow velocity for the microfluidic channel used in the developed Micro-BOAT. (b) Flow-induced shear stress increases as biofilm height increases in the 100µm tall microfluidic channel. These values are characterized at 20µL/h, the volumetric flow rate typically used for device experiments (see Chapter 5).

As seen above, the volumetric flow rate is directly proportional to the induced laminar flow velocity, allowing the rates of either to be tuned to achieve either environmentally relevant sheer velocities or to maximize new media flow to the developing biofilms. Additionally, sheer stress is found to vary inversely with h^2, which encourages the use of

such tall channels as those used here in order to achieve increased biofilm thickness at the expense of larger device sizes and increased sample volumes (see section 1.4.1 for the effects of sheer stress on biofilm development). Laminar flow is generally achieved for Reynolds numbers below R_e = 1000. For this system, the Reynolds number is on the order of 0.001 for most flow rates, making flows in this system dominated by diffusion effects rather than turbulence. This characteristic enables greater control over the conditions of experiments within the microfluidic chamber.

3.2.4 Bioelectric Effect for Biofilm Treatment

While much of this work focuses upon the development of a microsystem for drug screening applications, it is in many ways the use of this tool to conduct novel biofilm treatment studies that can express the full impact of this research. Recent work in our research group has validated an enhanced bioelectric effect for bacterial biofilm treatment at the macroscale [94]. In order to demonstrate use of the integrated biofilm growth and treatment system presented here, experimental work in this research area aims to establish the effectiveness of this novel treatment in microscale applications. The successful validation of this treatment has far-reaching consequences by providing a new and promising method of enhanced treatment of bacterial biofilms that do not involve the use of new or increased quantities of antibiotics.

In this work, the efficacy of the superpositioned bioelectric effect described in section 1.4.3 is tested in a microscale system by integrating electrodes with the microfluidic channels in order to provide the electric fields necessary for bioelectric treatment. Gold electrodes are fabricated upon the Pyrex^{TM} substrate of the microfluidic

channels in order to provide two functions simultaneously: (1) generate electric fields needed for the SP BE and (2) limit peripheral light from entering the charge-coupled device pixels, thereby limiting noise in the system. The pattern used for these electrodes is shown in figure 3.7 and the fabrication process is presented in the next chapter.

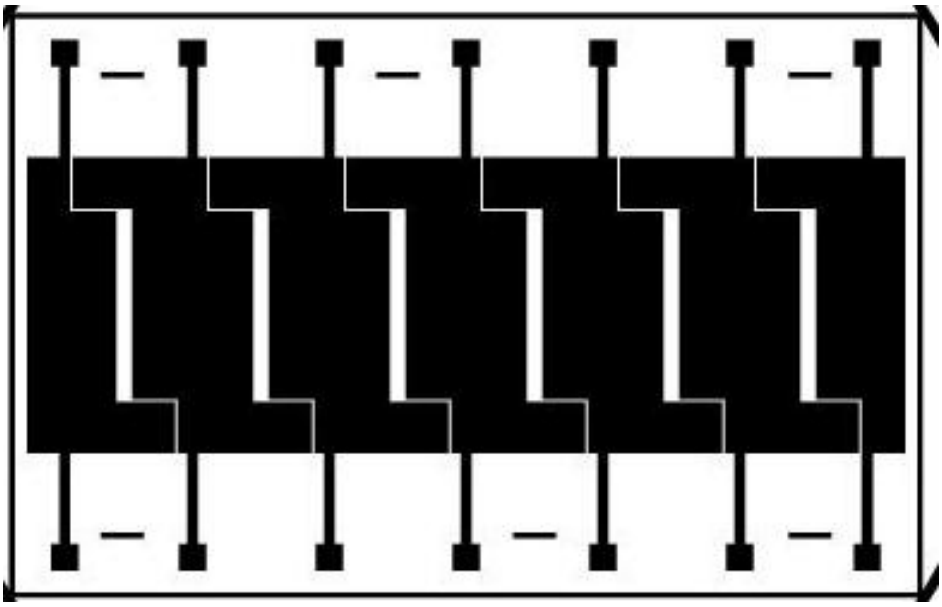

Figure 3.7: Pattern of the microfabricated gold electrodes used in the Micro-BOAT. The electrodes generate an electric field perpendicular to the direction of flow in the microfluidic channels and the rectangular spacing between the electrodes enables the limiting of peripheral light from polluting the changes in light transmission to the CCD devices due to changes in biofilm optical density.

Intensity of the electric field used in this work was characterized to operate within biocompatible limits while simultaneously avoiding hydrolysis of the aqueous media that occurs above a threshold voltage potential [95]. The frequency of the AC component of the SP electric field was selected based on previous literature in order to demonstrate maximum efficacy of biofilm treatment [45]. Based upon these factors and previous work in the MEMS Sensors and Actuators Lab, the SP electric field is composed of a 1.25V/cm sinusoidal signal at 10MHz with a 1.25V/cm DC offset. For an electrode spacing of 2mm, as we have in this system, this equates to an applied AC peak-peak

voltage and DC offset of 0.25V for both parameters. This electric field effectively avoids the hydrolysis potential of the system which is found to occur at 2.0V/cm or 0.8V applied. For this structure geometry, in which electrodes are evenly spaced along the full length of the microfluidic channel, the generated electric field is perpendicularly in-plane to the direction of fluid flow in the channel, with the resultant electrophoretic force being orthogonally out-of-plane with respect to the flow direction. As a result, based upon the theory presented previously for the effective mechanism of the bioelectric effect, the AC field will increase permeability of the bacterial cells, with those cells affected the most being towards the bottom of the microfluidic channel and directly between the two electrodes. The resultant electrophoresis provided by the presence of the DC electric field will apply a force upon antibiotic particles, driving them into the more permeable biofilm and increasing efficacy of the applied antibiotics. Results presenting experimental demonstration of the SP BE at the microscale are included in Chapter 4.

3.3 System-Level Design using Model-Based Systems Engineering

The opening sections of this chapter have introduced the different design considerations and relevant technologies required for the development of the Micro-BOAT system, utilized in this thesis as an example implementation of the systems engineering principles presented in Chapter 2 for the development of experimental biomedical systems. In this section, the methodologies used to integrate these components is presented and the verification of particular system components is shown at a high level in order to demonstrate the integral use of systems engineering principles within the design phase of biomedical device development, specifically with respect to

the presented Micro-BOAT system, utilized in this work as an application of the proposed system.

While high-level modeling was integral in the development of the Micro-BOAT system for component integration and the implementation of the on-chip superpositioned bioelectric treatment effect, additional lower-level simulations were required in order to design and validate individual system components such as the design of microfluidic channels, electrode design, optical electrical component circuitry, and PCB design. The images shown in Figure 3.8 demonstrate the modeling efforts that have led to the development of the physical modules of the Micro-BOAT system.

Ray tracing analysis in the ASAP modeling paradigm (Fig. 3.8a) validated design of the optical components of the system, including the need for masking of the microfluidic channels and the corresponding CCD components in order to avoid signal noise and increase sensitivity. A three-dimensional representation of the optical density monitoring system is created using the ASAP computer aided design (CAD) tool, and system parameters tuned to optimize system performance. Simulation of microfluidic channel geometries using finite element modeling in COMSOL (Fig. 3.8b) was utilized to confirm flow characteristics within the microchannels and to avoid areas of high flow stress that would incur a greater risk of device leakage during operation. Such simulations confirmed the theoretical calculations provided in Section 3.2.3 while also allowing for increased device reliability, by decreasing high-shear areas, and visualization of possible challenges of the interface between the microfluidic channel and the larger external flow tubing. Simulations of the electric fields generated within the microfluidic channel for the SP BE confirmed treatment biocompatibility as well as

electric field intensity in vital channel regions (Fig. 3.8c). Finally, circuit design and layout performed in the Cadence and EAGLE paradigms (Fig. 3.8d) confirmed CCD functionality and ensured proper PCB design for the integrated device system. Such circuits are based upon the wiring configurations of the CCD components when utilized in parallel (see Appendix A) and were performed to confirm power requirements of the system and investigate device cross talk.

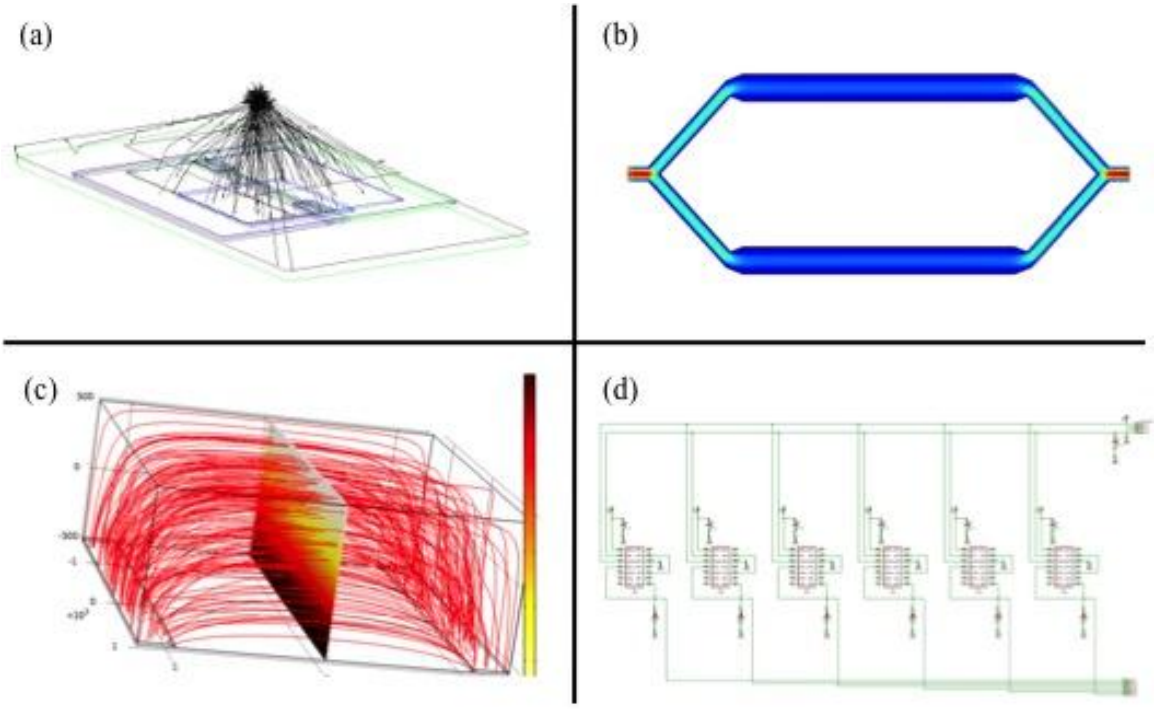

Figure 3.8: Various modeling performed in the design and development of the microsystem constructed for this research. (a) Optical detection modeling using the ASAP software paradigm (Breault Research Organization). (b) Fluidics modeling of a parallel two-chamber microfluidic system designed as an alternative to the utilized fluidics of the current Micro-BOAT architecture that may be implemented in future work (COMSOL Multiphysics, COMSOL Group). (c) Simulation of the electric fields utilized in the on-chip demonstration of the SP BE (COMSOL Multiphysics, COMSOL Group). (d) Simulation of the PCB design for six parallel charge-coupled devices (EAGLE Light Edition, CadSoft Computer USA and Cadence PSpice, Cadence Design Systems, Inc.).

Based on the analyses provided in Section 3.2 and the system-level approach provided by the modeling platform presented here in Section 3.3, a mapping of Micro-BOAT device components and subsystems to system functionality can be provided. Table 1, below, outlines such relationships, with the details of newly introduced components described in further detail in Chapter 4.

Table 1: Micro-BOAT component mapping to the system-level modeling platform for experimental biomedical and biological systems.

Micro-BOAT Device Component	**MBSE Platform Element**	**Component Simulation (Software Used)**	**Related/Affected Micro-BOAT Components**
Microfluidic Growth Chambers	Physical Experimental Device System	Microfluidic Channels (COMSOL)	• Gold Electrodes • Fluidic Tubing and Syringe Pump • CCD Photodetectors (via biofilm growth)
Gold Electrodes	Physical Experimental Device System	Electromagnetic Field Simulation (COMSOL)	• Microfluidic Growth Chambers • PCB
PCB	Physical Experimental Device System	Circuit Simulation (EAGLE, PSpice)	• Gold Electrodes • CCD Photodetectors • Data Acquistion System/Card (wire-to-board connections only)
Fluidic Tubing and Syringe Pump	Physical Experimental Device System	None	• Microfluidic Growth Chambers
CCD Photodetectors	Sensing Network	Optical Ray Tracing Modeling (ASAP)	• Data Acquisition System/Card • Microfluidic Growth Chambers (via biofilm growth)
LED Light Source	Sensing Network	Optical Ray Tracing Modeling (ASAP)	• CCD Photodetectors
Data Acquisition System/Card	Data Processor	None	• CCD Photodetectors • PCB • LabVIEW Data Readout Software
LabVIEW Data Readout Software	Data Processor	None	• Data Acquisition System/Card
Biofilm Simulation and Prediction Tool	Biological Component Simulation	Not Realized	Not Realized

The relationships presented via the "Related/Affected Micro-BOAT Components" column intends to show the interrelationships between various subsystems in the device system, and follows from figures 2.4 and 2.5.

The parallels of Micro-BOAT components to the overall biological/biomedical tool's architecture is shown further in Figure 3.9 below, which displays prototype versions of the Micro-BOAT subsystems as they were initially tested.

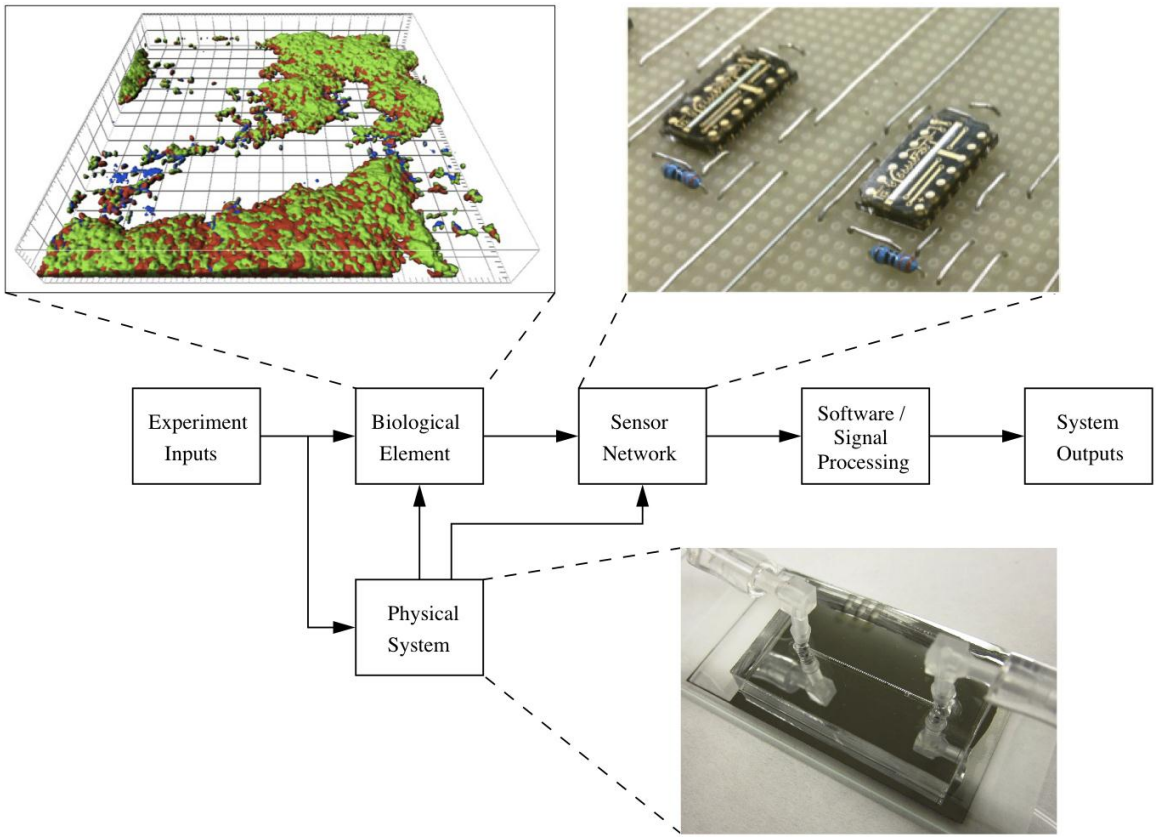

Figure 3.9: High-level visual representation of the mapping between modeling platform elements and the physical Micro-BOAT subsystems. Images are representative and do not show the physical structure of the Micro-BOAT or biofilms formed within the Micro-BOAT, but rather are prototype-stage devices testing individual subsystem operation [15].

This image represents general biomedical systems at an even higher level of abstraction than that presented in figures 2.3 and 2.5, by reducing such systems to a network of four interacting components: (1) a biological element (biofilm), (2) a sensor network (CCD components), (3) a physical system (microfluidic system), and (4) software/signal processing (data acquisition system/card and LabVIEW processing software).

Using this mapping, a full device design is achieved that is capable of satisfying performance requirements. Continued in the Testing and Results section of this thesis, a similar analysis is performed based on biological model utilized to represent development of a probabilistic, high-level bacterial biofilm within the microfluidic channels of the Micro-BOAT system. The discussion of this biological model differs from the current section, as this work is purely experimental and, while enabling for the future development of systems such as the Micro-BOAT platform presented here, did not directly drive the operating conditions and performance of the overall system. Rather, the Micro-BOAT device, as implemented, utilized the platform methodology developed, while limiting its use of biological models to mathematical models estimated independently of the system architecture, with the results of these simulations being considered by the system via an additional requirement set. Thus, the principles of the developed platform for the engineering of experimental biomedical devices remains a driving force in this effort, with the utilized mathematical model providing additional requirements in the Micro-BOAT design, while an empirically developed Markov Model is developed external of this analysis. Future work in this application area, as described subsequently in this thesis, will target the continued development of the Markov Model

and the integration of the model with a functional model of device structure and performance.

Collectively, the work presented in this chapter provides the background and support for full-system design of the Micro-BOAT system as well as the use of this system for biological and drug discovery applications such as the testing of the novel SP BE for bacterial biofilm treatment. The following chapter provides the full system design for the device as well as the fabrication and assembly process of the developed Micro-BOAT system. Subsequently, Chapter 5 presents the developed model of the biological bacterial biofilm system, as well as testing, characterization, and use of the developed Micro-BOAT system for a specific drug screening application, thereby presenting a potential method of future bacterial infection treatment in addition to a working example of the implemented systems engineering concepts.

Chapter 4: Micro-BOAT Design and Fabrication

4.1 Introduction

The following discusses the full-system design of the Micro-BOAT device that forms the crux of this research, as well as the fabrication and assembly processes required to achieve system functionality. Figure 4.1 reiterates the full system design developed in this work, which was first presented at the conclusion of Chapter 1.

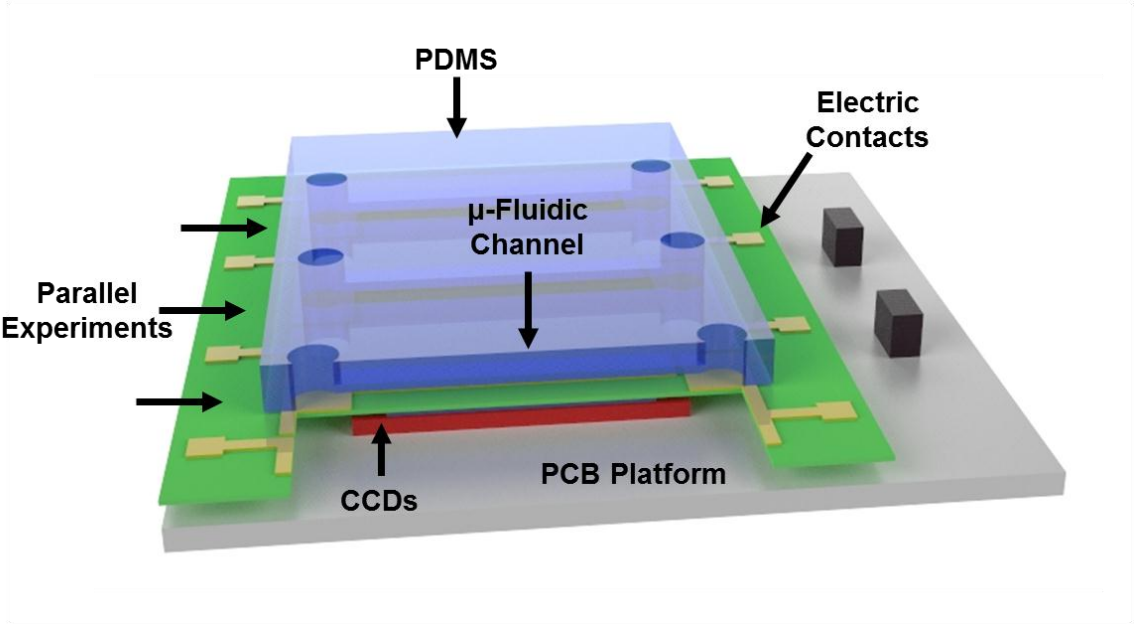

Figure 4.1: Full-system schematic of the integrated microsystem. The device is based on a PCB platform supporting system electronics, external connectors, and the charge-coupled devices used to detect changes in biofilm optical density. Microfluidic channels formed in PDMS enable six parallel experiments on a single chip. Patterned gold electrical contacts enable application of the SP BE.

The previous chapter of this thesis presented the systems-level analysis that contributed to the design of the Micro-BOAT system, achieved through the use of a modeling platform specifically tailored to experimental biomedical devices such as the Micro-BOAT. In the coming sections, each component and/or module of the system is discussed with regards to its final design and fabrication in order to enable future

optimization and use of the device for drug screening and biological study applications. This information provides a basis for the characterization and experimental demonstration of the microsystem in Chapter 5, in which the biofilm growth and treatment system is used to evaluate the effectiveness of the superpositioned effect biofilm treatment with respect to traditional biofilm treatments using exclusively liquid antibiotics.

4.2 Device Design

Here we present the full design and specifications of the Micro-BOAT system, beginning with the lowest level substrate, the PCB module and moving towards the top-most layer of the device, which is comprised of the PDMS-based fluidic component. Assembly of the system is discussed in the final section of this chapter, thus enabling full realization of the device.

4.2.1 Printed Circuit Board and Electrical Components

The PCB developed for the Micro-BOAT is designed to integrate easily with microfluidic devices fabricated out of PDMS on a 100mm diameter wafer mold. To meet this requirement while remaining small enough to fit inside of the small incubator for experiments, the final PCB pictured in Figure 4.2 is a 9.5 cm × 8.1 cm epoxy resin PCB (Advanced Circuits). The PCB features six evenly spaced charge-coupled devices (CCD, TSL202R, Texas Advanced Optoelectronic Solutions) integrated in parallel to enable biofilm detection in six channels simultaneously and in real-time. The PCB also features wiring and surface-mount electrical components to support operation of the CCD

components. 330Ω pull down resistors (0805 SMD, Panasonic Corporation) and 0.1μF capacitors (0805 SMD, TDK USA) are integrated and all external connections are achieved via on-chip MOLEX connectors (538-22-23-2061 and 538-22-23-2041, Molex, Inc), shown in black in Figure 4.1.

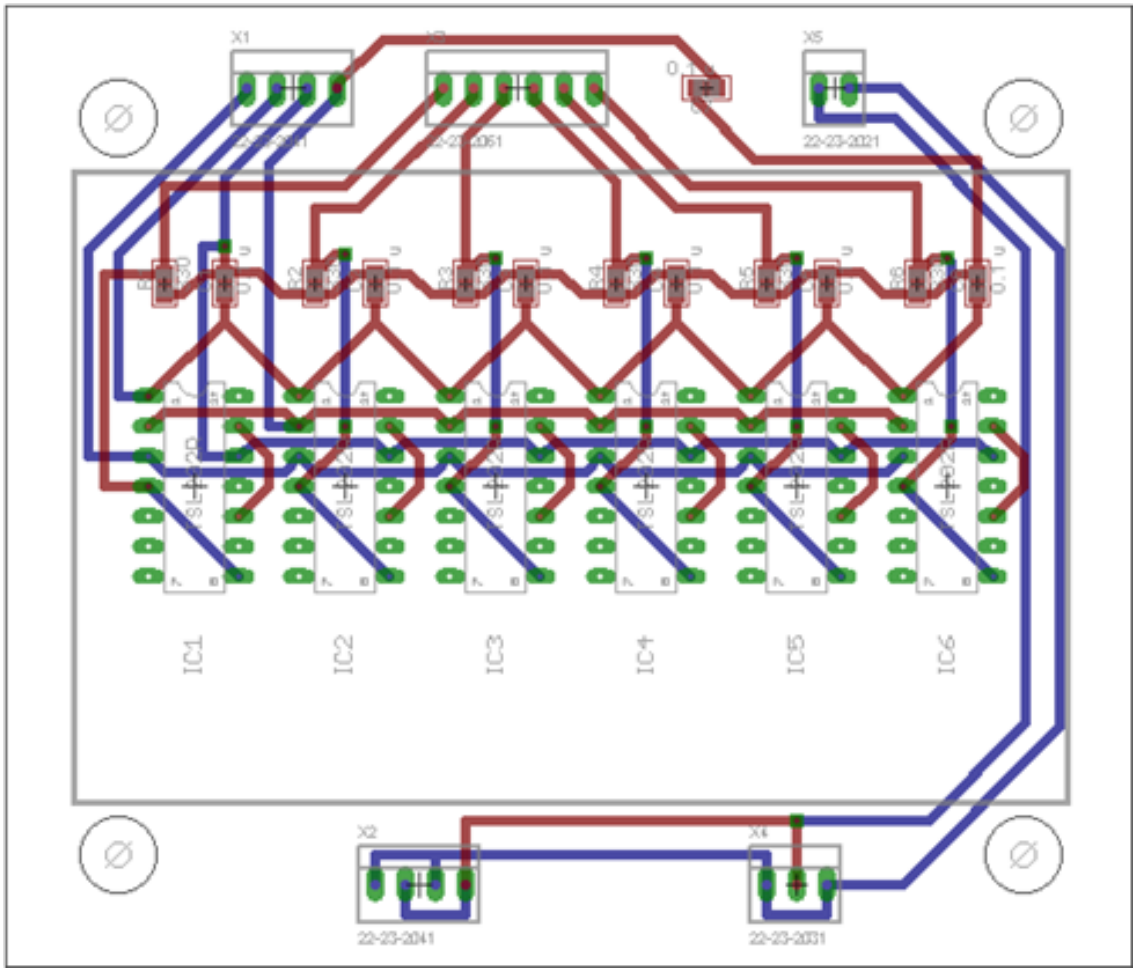

Figure 4.2: PCB Design showing the integration of six CCD components (IC1 - IC6) in parallel to enable six simultaneous biofilm experiments. The inset rectangle (shown in gray) defines the area covered by the electrode and microfluidic modules of the system, introduced in the next sections. Red and blue lines define the wiring pattern of the PCB, with red lines showing top-surface wiring and blue lines showing bottom-surface wiring patterns. Molex connectors (X1 - X6) allow connections to off-chip power and signal sources. Surface-mount resistors (R1 – R6) and capacitors (C1 – C7) are required for operation of the CCD components.

Four mounting holes on the PCB allow for suspended attachment of the fully assembled Micro-BOAT in the incubator (I5110, Labnet International, Inc) using ¼-inch bolts to avoid electrical shorts and enable easier fluid sample integration on-chip.

4.2.2 On-Chip Electrodes

Electrodes for the application of electric fields relevant to the superpositioned bioelectric effect are fabricated upon the top surface of the Pyrex™ substrate, allowing the electrodes to have direct contact with the fluids within the microfluidic channels. In so doing, the insulating electrical properties of the Pyrex™ and the rubber-like PDMS can be avoided, thus allowing for precise calculation of the electric field intensity used in the bioelectric treatment.

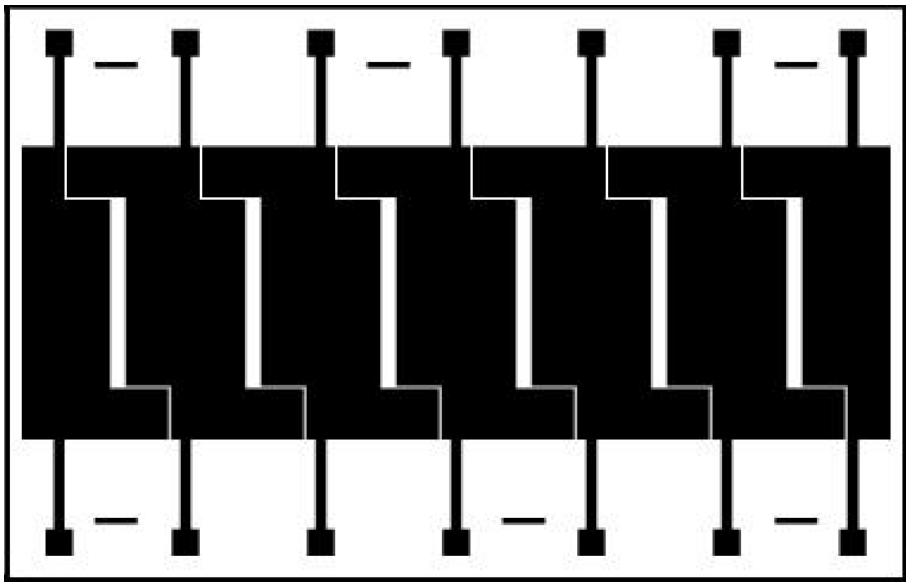

Figure 4.3: Electrode design fabricated upon the PyrexTM substrate for the application of the SP BE. Electrodes are configured to provide an electric field to the six parallel microfluidic channels of the system while simultaneously limiting peripheral light from entering the CCD components via a "window" pattern. Additional dashed horizontal lines at the top and bottom of the PyrexTM chip are patterned in gold and provide guidelines for the alignment of the microfluidic PDMS slab. Mask design is conducted using the software package L-Edit.

Seven electrodes form six individual electric field chambers and are fabricated on the substrate (see section 3.3.3) with 2.0 mm gap spacing. Spaces between electrodes in the narrowest areas measure 0.25 mm in order to create a "window" pattern that limits peripheral light from entering the CCD components during biofilm OD measurement. Contact pads corresponding to each electrode are symmetrically patterned on each side of the substrate and measure 2.5 mm × 2.5 mm square.

For the application of electric fields, electrode polarity is alternated from left to right between positive and negative (i.e., the left most electrode is positive, the one to its right negative, the next positive, and so on). Edge effects at the ends of the active area of the electrode pattern are not substantial and therefore are neglected in analysis of the system. Alignment marks for the bonding of the microfluidic PDMS slab are comprised of three patterned horizontal lines on the top and bottom of the substrate. Fabrication of these electrode structures is presented in section 4.3.2.

4.2.3 Microfluidic Module

The microfluidics module developed for the Micro-BOAT system is constructed of PDMS on a Pyrex™ substrate. Six parallel channels are integrated on a single Pyrex™ chip measuring 84 mm × 54 mm to accommodate the channels while maintaining reasonable surface area for adhesion of PDMS to the substrate. The individual channels are spaced 13 mm center-to-center, with each active chamber area measuring 100 μm deep, 2000 μm wide, and 2 cm long. The tapered portions of the chamber leading to the inlet and outlet measure 2.6 mm long and are 1000 μm wide at their narrowest. Inlets and outlet holes in the channels measure 2 mm in diameter and

create openings through the top of the PDMS slab. Overall the channels, including inlets and outlets, measure 2.9cm in length.

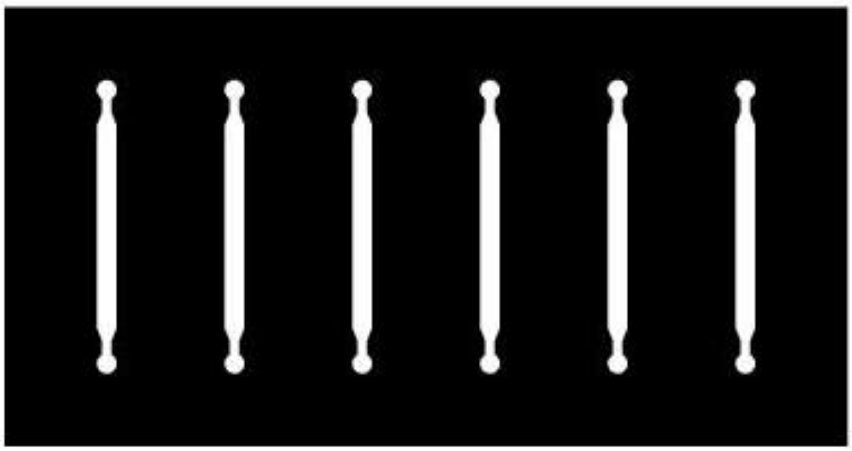

Figure 4.4: Microfluidic channel design for the Micro-BOAT system. Six parallel channels, shown in white, are integrated on a single slab of PDMS mounted on a PyrexTM substrate. Mask design for the microfluidic channels is conducted using L-Edit (L-Edit v11.0, Tanner Research, Inc).

Connections to the microfluidic channels are achieved via barbed connectors (Cole Parmer no 06365-15) and Tygon tubing (Cole Parmer no 95609-14) that link the microfluidic chambers to microcentrifuge fluid reservoirs and an external syringe pump (Cole Parmer 74900) operating in withdrawal mode to minimize device leakage. The fabrication and assembly processes relevant to the microfluidics module of the Micro-BOAT system are presented subsequently in section 4.3.3.

4.3 Device Fabrication

Since the Micro-BOAT is an integrated microsystem composed of multiple modules, the following section discusses the unique fabrication of each system component separately before providing the methods used to assemble the full device.

Discussion of system activation and operation as well as testing apparatus is discussed in the following chapter.

4.3.1 Printed Circuit Board and Electrical Component Assembly

The PCB used in this work is designed using PCB-specific software (EAGLE Light) and subsequently commercially manufactured (Advanced Circuits) to limit manual fabrication. Device assembly is required via soldering using standard tin/lead (60/40 ratio) multicore solder wire. Figure 4.5 provides an example of a fully-assembled PCB module.

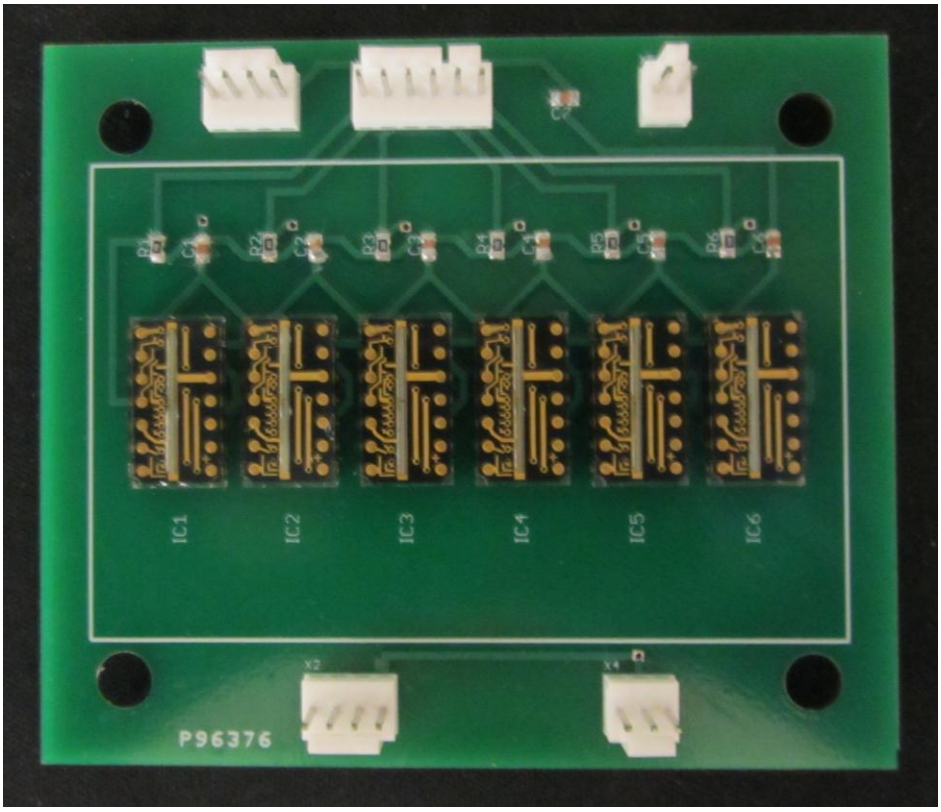

Figure 4.5: A fully assembled PCB featuring six CCD components in parallel to enable six parallel experiments on a single chip. Connector pins are visible in the white Molex connector housings.

4.3.2 On-Chip Electrode Fabrication

Electrodes are patterned on-chip for the generation of electric fields used in the superpositioned bioelectric treatment effect. The structures are microfabricated using a liftoff process on the Pyrex™ substrate. AZ-5214 negative photoresist (Clariant) in a 1.6 μm thickness profile is patterned using the transparency mask pattern presented in figure 3.2 using the process parameters provided in Table 2. For this process, hexamethyldisilazane (HMDS) is not required prior to the photoresist spin as it proved to sufficiently adhere to the surface of the Pyrex™ wafer without this step.

Table 2: AZ-5214 Process for On-Chip Electrode Liftoff

Step	1.6 μm thickness profile
Hexamethyldisilazane (HMDS)	None
Spin Cycle	Rate: 3000 rpm, Ramp: 500 rpm/s, Time: 30 s
Soft Bake	60 s at 100 ºC
Exposure	60 mJ/cm^2 for 405 nm UV exposure
Post-Exposure Bake	45 s at 125 ºC
Flood Exposure	2400 mJ/cm^2 for 405 nm UV exposure
Development	2 min in AZ400K (1:6 dilution in DI water)

For this application, in which the photoresist is developed on a transparent substrate, characterization and tuning of exposure parameters was required in order to obtain sufficient resolution of the photoresist pattern. Following the lithography step, full-wafer evaporation of gold is performed in a 200 nm thickness prior to the final liftoff step. Evaporation of chrome/gold (Cr/Au) is performed using a Metra thermal evaporator and the parameters prescribed in Table 3.

Table 3: Chrome/Gold Deposition by Evaporation Process

Film Thickness	15 nm / 200 nm (Cr / Au)
Chamber Pressure	2_{X10}^{-6} Torr
Filament Current	125 A
Chamber Temperature	> Evaporation points for Cr, Au

To complete the electrode structures on the Pyrex™ wafer, liftoff is performed using acetone as a photoresist stripper for approximately 5 minutes under agitation by ultrasonication. Rinsing using DI water full prepares the patterned base for bonding to the microfluidic structures in PDMS. The fully fabricated electrode devices are presented in figure 4.6.

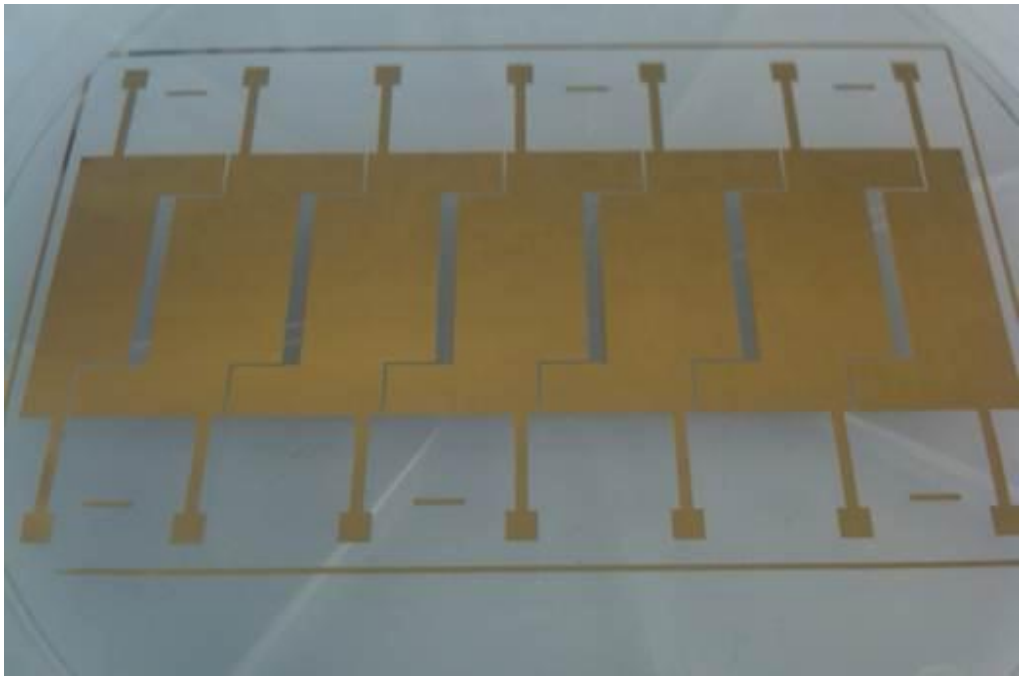

Figure 4.6: Photograph of fully fabricated gold electrode structures constructed on a PyrexTM substrate. Bonding of the PDMS microfluidic channels is performed on the patterned side of the substrate to enable application of the electric fields for the SP BE within the channels for biofilm treatment experiments.

4.3.3 Microfluidic Module Fabrication

As discussed previously in this chapter, the microfluidic module consists of microfluidic channels molded in PDMS bonded to a Pyrex™ substrate. These two elements are fabricated separately and bonded as a last step in order to create functional microfluidics. Here, we discuss the processes relevant to the fabrication of these channels and the steps required to achieve bonding and functional use of the microfluidic devices. Specific procedures for the fabrication of the electrode-patterned Pyrex™ substrate are included in the next section.

A full fabrication process flow for the microfluidics and electrode modules is presented in Figure 4.7, with the fabrication process for the electrode patterns (Fig 4.7d – 4.7e) following that outlined in Section 4.3.2.

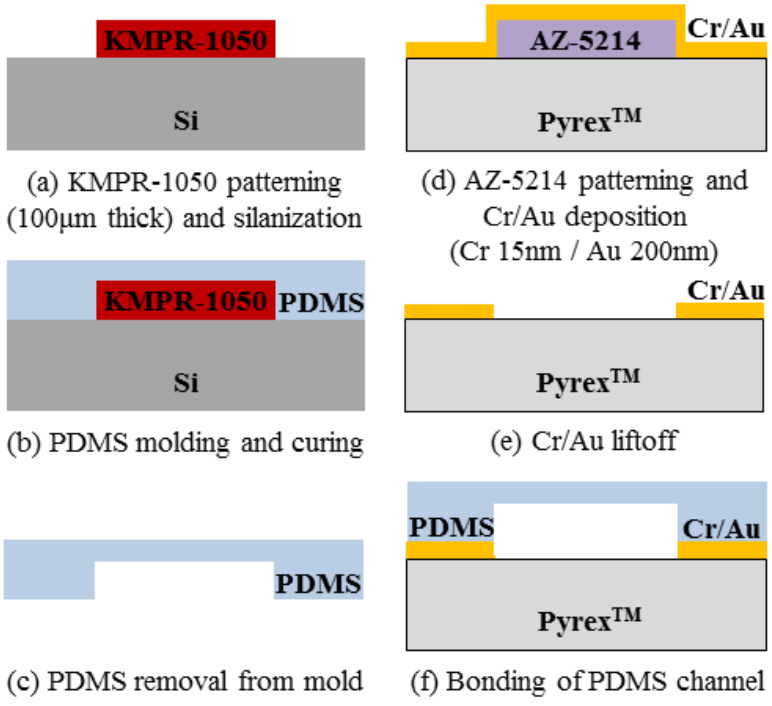

Figure 4.7: Fabrication process for the microfluidic module of the Micro-BOAT system. Here, the procedure relevant to the fabrication of the microfluidic mold (a-b), PDMS molding (c), electrode fabrication (d-e) and microfluidic channel bonding (f) are presented in sequence.

The PDMS-based microfluidic channels are formed from a reusable negative mold that is constructed of KMPR-1050 (MicroChem Corp, USA) negative photoresist on a test grade, 100mm diameter single-side polished (SSP) silicon wafer. KMPR-1050 is patterned using the process parameters specified in Table 4, with contact photolithography being performed using a transparency mask (5080dpi positive film, emulsion down, PageWorks, USA) mounted on a glass plate.

Table 4: KMPR-1050 Microfluidic Mold Preparation Procedure

Step	100 µm thickness profile
Wafer Dehydration	10 min at 100ºC
Spread Cycle	Rate: 500 rpm, Ramp: 100 rpm/s, Time: 10 s
Spin Cycle	Rate: 1100 rpm, Ramp: 300 rpm/s, Time: 30 s
Soft Bake	25 min at 95 ºC
Exposure	1600 mJ/cm^2 for 365 nm UV exposure
Post-Exposure Bake	6 min at 95ºC
Development	6 min in SU-8 developer

Using this process, a 100 µm thickness profile is achieved corresponding to the depth of the microfluidic channels. Wafer dehydration and baking processes are conducted using a DATAPLATE® hot plate (PMC Industries, USA), with photoresist spins conducted on a P-6708 unit and exposure performed using a Quintel Q4000 Contact Aligner. A contact profilometer (6M Surface Profiler, Veeco Dektak) is used to confirm channel geometry, which shows low variability (<10%) across the wafer mold, with most channels ranging from 95 µm to 105 µm in depth. For this process, a post-development hard bake step was not required to generate permanent mold structures and the addition of such a step did not show any advantages in mold longevity.

Prior to using the mold for the fabrication of microfluidic devices, silanization of the master must be performed in order to avoid adhesion of PDMS to the mold structures [96]. While it is often suggested that this process be utilized for the first 4-5 iterations of PDMS molding, verification of this technique has shown that as little as one silanization process is sufficient to prevent adhesion of the PDMS to the photoresist/silicon mold during curing. Silanization is performed by suspending the wafer mold for one hour in a vacuum desiccator in the presence of approximately 4 mL of trimethylchlorosilane (Silane M3, Gelest, Inc) in a micro weigh boat. Chamber pressure is reduced to 685 mmHg to enable evaporation of the silane solution and coating of the mold. Upon completion of this step, the wafer master is sufficiently protected for the molding of PDMS channels without the risk of fatal adhesion of the two.

Microchannels are fabricated using PDMS (Sylgard 184, Dow Corning) in a 10:1 ratio that is mixed to a 35 g volume and degassed in order to remove all imbedded bubbles. The silicone mixture is poured over the wafer mold and cured in a furnace (BF51732BC, Thermo Scientific, Lindberg/Blue M) for 20 minutes at 80 ºC. After cooling, the PDMS is peeled from the mold and manually diced to size. Ports for integrating the PDMS-based microfluidics with Tygon tubing are drilled through the top surface of the PDMS using a 2 mm-diameter dermatological punch (#BP20, HealthLink).

The PDMS microchannels are reversibly bonded to the patterned side of the Pyrex^{TM} substrate by applying methanol to the PDMS layer, then aligning and placing it onto the substrate until full evaporation of the methanol has occurred, thereby ensuring a waterproof seal between the two surfaces. Here, reversible bonding is preferred over permanent methods such as oxygen plasma bonding to allow for disassembly, cleaning,

and reuse of the patterned Pyrex^{TM} substrate for multiple biofilm growth experiments [97]. Additionally, since the methanol bonding method is a reversible process, any misalignment in initial bonding of the microfluidic device can be easily corrected. A fully fabricated microfluidic module for the Micro-BOAT is presented in Figure 4.8.

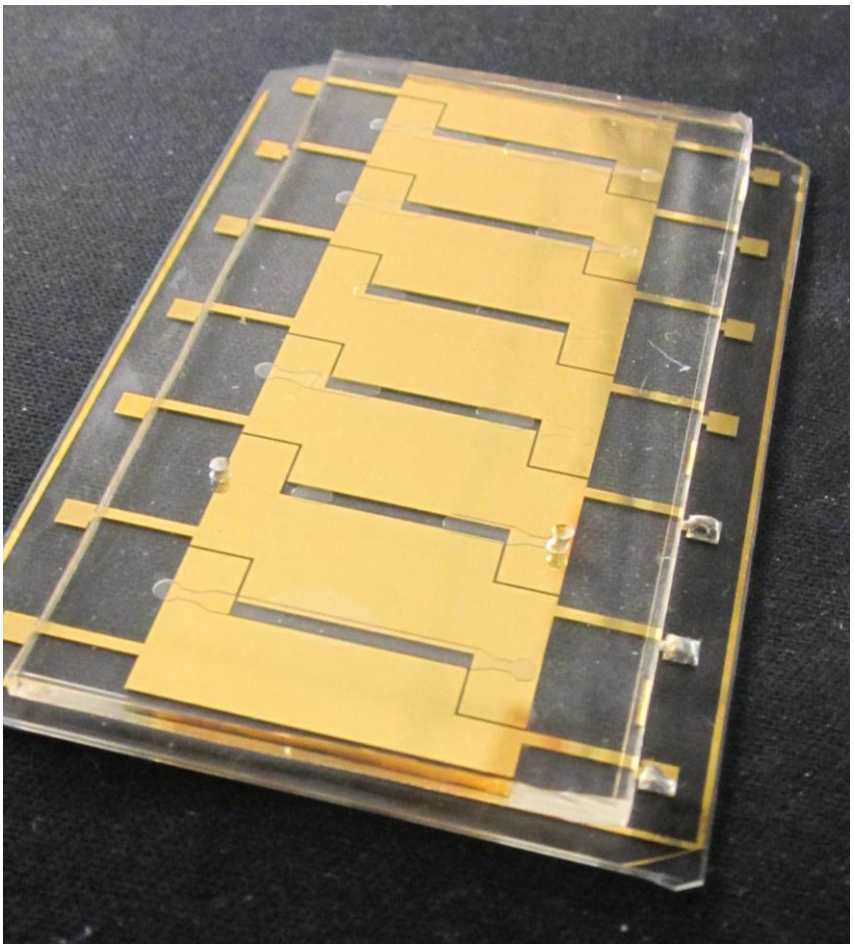

Figure 4.8: Photograph of the fully fabricated microfluidic module offering six channels on a single chip for parallel biofilm growth and treatment experiments. The PDMS-based microfluidic channels are shown here after methanol binding to the PyrexTM substrate with electrode structures.

4.3.4 Full System Assembly

Full-system assembly of the Micro-BOAT incorporates the three components discussed in sections 4.3.1 through 4.3.3 and requires no additional fabrication. The

process is presented in the following steps, with figure 4.9 providing an example of a fully fabricated and assembled device.

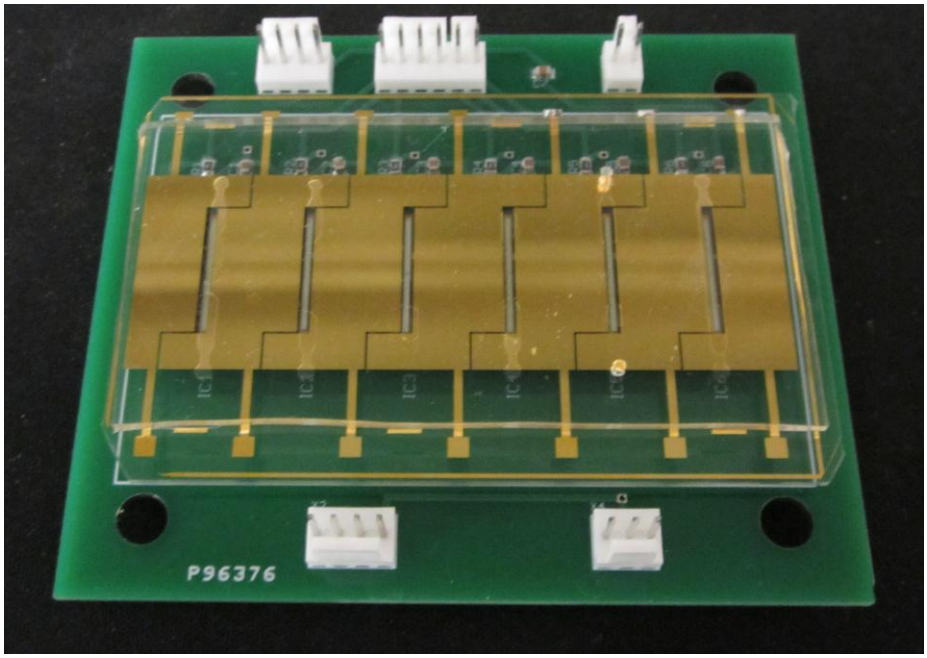

Figure 4.9: Fully assembled Micro-BOAT system prior to mounting in the Labnet incubator. Following this mounting process, the microfluidic channel inlets and outlets are connected to external fluidics for the flow of bacterial cultures and media needed to conduct biofilm experiments.

1. Beginning with the PCB module discussed in section 4.3.1, small adhesive strips are cut to size and attached to the non-sensor portion of the charge-coupled device packaging (IC package). These strips enable firm attachment of the microfluidic module to the PCB.
2. Using the methanol binding method discussed previously, the PDMS-based microfluidic structures are adhered to the Pyrex™ substrate with patterned gold electrodes. The two structures are compressed until the methanol has fully evaporated in order to ensure a leak-free bond.

3. Visual aligning and placement of the microfluidic module is performed. Assembly is conducted with the Pyrex™ substrate facing down, contacting the adhesive strips / CCD IC packages and allowing alignment of the electrode "windows" to the linear arrays of the CCD components. This constitutes full assembly of the Micro-BOAT system.
4. The complete device platform is mounted on the shelf in a miniature incubator using ¼-inch bolts. The holes in the PCB for these mounts align to the microwell plate holders in the aluminum shelf of the I5110 Labnet incubator.

After the microsystem is fully assembled, it must be connected to external fluidics to enable the flow of bacterial cultures, growth media, and aqueous treatment samples (i.e. liquid antibiotics). To achieve this, Tygon tubing (Cole Parmer no 95609-14) with barbed connectors (Cole Parmer no 06365-15) interface with the fluidic channel inlets and outlets and are sealed using quickset two-part epoxy (no 1293758, Loctite) to prevent the influx of air when the system is under flow. Fluid flow is achieved with an external syringe pump (Cole Parmer 74900) operating in withdrawal mode. Fluid samples are contained in 1.5 mL microcentrifuge reservoirs (02-681-285, Fisher Scientific) that are placed in the incubator during experimental cycles in order to avoid temperature shock to the bacterial cultures and/or films. A full description of device operation and experimental procedures is presented in the following chapter. Figure 4.10 demonstrates a fully assembled Micro-BOAT system that is prepared for experimental use, including microfluidic connections and electrical connections for the powering of PCB-mounted devices and on-chip electrodes for the bioelectric treatment effect.

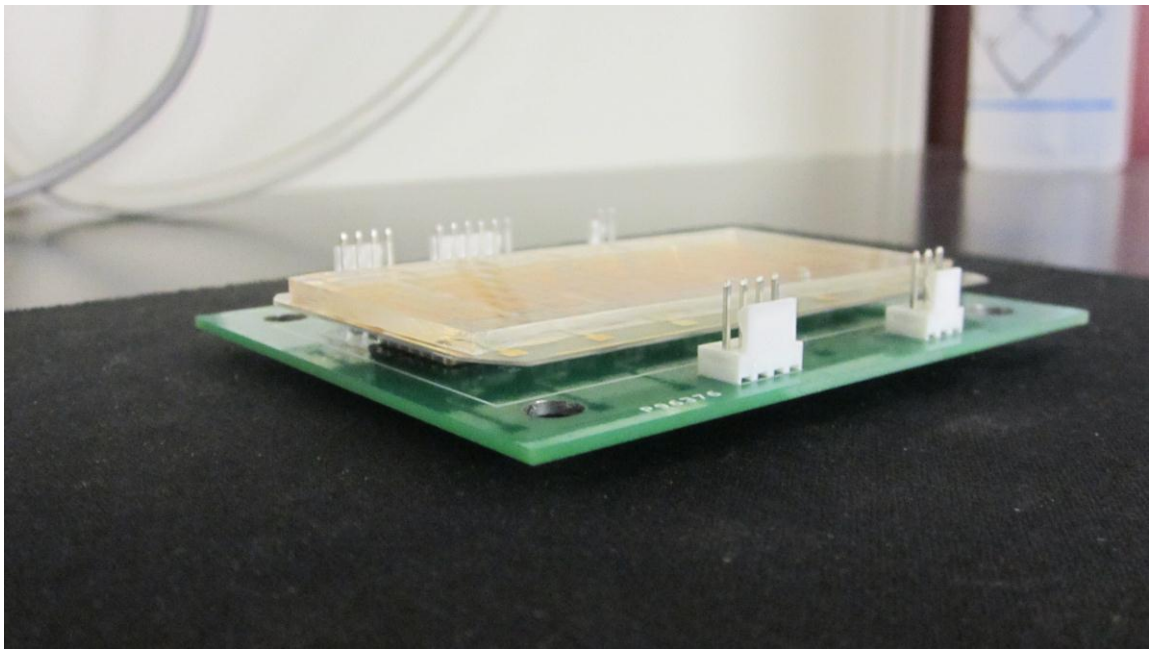

Figure 4.10: Photograph of a fully assembled and experimentally prepared Micro-BOAT system. Fluidic Tygon tubing provides connections to an external syringe pump and fluid sample reserves, while various electrical connections to the PCB allow for powering of on-chip electronics components and application of electric fields for the SP BE. In this image, connections between the electrodes for the bioelectric effect and the source of the electric field are not connected. The LED light source (not pictured) is positioned directly above the complete system to provide diffused light for OD detection.

In this following chapter, specific procedures for the actuation and operation of the device are provided, as well as experimental procedures and results obtained from characterization experiments and experiments comparing the novel SP BE to traditional biofilm treatments.

Chapter 5: Testing and Results

The following chapter presents the full testing apparatus and procedures used to conduct experiments in the Micro-BOAT system, including both characterization experiments and those testing the novel superpositioned bioelectric effect presented previously for biofilm treatment. Characterization experiments effectively validate and verify the Micro-BOAT as a viable system for investigations involving bacterial biofilms. Similarly, use of the microsystem to evaluate the potential benefits of the SP BE displays encouraging results in which the treatment method drastically increases the efficacy of localized biofilm treatments in comparison to traditional antibiotic therapies.

5.1 Bacterial Biofilm Markov Chain Modeling

The proposed platform for the modeling of experimental biomedical systems utilizes Markov Chain models to integrate the performance of biological systems within the construct of the larger biomedical system in order to determine overall system performance. In enabling this platform, a focus of this work examined the efficacy of utilizing Markov Chian models to achieve (1) predicting and determining the functionality and response of biological systems and (2) of integrating these models with physical models of a device system. To demonstrate this as an enabling approach to full-system biomedical device development, a simplified architecture of a bacterial biofilm is implemented and demonstrated in this work.

In order to achieve biological modeling of the bacterial biofilm system within the microfluidic channels of the Micro-BOAT system, the bacterial biofilm is mapped as high-level segments of biofilm to the structure of the microfluidic channel. Visually, this

can be represented using figure 5.1 below, which provides a conceptual abstraction of the biofilm within the microfluidic channel to the system level modeling via SysML or UML.

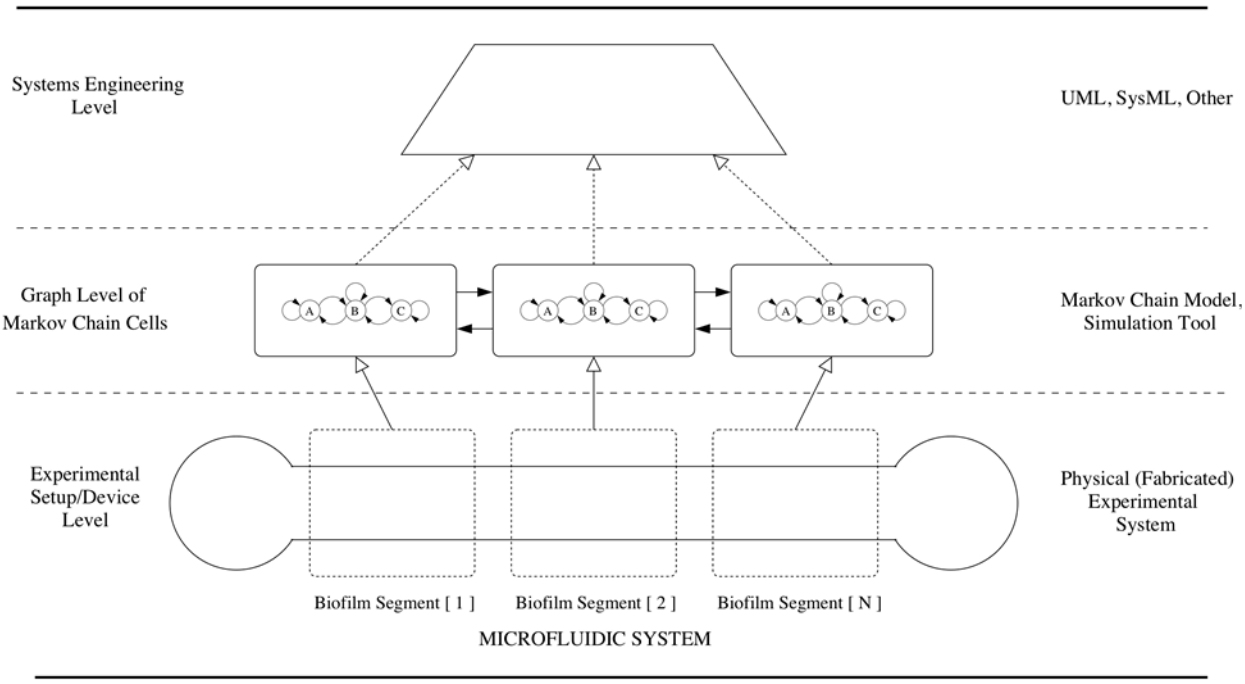

Figure 5.1: Implementation of the bacterial biofilm Markov Model. Here, biofilm within the microfluidic channels of the device are segmented along the channel as biofilm segments (1-N), each represented as a network of interdependent Markov Chains. High-level system modeling at the SysML or UML level facilitates alteration of the biofilm structure and modeling parameters.

Each segment of the bacterial biofilm structure within the microfluidic channel is represented as a segment of biofilm modeled using a Markov Chain. At a graph level of the biological system model, the biofilm segments (1-N) are interdependent upon one another. Thus, the growth characteristics and trends of a single biofilm segment affect the segments of surrounding biofilm, thus creating a full biofilm system model that, from a high level, represents the biofilm growth within a microfluidic environment. Proceeding a level higher in abstraction, system-level engineering can provide access to this model as well as the ability to readily modify model parameters, such as growth

parameters, in order to quickly detect the effects of various changes on the biofilm structure.

In the implementation explored in this work, a simplified biofilm structure was explored utilizing biofilm segments that can exist in one of three biofilm growth states, corresponding to physical states of biofilm maturity. Thus, each biofilm state is described as existing as either a *depleted biofilm*, a *moderate biofilm*, or a *mature biofilm*, corresponding to a particular level of biofilm viability. While these terms are somewhat general in the context of the complicated biological system, the terms could alternatively correspond to physical descriptions of biofilms, e.g., a biofilm viability metric (i.e., a ratio of metabolically active to metabolically inactive bacteria), an average biofilm height metric (i.e., a height in microns or a percentage of the height of the overall microfluidic channel, in this case the height of the biofilm structure within a 100 μm deep channel), or a surface coverage metric of the biofilm structure (i.e. as a percentage of the microfluidic cell substrate or as an area/units^2). In addition to the three biofilm system states defined for this model, the biofilm system as a whole is defined as being dependent upon two global variables, which exist as a set of two environmental conditions affecting the development of the bacterial biofilms within the microfluidic systems. These global variables are defined as including (1) nutrient concentration within the bacterial biofilm and the biofilm growth environment/media, and (2) biofilm surface shear stress as a result of fluid flow within the channels. For this model, each of these parameters is defined as being one of a pair of values: either High or Low. While defined qualitatively for this example, in practice, these global variables can correlate to physical values, e.g., a value for an oxygen concentration in terms of g/L, or a value for shear stress expressed in units

of Pascals or as a function of flow rate and biofilm height within the microfluidic channel, as expressed previously in equation (10) of this thesis. Each of these two global environment variables are independent variables that affect each of the interdependent biofilm segments, as described subsequently.

In implementing the Markov Chain model of the bacterial biofilm system, each biofilm segment is describe according to Figure 5.2 as shown below.

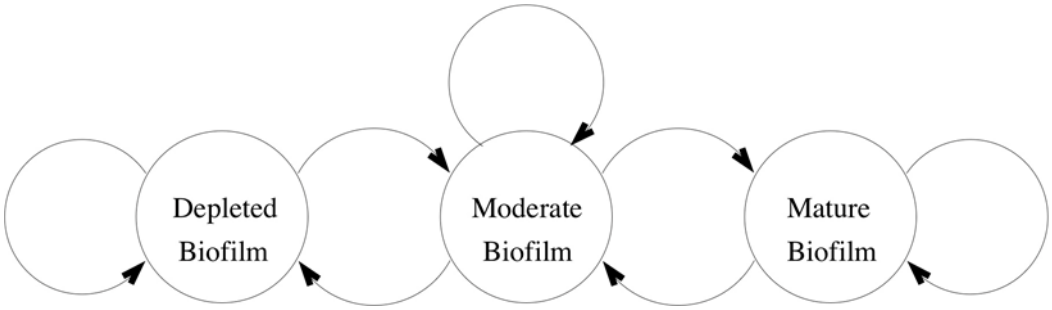

Figure 5.2: Markov Chain model used to implement the bacterial biofilm segments of this system. Each system state of the biofilm model can propagate by only one state per increment of time (e.g., a depleted biofilm can become a moderate biofilm, but not a mature biofilm, in one increment). The propagation probabilities are specific to the current state of the surrounding biofilm segments, as well as the environmental (global) variables.

As implemented, each biofilm segment can propagate only from its current state to a state one 'position' away per iteration of the cycle. For example, a biofilm segment that is in a *depleted biofilm* state can only remain as a *depleted biofilm* or propagate to a state of *moderate biofilm*, it cannot progress, in a single step, from a *depleted biofilm* to a *mature biofilm*. This is done not only for computational reasons, as it drives down the number of potential combinations associated with the Markov Chain system, but also for logical reasons, as it is not natural to expect a biological biofilm system to immediately develop from a minimal (depleted) state to a maximal (mature) state, but rather to have to

progress from one to the other through an intermediate (moderate) state. Additionally, while time is removed from this example and is represented only as a function of the number of unitless steps that the system is simulated for, the time associated with each of these steps, e.g., 1 hour or 1 day per step, can be tuned to match the Markov Model so as to most accurately represent an actual biofilm.

When considering the biofilm system as a whole, the biofilm segments in the current implementation are not interdependent in such a way that every biofilm segment is dependent upon every adjacent biofilm segment, i.e., that every biofilm segment *i* is dependent upon the states of the environmental conditions (global variables) as well as the state of biofilm segments *i-1* (upstream segment) and *i+1* (downstream segment). Rather, in order to represent a biological biofilm system in a manner that is both accurate and computationally simplistic, the Markov Chains representing biofilm segments 1 through N for this implementation are dependent solely upon the upstream biofilm segments (*i-1* segment) in addition to the environmental conditions (global variables). In the case of the *i=1* biofilm segment, representing the most-upstream segment of the biofilm, the biofilm is defined as being dependent upon the *i=1*segment in addition to the environmental conditions, in order to maintain simplicity of the model. Overall, the implemented biofilm model can be visualized via Figure 5.3 below, where biofilm segments (1-N) are defined in addition to the interdependencies of the segments.

For the specific model implemented in this work and presented as demonstration of the efficacy of biofilm modeling using Markov Chains as a generalization of biological modeling using the same method, a network of 10 biofilm segments is implemented using the arrangements and specifications provided.

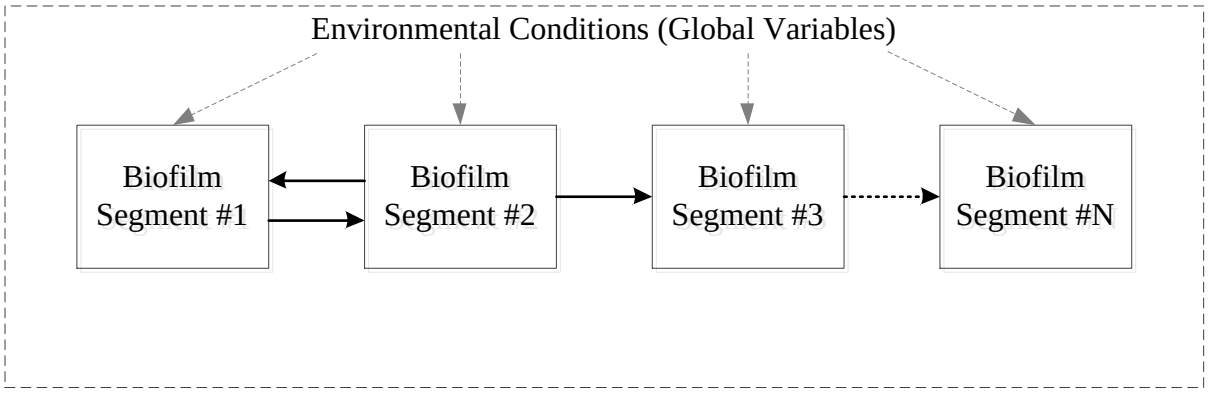

Figure 5.3: Graph level visualization of biofilm segments and their interdependencies as defined in the performed simulation. Each box represents a singular Markov Chain biofilm segment, with interdependencies represented through the provided arrows. Environmental conditions (global variables) uniformly influence the biofilm Markov Chain segments.

To implement the biofilm Markov Model, a Markov Model Simulation Tool developed by Yang, et al. and using the Java programming language is utilized in order to determine the probabilistic outputs of the system [75]. The developed tool enables the structure and transition probabilities of a specific system to be encoded, where the tool then determines the outcomes of the system based upon the transition probabilities and each of the potential combinations of variables (e.g., the environmental conditions) within the system. Additionally, the tool utilizes techniques capable of recognizing model symmetry of the particular set of Markov Chains, and of reducing the computations needed to determine the outputs of the particular system based upon this symmetry [75]. The simplified 10-segment system was chosen in order to minimize the computing overhead of the application, while maintaining the usefulness of the model as an example system for the modeling of a bacterial biofilm biological system within the microfluidic environment. Full coding of the biofilm model, as utilized for this work, is presented in Appendix B of this thesis for further reference. For the particular system presented here,

transition probabilities between the various states were determined based upon expected biofilm system development, supported by the relationships that determine bacterial biofilm growth and development, i.e., the set of partial differential equations, and otherwise approximated based upon the qualitative effects of shear stress and nutrient concentrations on bacterial biofilms. Using the initial transition probabilities defined, the values were adjusted slightly to achieve a biofilm model that matches the anticipated output of the biological system. The probabilities utilized for the final simulation are provided in Appendix B, where an abbreviated set of the code is presented, describing the first four segments of the 10-segment biofilm model implemented in this work. As the model is symmetric for each biofilm segment, with only the connections between the various segments being unique, the remaining code of the biofilm segments is in this thesis. Overall, through Bayesian statistics, the number of probabilities computed by the system are found to be:

$$X = A * a * n^N \qquad (12)$$

Where X is the total number of system states, A represents the number of global variables (i.e., environmental conditions), a is the number of possible states of each of the global variables (i.e., high and low), n represents the number of Markov Chain segments (i.e., biofilm segments), and N is the number of segments (i.e., the number of segments in the total biofilm). For this particular model, the number of states equates to:

$$X = 2 * 2 * 3^{10} = 236{,}196 \qquad (13)$$

Due to the symmetry in the system that is recognized using the tool developed by Yang, the total number of states is reduced by 25%, or a total of X = 177,147 states, or a reduction of 59,049 states.

The results of the performed simulation are presented below. Due to the presence of symmetry within the model, the overall simulation was capable of being computationally reduced by a factor of 25%. In Figure 5.4 below, a simulation is performed in order to determine the number of biofilm segments existing in each state for a large number of iterations (N=100) of the system for all of the four combinations of global variables. Cumulatively, among the four combinations of environmental conditions (high shear stress – high nutrient concentrations, low shear stress – low nutrient concentrations, high shear stress – low nutrient concentrations, and low shear stress – high nutrient concentrations) 31.915% of biofilm segments exist in a *depleted* state, 41.832% of biofilm segments exist in a *moderate* state, and 26.252% of biofilm segments exist in a *mature* biofilm state. This result demonstrates that the biofilm model designed for this system provides, at a high level, an accurate qualitative representation of biofilm structure. Based on the proposed set of environmental conditions, one expects that biofilms subjected to limiting environmental conditions, i.e., high shear stress and low nutrient concentrations, will display depleted growth. Similarly, those biofilms subject to growth conducive conditions, i.e., low shear stress and high nutrient concentrations, will display mature growth, and those biofilms subject to neutral environmental conditions, i.e., high shear stress and high nutrient concentrations and/or low shear stress and low nutrient concentrations, result in a moderate growth of biofilms. In this case, since there are essentially two combinations of environmental conditions

promoting moderate growth and one combination of environmental conditions promoting both depleted and mature growth, one anticipates that the ratio of moderate biofilm segments (41.832%) to depleted (31.915%) or mature (26.252%) biofilm segments would be approximately 2:1, a ratio that is supported through this high-level simulation. In the Discussion chapter of this thesis, further discussion of this result, as well as its implications for the use of the platform for the engineering of biomedical systems as a whole, is presented. The remainder of the results presented in this chapter follow from the model developed here, where the Micro-BOAT system is explored for its use in the growth of bacterial biofilms and the evaluation of various biofilm treatments, including the SP BE discussed as a focal point of this work.

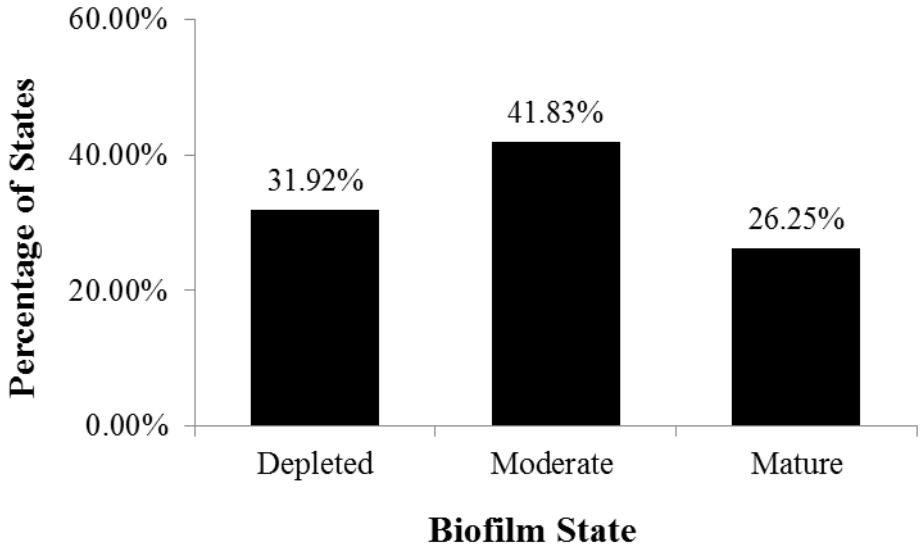

Figure 5.4: Results of the simulation conducted for a ten segment qualitative biofilm model based on qualitative characterization of biofilms. The model is simulated for biofilm segments that are interdependent and characterized by a set of three states, being one of depleted, moderate, or mature biofilm. The model is tested against two environmental conditions, environmental nutrient concentration and flow induced shear stress, each provided a binary high/low value.

5.2 Testing Apparatus and Actuation

The following section discusses the experimental setup developed for the actuation and use of the Micro-BOAT platform, as well as the signals required to actuate the device under operation. Subsequently, characterization and demonstration of the device is presented as an enabling step towards the utilization of the Micro-BOAT system for biofilm growth and treatment experiments.

5.2.1 Experimental Testing Setup

Borrowing from the device design and fabrication presented in Chapter 4 of this thesis, a high-level representation of the full experimental apparatus used for the Micro-BOAT is presented in figure 5.5. The full system is contained within an incubator at 37ºC to provide control of environmental conditions, which also houses fluid samples that are supplied to the microfluidic channels of the system and an edge-lit LED light panel (Luminous Film USA) that is used to uniformly illuminate the CCD components of the system. Light emission is tuned to 630nm red light by a polycarbonate lighting gel film (Roscolux #120, Rosco Laboratories) in order to match the peak sensitivity of the CCD photopixels. Interconnections via Tygon tubing connect the outlets of the microfluidic channels to the external syringe pump, which operates in withdrawal mode to prevent device leakage. A power supply and three function generators used to actuate the CCD components, discussed fully in section 5.2.2, are situated outside of the incubator and provide the necessary electrical signals via BNC cables (L-Com Global Connectivity) and the PCB-mounted wire-to-board connectors. Signal readout from the CCD components is achieved using a data acquisition (DAQ) device (NI USB-6221,

National Instruments) that integrates directly with the customized LabVIEW macro application developed for the application (LabVIEW 2010 SP1, National Instruments) running on an external PC (Optiplex 790, Dell).

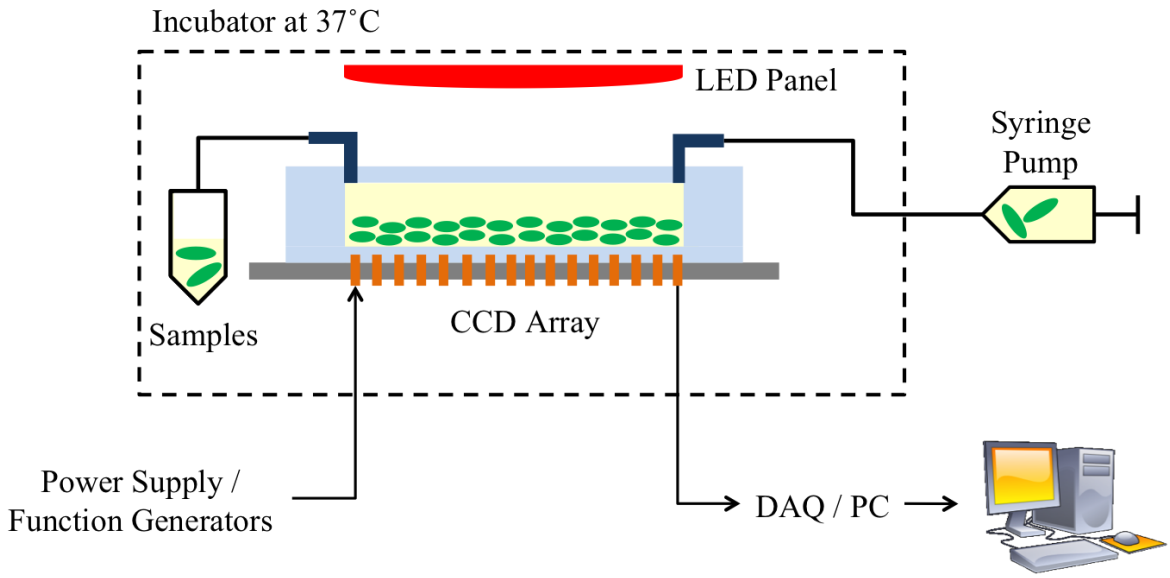

Figure 5.5: High-level schematic of the system's experimental setup. Samples and the Micro-BOAT system are contained in an incubator at 37ºC while an external syringe pump operating in withdrawal mode enables flow through the microfluidic chambers. External power supplies and function generators enable actuation of the CCD sensors, while a DAQ device and PC are used to obtain and analyze OD measurements.

5.2.2 Charge-Coupled Device Operation

Actuation of the linear pixel array CCD components is achieved via the signal waveforms outlined previously in section 3.2.2. For convenience, the timing diagram for the TAOS TSL202R components is reproduced here.

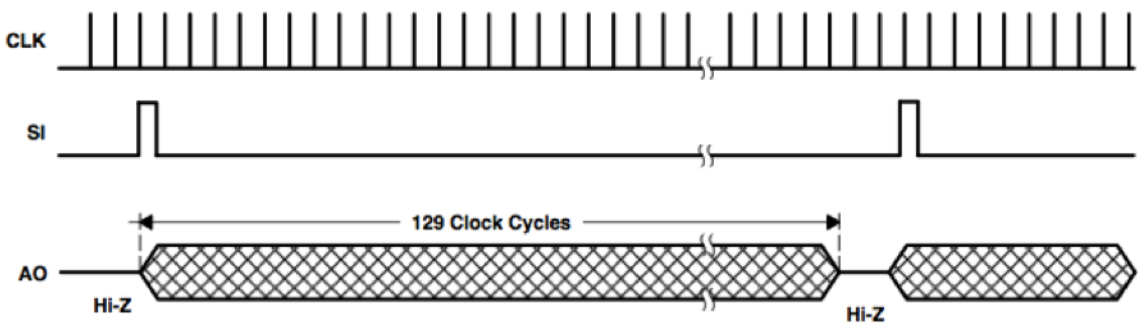

Figure 5.6: Timing diagram of the TAOS TSL202R linear array charge-coupled device. A drive clock (CLK) in combination with an out-of-phase serial input bit (SI) triggers integration and output of the CCD photopixels, given as a series of analog voltages on the output pin of the device (AO) [90].

The output of the system is governed by a drive clock (CLK) supplied by an external function generator (Agilent 33220A) providing a square wave signal at 150 kHz (6.67 µs period) with 5.0 Vpp centered at 2.5 Vdc. Using this drive frequency, the full output of the 128 pixels of the CCD occurs in 0.853 ms. Clock frequency is optimized in this case to allow the CCD pixels to output voltages in the linear range of output for the device, which occurs in the 1.0 Vdc – 2.5 Vdc output range and is presented further in section 5.3. The serial input (SI) bit, which triggers the integration and output of the CCD device, is provided by a second function generator (Agilent 33220A) operating in pulse mode to provide a periodic signal with a 1.0 ms period, 1.5 % duty cycle, and 5 ns rise/fall time. Since the active time of the SI bit (0.015 ms) is approximately the same as two full periods of the CLK signal (0.013 ms), there is no possibility that the SI bit will miss the rising clock edge needed to trigger output and next-cycle integration of the CCD device, despite the fact that the two signals are not triggered off of one another. In the event of consecutive rising edges of the CLK signal being captured by the SI bit, effectively resulting in a secondary output of the CCD pixels after an integration cycle of only 6.67µs, the processing software described in section 5.2.3 guarantees that only the

relevant data will be measured and stored for analysis. Actuation of the CCD components is enabled via a 5.0 Vdc source provided by an external power supply (Agilent E3631A). Connections between the external power sources, function generators and the PCB-mounted CCD devices are achieved via BNC cables and wire-to-board connectors as mentioned previously. Wiring of the individual CCD IC chips is performed in parallel according to specification (see Appendix A) [90].

5.2.3 Data Acquisition

In order to perform data readout and analysis of the optical density measurements recorded from the six parallel CCD components, a National Instruments DAQ card and LabVIEW are integrated with the system to store data on a local PC. For this application, a customized macro was developed in LabVIEW that allows data acquisition throughout a full experiment, which may last between 24 h and 72 h, with minimal user intervention.

The DAQ device is integrated with the device using BNC cables and wire-to-board connectors as described previously and with the local PC via a USB connection. The DAQ is a 16-bit device featuring 16 parallel analog I/O channels and a maximum sampling rate of 250 kS/s on a single channel. Since the device cannot sample multiple channels in parallel, the LabVIEW program designed for the application operates using a sequential method in which each of the six CCD devices is sampled in series. While this is not optimal, the continuous activation of the CCD devices (e.g., the clock and serial input bits are continuous, with a full cycle of device operation occurring every 1.0 ms) and the slow changes in biofilm OD allow this method to provide accurate measurements of each channel at specified measurement points.

The developed LabVIEW program utilizes the sampling and data analysis/storage schema provided in the high-level flow diagram in figure 5.7. Appendix D provides the full LabVIEW documentation, including front panel interface, block diagram programming, and virtual instrument (VI) configuration parameters.

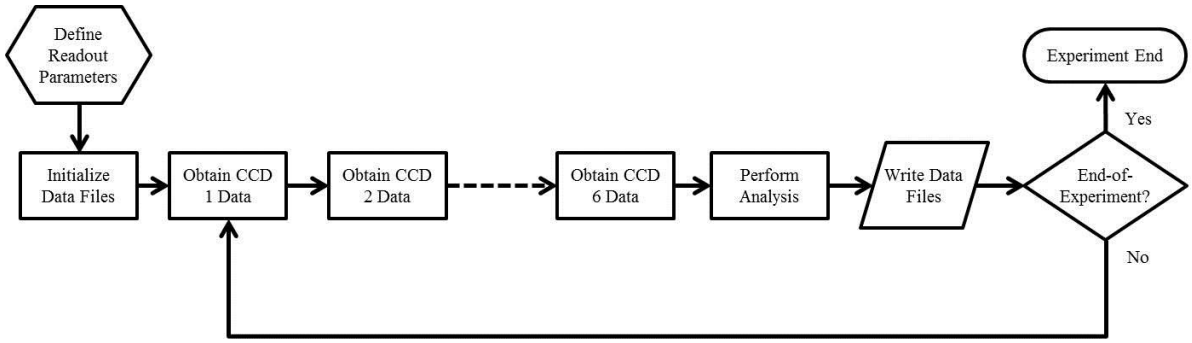

Figure 5.7: High-level flow diagram of the data acquisition process using LabVIEW. After defining experimental operating parameters, the program initializes the required files, before sequentially obtaining measurements from each of the six CCD components. This data is then analyzed for basic metrics and appended to the proper data files. The program then detects if the experiment time has been exceeded and assumes a wait phase until the data readout and writing processes are called upon.

Operation of the LabVIEW program begins with the user input of key variables that define the operation of the experiment including: (1) time in minutes between measurements, (2) full experiment time span in hours, (3) CCD drive clock frequency, (4) DAQ sampling frequency, (5) number of samples to read from each DAQ channel, and (6) append/overwrite data from each channel. Cumulatively, these six variables define how often the program should obtain data from the CCD components, how data readout should be performed with respect to DAQ sampling, and how the data should be stored in the specified files. With these parameters set, running the program begins with the initialization of the data storage files. The program then proceeds to sequentially read the specified number of data points from each channel, using a rising edge trigger to define the beginning of the CCD output from the dark voltage (approximately 0 Vdc) to the

active pixel output voltage (above 1.0 Vdc). Due to the use of high-pass filtering to remove noise from the CCD analog output signal, the first few samples from the DAQ are eliminated in data analysis in order to avoid the effects of slower transitions between dark voltage and active voltage output signals. Following data reads, basic analysis is performed on the data, including average pixel voltage output for each channel, as well as maxima and minima. Average optical density measurements are obtained by collecting voltage data from each of the 128 pixels of the CCD and averaging their output values at each measurement period. These values, as well as individual analog voltage data points, are then appended to the generated Excel files along with a relevant time stamp. Following this data write process, the system then enters a wait phase until the next program call for data readout, which is user-defined. A summary of typical measurement processing parameters is provided in Table 5 below, although other parameter values were often used in preliminary experiments. Since the NI USB-6221 DAQ is limited to 250 kS/s, the system is unable to exceed the Nyquist rate (twice the CCD drive clock frequency) thereby posing a current limitation to precise data acquisition and analysis that can be addressed in future work [98]. Here, both 150 kS/s and 225 kS/s were used as sampling frequencies for the 150 kHz CCD drive clock in order to allow the highest accuracy of sampling with limited ghosting and noise. Using this designed LabVIEW macro, successful data acquisition of six parallel channels was performed in real-time, thereby validating this high-throughput method for biofilm monitoring applications and providing an advantage over current monitoring techniques.

Table 5: Typical Operating Parameters for the LabVIEW Program

Parameter	With 150kS/s sampling	With 225kS/s sampling
Time Between Measurements	8 min	8 min
CCD Clock Frequency	150 kHz	150 kHz
DAQ Sample Frequency	150 kS/s	225 kS/s
# of Samples to Obtain	128 (-4 Presamples)	191 (-5 Presamples)
Low-Pass Filter Frequency	15.0 kHz	22.5 kHz
Trigger Threshold Voltage	0.3 V (0.25 V Hysteresis)	0.3 V (0.25 V Hysteresis)

5.3 Device Characterization

To perform validation and verification of the developed Micro-BOAT system, a series of characterization studies are presented that demonstrate the sensitivity, capabilities, and potential limitations of the device system for the monitoring of bacterial biofilms via changes in optical density. The three studies described in this section effectively define these characteristics for the current microsystem, thereby supporting its use for biofilm treatment experiments.

5.3.1 Operating Region for CCD Components

As described previously in section 3.2.2 and equation (4), the outputs of the CCD components are linearly correlated to the total energy incident on the photopixels whenever all other variables are kept constant. In order to verify this relationship and define the range of output voltages for which the relationship is applicable, an initial experiment was conducted in the system. The experiment performs a sweep of integration periods (t_{int}) between 0.1 ms and 50.0 ms for three different irradiance levels

that are achieved by covering the top of the CCD components with three filters of differing opacity.

Experiments are performed using a fully prepared microsystem that is operated under identical conditions to those utilized for biofilm experiments, aside from the flow of fluids through the microchannels, which is not required for this characterization procedure. The top of the device (where LED light is incident) is covered with one of three adhesive films of varying opaqueness including: (1) a transparent film to define normal operation conditions, (2) a semi-transparent white film that absorbs approximately half of the light incident on the CCD components, and (3) an opaque black film that absorbs almost all incident light. For each film, the integration period of the CCD components is varied across 25 different values ranging from 0.1 ms to 50.0 ms, with the CCD drive clock frequency and serial input pulse width adjusted to match the needs of each integration setting (e.g., a 0.1 ms integration period cannot utilize a 150 kHz drive clock since that clock rate would require 0.83 ms to output all 128 bits of the CCD signal, thus resulting in unreliable device operation). For each sample, the maximum CCD pixel output is recorded and plotted against the integration period, as shown in Figure 5.8. Results of this experiment demonstrate a linear CCD response in the range of approximately 0.75 V to 3.0 V regardless of the light irradiance level, thus validating the use of the tool for optical density monitoring when CCD output is maintained within these voltage levels. In the case of the highly opaque film, such a relationship is not observed as the total amount of light energy detected by the CCD components was too low given the tested range of integration times to allow signal outputs in this range. Device saturation is observed to occur around 3.4 V and the dark

voltage level is demonstrated at a negligible level tending towards 0 V, both of which agree with device specifications [90].

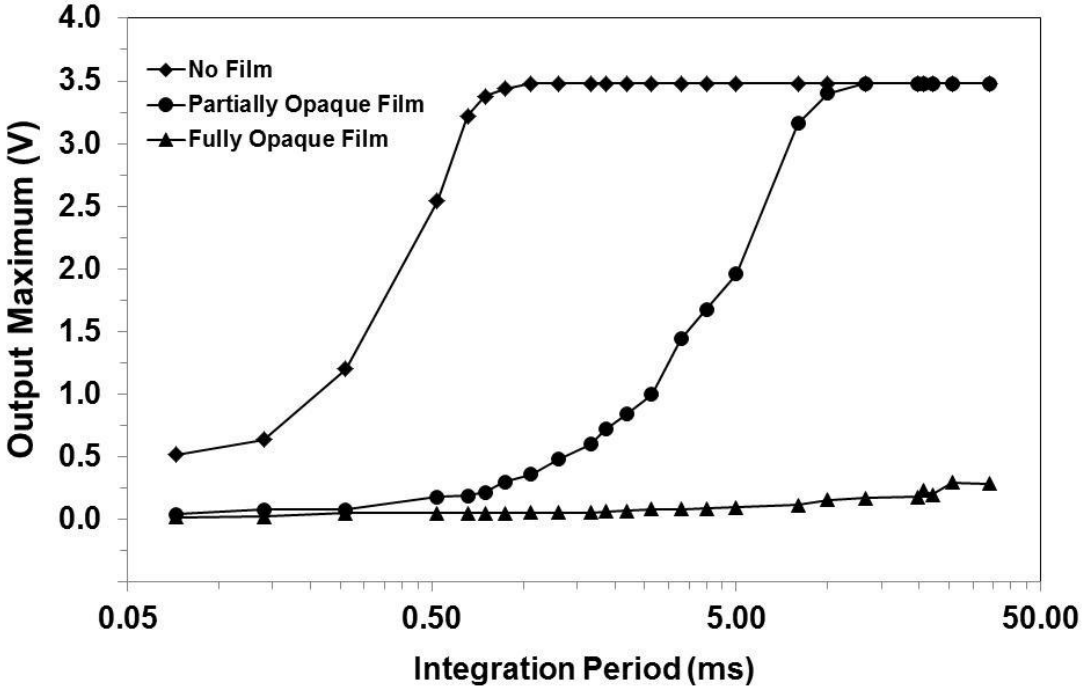

Figure 5.8: Maximum CCD pixel output for varying pixel integration times subject to three levels of irradiance. The linear CCD output range is observed to occur from approximately 0.75 V to 3.0 V regardless of the irradiance level, thus validating the use of this system for biofilm monitoring when CCD output is maintained within these voltage levels. Each data point is an average of three samples from the same CCD device on a fully functional Micro-BOAT.

The usable operation range of the OD detection module is defined by affirming the linear output region for the CCD components in the integrated system. Biofilm experiments performed within the Micro-BOAT require CCD pixel outputs within the defined range of 0.75V to 3.0V in order to obtain results that are linearly correlated to changes in biofilm optical density, with the ideal initial voltage level being approximately 2.0 V in order to provide the largest usable range for both increases and decreases in OD.

5.3.2 Micro-BOAT OD Measurements Correlated to Standard Methods

A second characterization experiment demonstrates the optical density measurement response of the CCD components to known changes in bacterial culture optical density at 600nm light (OD_{600}) in order to demonstrate device sensitivity and derive the relationship between optical densities measured using CCD components and those measured using a standardized spectrophotometry method. The response of the system to known changes in optical density are provided in figure 5.9 and demonstrates a linear relationship between optical densities measured at OD_{600} and the change in optical density as measured using the microsystem. This linear relationship is expected due to the irradiance response of the CCD photopixels presented in section 5.3.1.

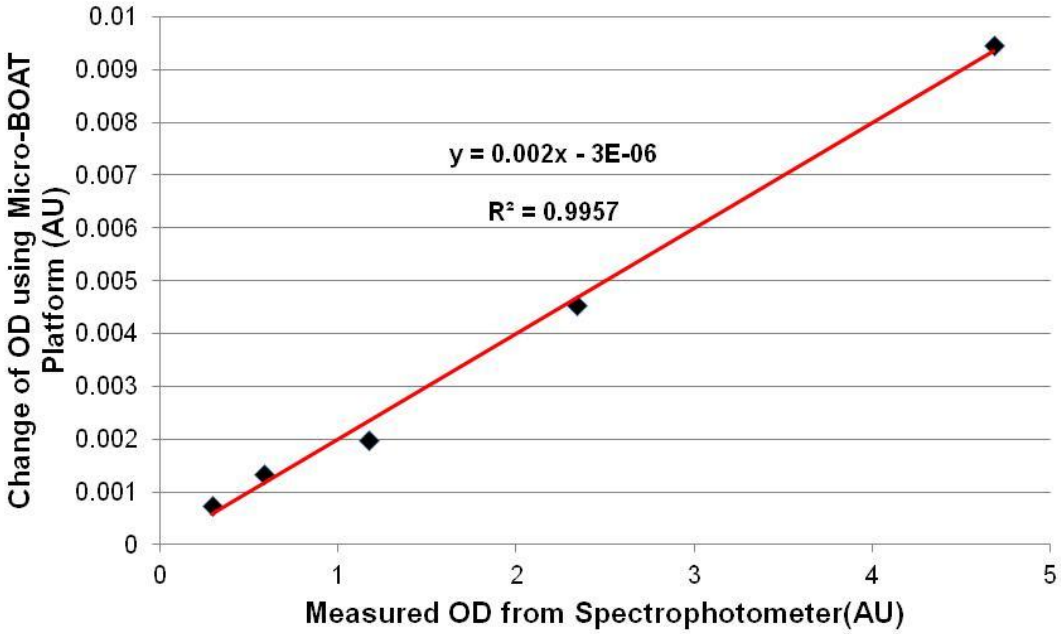

Figure 5.9: Correlation between optical densities measured using the Micro-BOAT and known OD600 values obtained from a commercial spectrophotometer. The linear relationship further validates the performance of the CCD method for optical density monitoring and enables approximation of OD600 using the developed system. Each data point is an average of 25 unique optical density measurements from the Micro-BOAT system.

The use of linear regression to obtain an approximate relationship between OD measured using the developed instrument and OD_{600} as measured by a spectrophotometer allows the conversion of measurements made using the Micro-BOAT system to standard measurements using commercial devices. Here, the slope of the curve in figure 5.9 demonstrates that a change of 0.002 AU as measured by the CCDs (hereafter termed AU_{CCD}) corresponds to a change of 1.0AU measured at OD_{600} (hereafter termed AU_{SOD}). The linear correlation between OD_{600} values measured from the spectrophotometer and the CCD OD measurements permit calculation of the detection limit of the system as well as the approximation of spectrophotometer-measured OD_{600} using the Micro-BOAT device. The device detection limit is calculated using the following equations and specifications supplied by the CCD manufacturer for device noise limits:

$$Detection\quad Limit\ \ (AU) = \frac{Noise\quad Limit\ \ (V)}{Sensitivity\quad of\quad Device\ \ (V/AU)} \qquad (15)$$

$$Detection\quad Limit\ \ (AU_{CCD}) = \frac{Noise\quad Limit\ \ (V)}{Sensitivity\quad of\quad Device\ \ (V/AU_{SOD})}$$

$$Detection\quad Limit\ \ (AU) = \frac{1.0\quad mV}{10.5\quad mV/AU} = 0.095\quad AU \qquad (16)$$

$$Detection\quad Limit\ \ (AU_{CCD}) = \frac{1.0\quad mV}{10.5\quad mV/AU_{SOD}} = 0.095\quad AU_{SOD}$$

$$Detection\quad Limit\ \ (AU_{CCD}) = \frac{1.0\quad mV}{10.5\quad mV/AU_{SOD}} = 0.095\quad AU_{SOD}$$

$$Detection\quad Limit\ \ (AU_{CCD}) = Detection\quad Limit\ \ (AU_{SOD}) \times Conversion\quad Factor \qquad (17)$$

$$Detection\ \ Limit\ \ (AU_{CCD}) = 0.095\ \ AU_{SOD} \times 0.002 = 0.00019\ \ AU_{CCD}$$

From this, we see that the theoretical detection limit for changes in sample OD_{600} is $0.095AU_{SOD}$, which equates to a CCD-measured OD detection limit of 0.00019 AU_{CCD}.

To perform this experiment, *E. coli* BL21 pGFP samples were prepared and the optical density of these samples tested using a spectrophotometer to determine OD_{600} in AU_{SOD}. Samples are then repeatedly diluted by a factor of 2 in LB media to generate the spectrum of known optical densities shown in figure 5.9. To test the sensitivity of the CCD biofilm monitoring system, each of these samples was briefly inoculated in the microfluidic channel in order of increasing optical density and OD measurements recorded using the Micro-BOAT system. Deionized water is used to flush the channel of bacterial cells between each sample. Average optical density measurements are calculated by averaging the outputs of the 128 photopixels over a series of 25 measurements and by using equation (6) provided in section 3.2.2.

5.3.3 Demonstration of Spatiotemporal Detection Capabilities

Spatiotemporal detection of biofilm growth and treatment is a critical advantage of the developed system, as it provides additional insight into the stochastic nature of biofilms that is difficult to obtain using established methods. To verify use of the device for the spatiotemporal detection of biofilm development within the microfluidic channels, a characterization experiment demonstrates the monitoring of optically dense droplets flowing through the microchambers of the system in real-time. To perform this test, samples of deionized water were prepared in a 25:1 ratio with a green propylene glycol dye (McCormick & Company, Inc) to create a homogeneous solution with a measured

OD_{600} of 20.3 AU_{SOD}. Since optical density values above 1.0 AU_{SOD} are outside of the linear range of the spectrophotometer, the OD_{600} of this solution was measured by first diluting the initial mixture by a factor of 40 (overall water to dye concentration of 1000:1) and recording its optical density, then multiplying this value by the dilution ratio. Droplets of the dye solution are inserted in a flow stream of translucent mineral oil by puncturing the Tygon tubing used for sample flow with a 27-gauge, 0.5-inch needle (Becton, Dickinson and Company) and injecting the droplets into the flow stream. The flow of oil with separated, water-based droplets is provided at a volumetric flow rate of 0.25 mL/h and detected using the Micro-BOAT as described previously in Section 5.2.3.

Results of this detection experiment are provided in figure 5.10, which displays both the spatiotemporal and averaged changes in optical density due to droplet flow within the microfluidic channel. The measured flow velocity of droplets within the microchannel concurs with theoretical calculations given the channel geometry and volumetric flow rate of the experiment, thereby validating the device's use for detecting the propagation of biofilms within the channel due to growth and flow-induced shear stress.

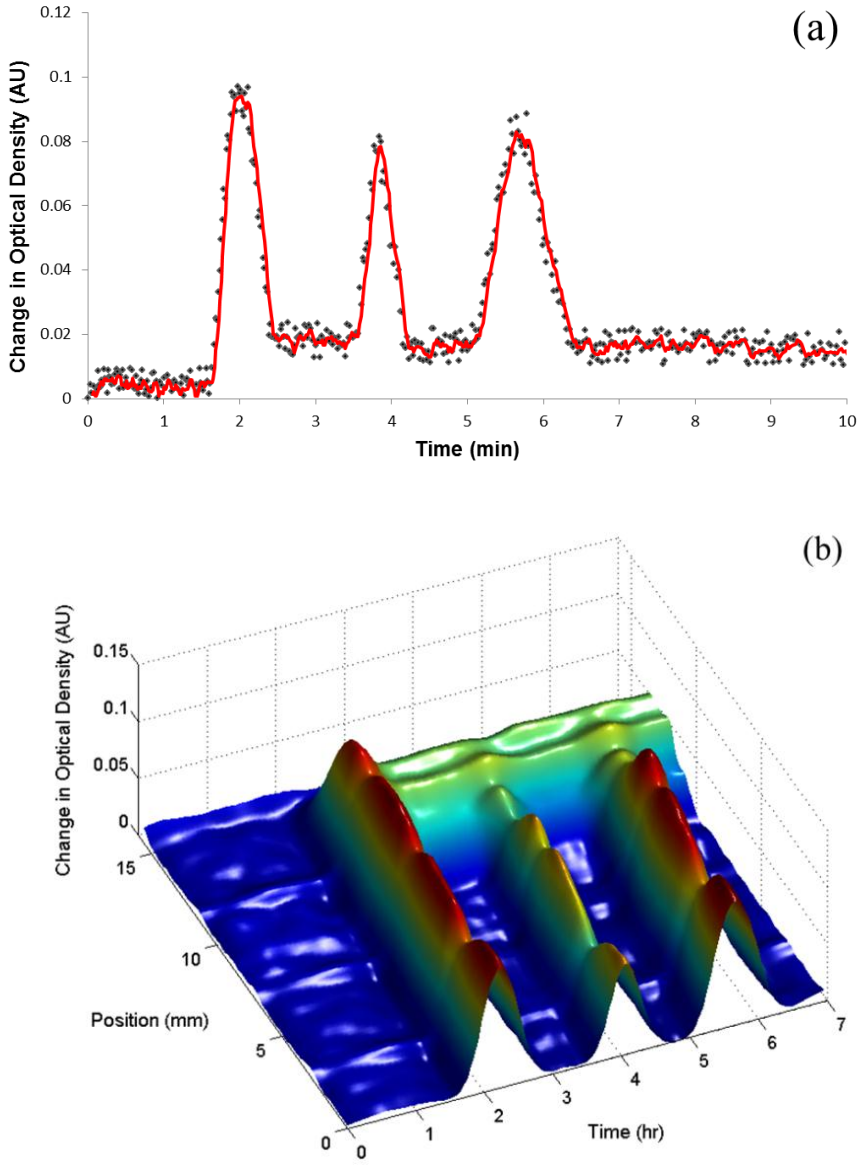

Figure 5.10: (a) Average change in optical density within one microfluidic chamber of the Micro-BOAT due to the flow of optically dense droplets in a translucent fluid. (b) Spatiotemporal detection of droplet flow within the same microfluidic channel. The enhanced waterfall plot is obtained via a customized MATLAB script (see Appendix C) based on the GridFit plug-in.

5.4 Biofilm Treatment Experiments

Upon validating the optical density monitoring capabilities of the Micro-BOAT, the device is utilized for a series of experiments testing the relative efficacy of various

methods of biofilm treatment, including the viability of the SP BE for the treatment of bacterial films. Cumulatively, these experiments aim in demonstrating the enhanced treatment effects of the SP BE in comparison to treatment by antibiotics alone. Demonstration of this treatment in microscale environments emulating *in vivo* conditions enables its use for potential clinical applications in the future. Furthermore, use of the integrated Micro-BOAT system for biofilm growth and treatment experiments validates its use and sensitivity for bacterial growth and treatment monitoring.

5.4.1 Bacterial Strains Used

E. coli BL21 is frequently used in clinically relevant bacterial studies, as this species is a well-studied microbiological system and well-suited for protein overexpression [99]. It has been used extensively with both native and heterologous proteins and provides a high protein yield per culture volume. In this study, *E. coli* BL21 modified with a plasmid encoding green fluorescent protein (pGFP) is used for bacterial biofilm studies to enable fluorescence microscopy in which metabolically active bacteria fluoresce green when excited by ultraviolet light. To conduct the experiments presented in this work, bacterial cultures are initially grown to an OD_{600} of 0.25 AU_{SOD}. All cultures are grown in LB growth media.

5.4.2 Bacterial Biofilm Treatments Tested

The testing of biofilm treatments using the microsystem developed in this work focuses principally upon the SP BE and its demonstration at the microscale. As defined previously in section 2.4, the electric field utilized for the SP BE is comprised of an AC

and DC signal characterized to be a 1.25 V/cm sinusoidal signal at 10 MHz with a 1.25 V/cm DC component that is applied to the established biofilms via thin-film gold electrodes patterned on the substrate of the microfluidic module. To conduct the treatment evaluation study, four distinct methods were compared to determine their relative efficacy and demonstrate the prospective suitability of the SP BE for bacterial infection treatment. The first of these treatments represents a control, in which bacterial biofilms are not treated using either antibiotics or electric fields, but rather are continuously supplied nutrient-rich LB growth media in order to provide a consistent growth environment. The second method utilizes traditional antibiotic therapy, where gentamicin sulfate (Invitrogen Inc, USA) is applied to established biofilms at a concentration of 10 μg/mL in LB media [45]. A third treatment method utilizes only the superpositioned electric field utilized for the SP BE without the presence of antibiotics in order to determine the biocidal effects of applying SP electric fields to biofilms. The use of this combinatorial electric field in the presence of traditional antibiotics, known as the superpositioned bioelectric effect, represents the fourth treatment used in this study [45, 94]. For this treatment, both the antibiotic concentrations and applied electric fields utilize the same parameters specified for antibiotic- and electric field-only treatments and demonstrate use of the SP BE for biofilm treatment. These four treatments are performed simultaneously within the biofilm growth and treatment microsystem and are repeated three times in order to determine the efficacy of each method. Detailed experimental procedures are provided in the following section.

5.4.3 Experimental Procedures

Testing is performed by initially creating *E. coli* bacterial suspensions with an OD_{600} of 0.25 AU_{SOD} in LB media. Small quantities of frozen cell cultures maintained at a temperature of -80 ºC are introduced to 10 mL of LB growth media and incubated at 37ºC in a shaker for approximately 24 hours in order to foster bacterial multiplication and maturation. The bacterial suspension, which typically has an optical density in the range of 4.0 AU_{SOD}, is then diluted in LB media to an OD_{600} of 0.25 AU_{SOD} measured by a commercial spectrophotometer (Beckman Coulter Inc).

To sterilize the microfluidic channels before placing the bacterial suspensions, experimentation is begun by initially disinfecting each channel using 70% ethyl alcohol under flow. After rinsing with deionized water, the channel is inoculated with the bacteria suspension for 2 hours without flow to allow for bacterial attachment to the microfluidic substrate [6]. LB media is then continuously supplied to the channel for 24 hours at 20 µL/h, an effective flow velocity of 30 µm/s given the dimensions of the microfluidic chamber, to replenish nutrients and facilitate biofilm growth. Sources of LB media are replaced as needed in order to avoid contamination and maintain steady supply to the developing biofilms within the microfluidic channel. Treatments are started after 24 hours of growth as described previously and continued for an additional 24 hours. To achieve the exchange of fluid sources during experiments with minimal effects, flow is stopped and the inlet tubing quickly transferred to the new source before reinitializing flow.

Optical density measurements are taken non-invasively in real-time with respect to both average and localized changes in biofilm optical density as described previously

in section 5.2. Initial optical absorbance of the biofilm is measured 30 minutes after the preliminary inoculation period has ended and the flow of LB media has begun. Measurements are obtained every 8 minutes and recorded using LabVIEW. For the length of experiments used in this work, which approach 48 hours, and the amount of data collected in each data read cycle, the frequency of measurement at 8 minutes is limited by the current data storage capabilities of the developed macro application in LabVIEW. Future work can utilize more advanced data storage techniques in the LabVIEW interface in order to increase the size limits of these data files, thereby increasing the frequency of measurement used in this work. However, due to the slow rate of change of bacterial biofilms as biological systems, in which the doubling time is metabolically limited to 20 minutes under ideal conditions, an 8-minute measurement interval is acceptable for determining both morphological and overall changes in film optical density.

In addition to the quantification of biomass changes using optical density measurement, the efficacy of each treatment method is further evaluated at the end of the experiments by a conventional cell viability quantification assay using live/dead cell staining and fluorescence microscopy. Red cells in the biofilms are stained red, while metabolically active bacteria appear green based on the expression of green fluorescent protein. To perform dead cell staining at the conclusion of the biofilm experiments, the microfluidic channel is first rinsed with phosphate buffer solution (PBS) at a rate of 200 µL/h for 1 hour in order to remove non-adherent bacterial cells. The remaining biofilm is then treated using a red fluorescent propidium iodide stain (Invitrogen no L7012) to allow imaging of the dead bacteria in the biofilm structures. The stain is provided in a

1.5 µL per 1000 µL PBS concentration at a rate of 200 µL/h for 2 hours in order to ensure complete staining of non-living cells. Subsequently, the channel is rinsed using PBS at 200 µL/h for 1 hour to remove unabsorbed propidium iodide, thereby limiting imaging background noise caused by the presence of residual dye. Microscopy is performed using a fluorescent microscope (Olympus BX60) at 20× magnification. Both total and green fluorescence images are obtained from multiple locations within each labeled sample (N=7 for each of the treatment 3 samples, corresponding to 21 images per unique treatment). Quantitative analysis of the images is performed using the image processing software ImageJ (Image J 1.44, USA). After the green fluorescence mode images of the biofilm are filtered to remove any red and blue color hues, the image undergoes a binary image conversion with respect to the green fluorescence color to produce a black-and-white image. Similar steps are performed (using only blue hue filtering) to provide binary interpretations of the bright field fluorescence images of the biofilms, such as that shown in Figure 5.11 below.

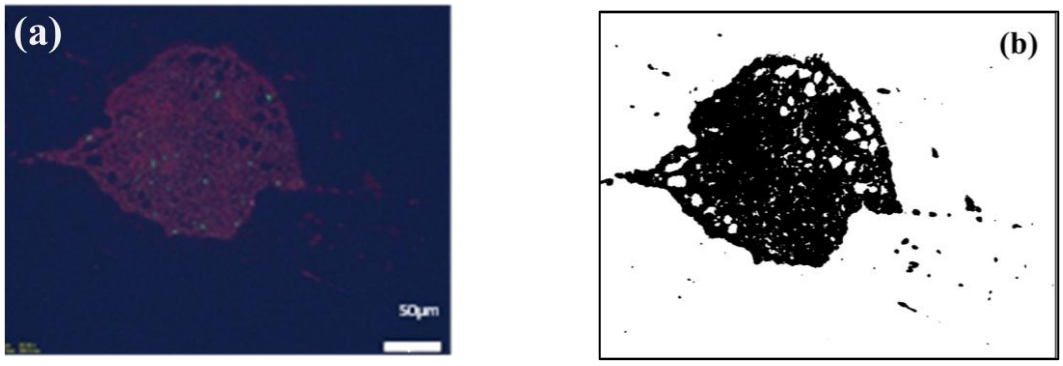

Figure 5.11: Example of the bright field binary conversion using the image processing software ImageJ. An initial bright field fluorescence image (a) is filtered and converted to a binary black-and-white image (b) to enable quantitative analysis of biofilm growth and treatment.

The percentage of viable bacteria is calculated based on the surface coverage of green fluorescence with respect to the total fluorescent surface coverage obtained from the binary image conversions. For each sample that is imaged for live/dead cell staining studies, 7 points within the microfluidic channel are imaged in order to obtain results that are representative of the average biofilm state within that channel.

Following experimentation, system component disposal and cleaning is performed to enable reuse of critical system modules for future biofilm experiments. Bacterial suspensions, used syringes, connection tubing, and the PDMS channels are disposed of, while the patterned Pyrex^{TX} substrate and other remaining system components are cleaned for immediate reuse.

5.4.4 Biofilm Monitoring by Optical Density Measurement

Using the Micro-BOAT system as a testing apparatus, the four biofilm treatments presented in section 5.4.2 are performed. For each treatment, three samples were tested in order to determine the relatively efficacy of each. The result presented in Figure 5.12 provides the change in overall optical density of the biofilms due to treatment. Following the 24-hour growth period, the optical densities of each sample are normalized to an initial starting point (0.0 AU), with subsequent changes being represented with respect to this point. Therefore, this figure provides the change in average optical density during the treatment phase for each therapy method, correlating to similar changes in bacterial biomass. As anticipated, the control and superpositioned electric field-treated biofilms demonstrate increases in optical density corresponding to further biofilm growth and an increase in biofilm mass. At the conclusion of the treatment phase, control biofilms averaged a 0.007 AU_{CCD} increase in overall optical density, while those treated only by

electric fields without antibiotics demonstrated an average increase in optical density of 0.004 AU_{CCD}. Standard biofilm treatment using the antibiotic gentamicin demonstrated a net decrease in averaged optical density of 0.003 AU_{CCD}, representing a reference for the efficacy of current bacterial infection treatments. By comparison, treatment using the SP BE displays an overall biofilm optical density decrease of 0.008 AU_{CCD}, a 167% increase in treatment efficacy over traditional antibiotics alone. This result verifies the capability of the SP BE to induce substantial biomass inhibition with respect to currently available antibiotic techniques.

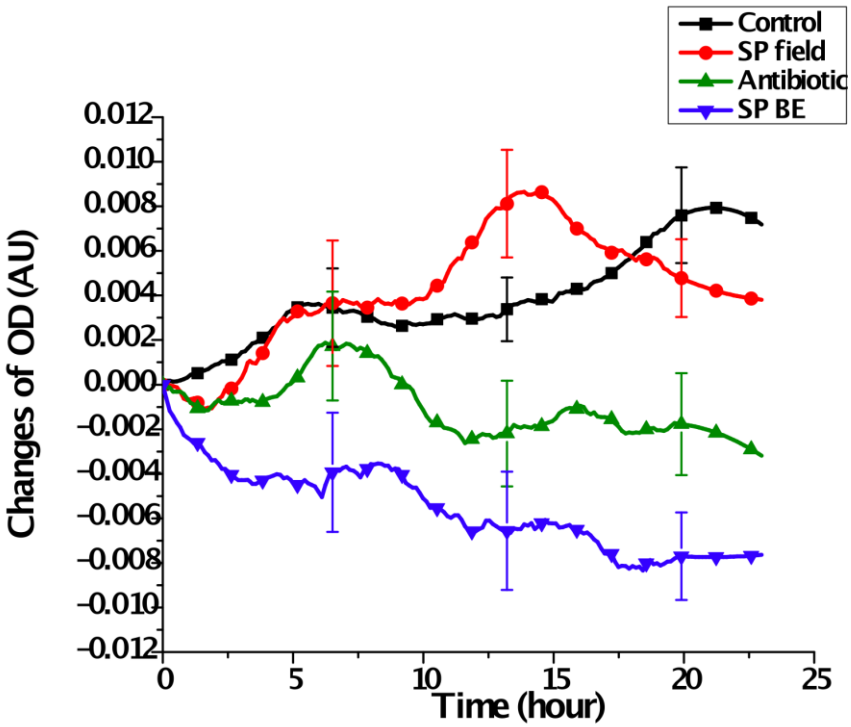

Figure 5.12: Measured changes in biofilm optical density during treatment using the Micro-BOAT system. Each curve represents the average optical density change for three samples with standard deviations shown at representative time points. The differences in optical density are statistically significant (ANOVA P<0.001).

In addition to the absolute change in optical density of biofilms over the course of treatment, calculations were performed to determine percentage changes in optical

density as a result of the different therapies. Figure 5.13 provides this result, in which the optical density of the sample at the conclusion of the treatment phase is presented as a percentage of its optical density at the conclusion of the growth phase of the experiment.

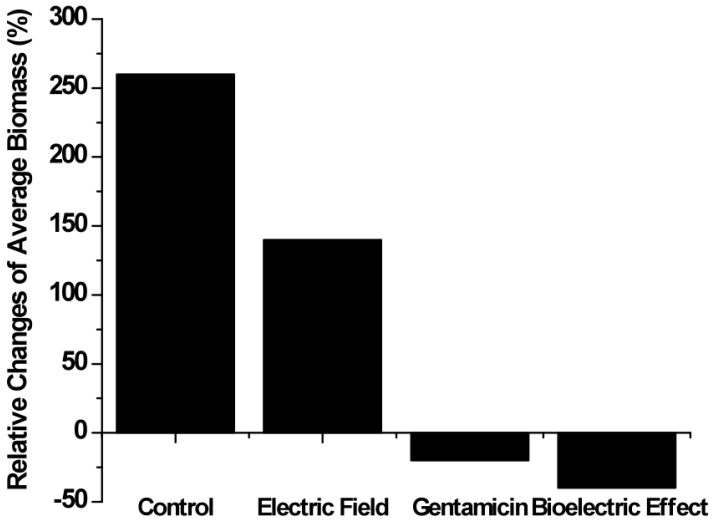

Figure 5.13: Relative changes in bacterial biomass as a result of the performed treatments. Overall, control biofilm samples demonstrated a 260% average increase in bacterial biomass during the treatment phase of the experiments, while those treated using only electric fields increased by an average of 140%. Gentamicin effectively reduced bacterial biomass by 24% during treatments and the SP BE achieved the greatest decrease in biofilm mass with a 40% average decrease during the treatment phase of experiments.

Cumulatively, these two results demonstrate the capabilities of the Micro-BOAT to determine the relative efficacies of various biofilm treatments. Further analysis of these results is reserved for the discussion portion of this chapter in Section 5.4.

In addition to providing results that compare the relative efficacy of the performed treatments based upon changes in average optical density, the spatiotemporal monitoring capabilities of the optical density method provide insight to qualitative changes in localized biomass OD and the resulting biofilm structural morphologies that accompany

each of the tested treatments presented in this work. As provided in Figure 5.14, control samples and those treated only with the SP electric field (shown) without antibiotics tend to develop widespread, thicker biofilms with areas of high-density biomass. Samples treated with antibiotics generally demonstrate thinner biofilms with fewer clusters of high-density film at the conclusion of treatment, while those treated with the enhanced bioelectric effect display extremely limited surface coverage and even thinner layers of biomass where the films remain established.

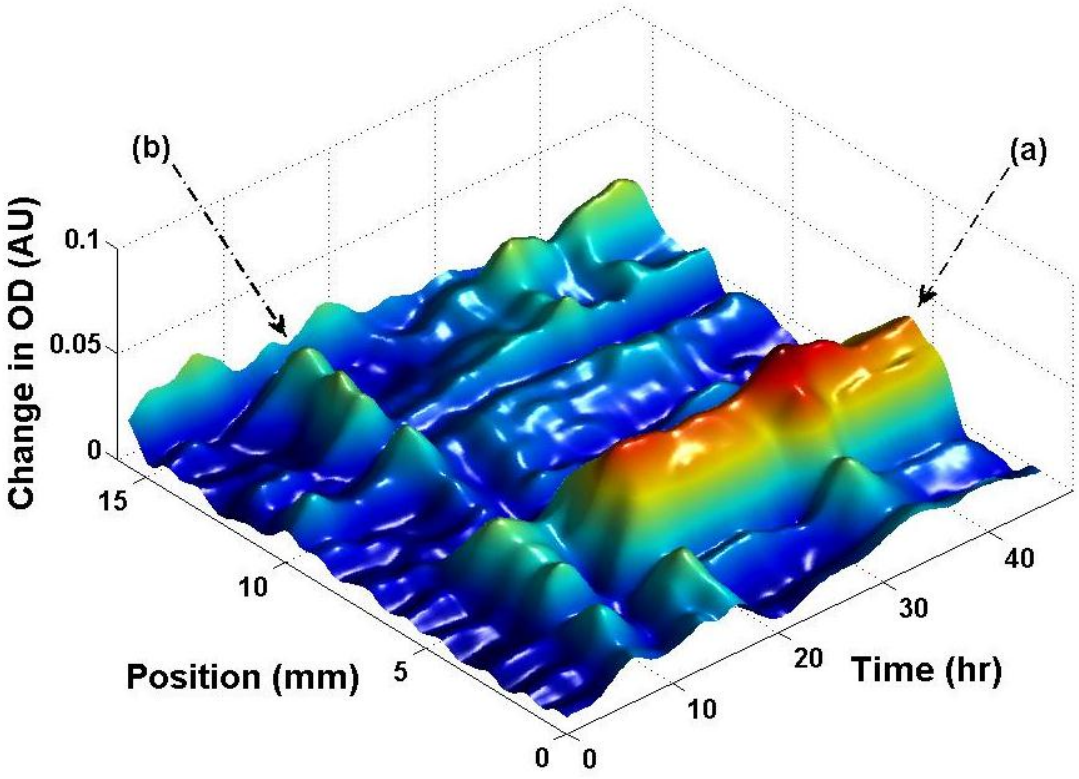

Figure 5.14: Surface reconstruction of biofilm surface morphology showing (a) stationary biofilm and (b) biofilm drifting through the channel with time. The surface reconstruction is created using the spatiotemporal data from CCD optical density measurement using the Micro-BOAT system. This particular plot is from a biofilm sample treated only using the SP electric field used for the SP BE without antibiotics.

5.4.5 Results using Cell Viability Studies

In addition to the quantification of biofilm growth via optical density measurement in the Micro-BOAT system, each of the treatments is evaluated for efficacy using the live/dead cell staining method presented in section 5.4.3 for further verification. Dead cells in the bacterial biofilms are stained red, while metabolically active cells appear green based upon the expression of green fluorescence protein by the *E. coli* BL21 pGFP bacteria. Figure 5.15 presents representative images of each biofilm treatment used in this work. Left column (a)-(d) images demonstrate bright field fluorescence of biofilms after each treatment while right column images (e)-(h) present live cell green fluorescence for each of the four treatments. The bright fluorescence images correspond to the two-dimensional projection of overall biofilm mass in the microfluidic channel following treatment, where both live and dead cells are visible due to fluorescence. Similarly the green fluorescence images provide a two-dimensional projection of the overall biomass with respect to only those cells that are metabolically active. As shown in Figure 5.15(d), biofilms treated using the SP BE display the lowest amount of bacterial biomass following treatment, demonstrating the enhanced effect of this method compared to traditional antibiotic treatment. Additionally, biofilms treated with the SP BE in the microfluidic chambers show a lower density of live cells compared to the other treatments, as seen in Figure 5.15(h). Therefore, we see that this method is capable of reducing not only the total amount of biofilm mass, but also of reducing the viability of biofilms by decreasing the percentage of live cells within the biofilm structure.

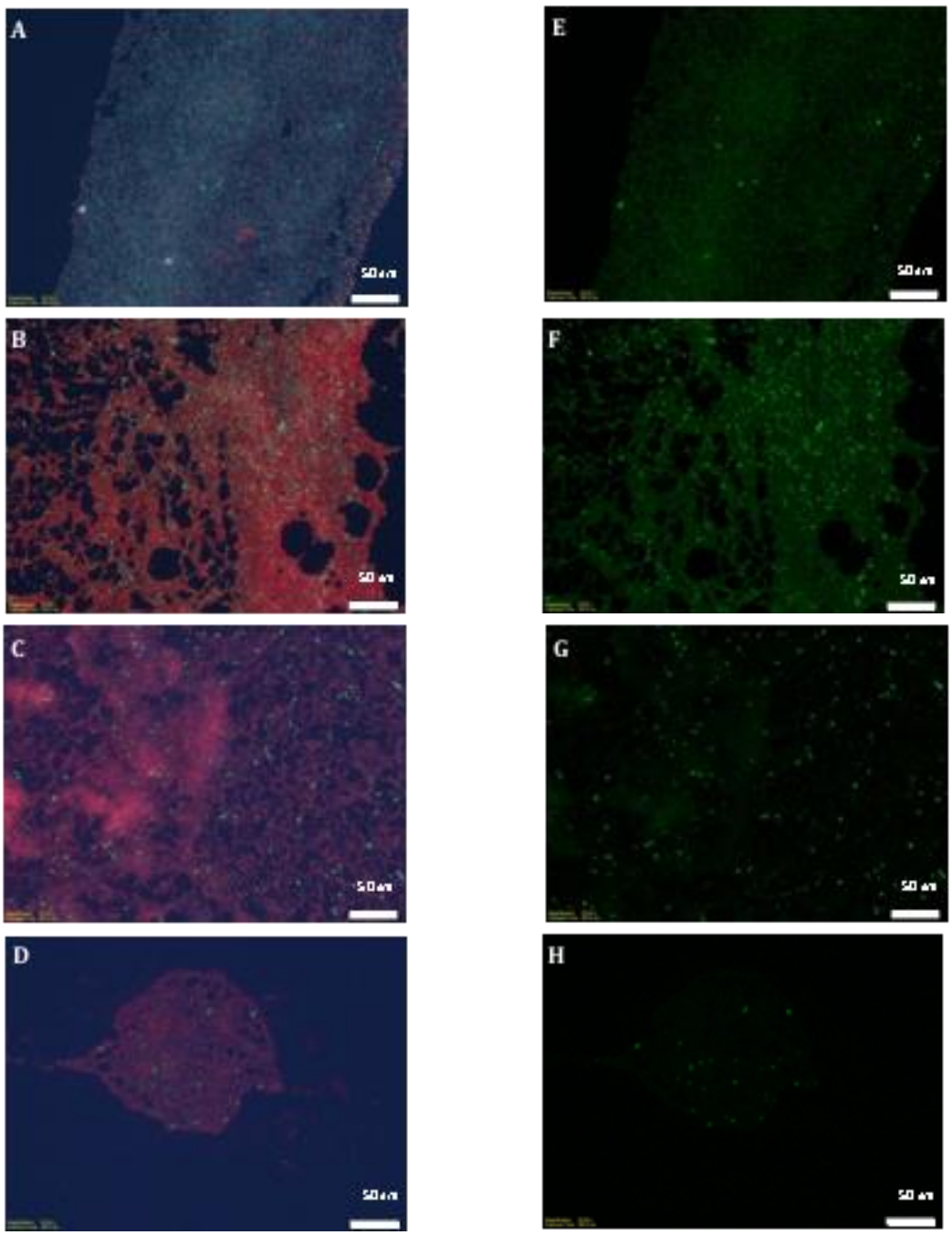

Figure 5.15: Representative bright and green fluorescence microscopy images of biofilms in the microfluidic channels after treatment. The total biomass and mass of live bacteria are shown for control biofilms (a,e), biofilms treated solely with the SP electric field (b,f), samples treated only with antibiotics (c,g), and biofilms treated with the SP BE (d,h). Biofilms treated using the SP BE showed less overall biofilm mass (d), as well as low live bacterial cell density (h).

The microscopy images of other treatments further demonstrated that the use of biocidal therapies produced thinner, more sporadic biofilms with low viable cell density, while control samples and those treated only with the SP electric field demonstrated more mature biofilm structures with considerably higher densities of both overall biofilm mass and live bacterial cells.

Using the image processing procedure described previously, binary transformations of each total (bright field) and green fluorescence image are created in order to quantify the percentage of viable bacteria within biofilms treated using each method. By calculating the surface coverage of the green fluorescence image with respect to the total surface coverage of the fluorescing biomass, the ratio of live to dead bacterial cells can be determined for each biofilm (Fig. 4.16).

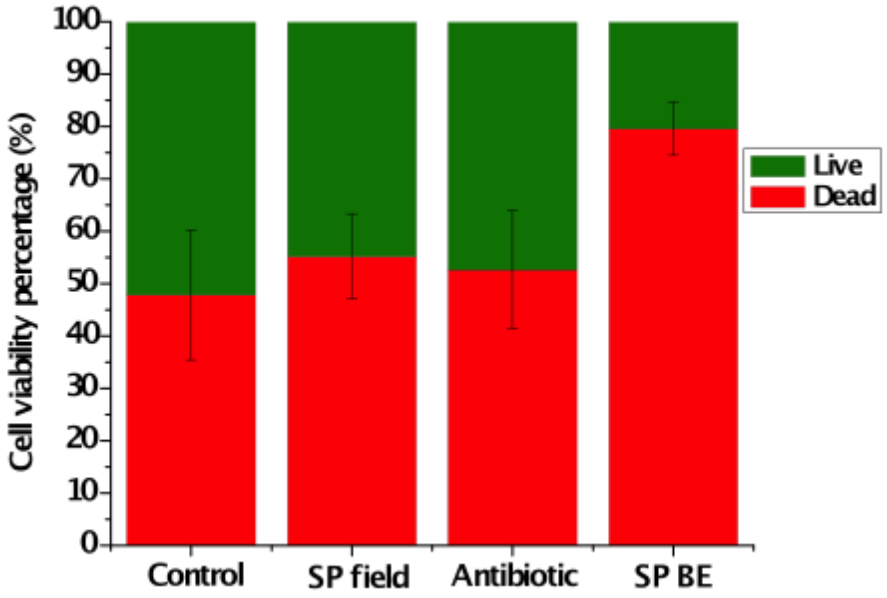

Figure 5.16: Results of cell viability studies. The percentage of viable bacteria with respect to the total bacterial biomass is calculated following treatment using the image processing software ImageJ. The results include the average of seven (7) images from each of three (3) samples for each treatment method. The SP BE showed the highest efficacy of the four treatments, with a 56% increase in dead cell density compared to antibiotic treatment (ANOVA, P=0.019).

Results demonstrate that biofilms treated using the SP BE showed the lowest percentage of viable bacteria after treatment, with 80% of bacterial cells being metabolically inactive. This is compared to traditional antibiotics, which showed 51% of bacteria are non-living after treatment, treatment using only the SP electric field, which demonstrated that 55% of biofilm bacteria were non-living, and control samples, in which an average of 48% of biofilm bacteria were metabolically inactive after the treatment phase of experimentation. The 56% increase in dead cell density present in biofilms treated using the SP BE poses strong evidence for the efficacy of this new method for localized biofilm treatment as well as the inhibition of total biofilm mass, discussed further in the coming discussion.

5.5 Discussion

The following provides a discussion of the various results presented in this thesis, with the aim of providing analysis and further insight into the future utilization of this work for related studies in the various regimes discussed, including further developments in the use of systems engineering approaches towards the engineering of systems for experimental biomedical applications.

5.5.1 Markov Modeling of Biofilm Systems

The modeling presented here for a high-level structure of a bacterial biofilm system forms a basis for the future use of Markov Chain techniques to represent biological systems in full system models of biomedical devices. Here, the biofilm model utilized qualitative descriptions of bacterial biofilms (*depleted*, *moderate*, *mature*) and

segmentation in order to represent a biofilm system as it exists within a microfluidic environment. A graph level of Markov Chain cells was demonstrated, showing the method by which the segments of bacterial biofilm can interact. Cumulatively, the biofilm system, represented by this interacting Markov Chain system, stands as a foundation for the future development of this model to describe bacterial biofilms. The model has demonstrated results that conform to expectations when subjected to a set of two environmental conditions, specifically flow-induced shear stress and available nutrient concentrations within the microfluidic environment.

Future developments and implementations of this model can enable more accurate predictions of bacterial biofilm development that include additional environmental conditions affecting the growth and development of bacterial biofilms, as well as potential treatment variables that may, for example, be able to predict the efficacy of a candidate treatment upon an established bacterial biofilm, such as those related to clinical infections. To develop such a model, data from prior bacterial biofilm studies can be integrated in an established model structure such as that presented here. Through learning techniques, such as iterative learning techniques including the Viterbi method and others, this data can be utilized to tune the transition states as well as the transition probability values of the system, overall resulting in a biofilm model that is more representative of the biological system. While it is desired that such a model would be uniform across any number of environments, e.g., microfluidic, *in vivo*, and macro-scale flow cells, and bacteria types, e.g., *E. coli* and *Pseudomonas*, there is a certain likelihood that such a model would also need to be tuned depending upon the application. In such a case, biofilm models describing the system for a particular environment and a particular

bacteria type may exist, in which the general structure of the system remains the same, with only slight parameters being variant depending upon the application space. Future work in the area of biological system modeling using Markov Chains can aid in the development of specific models for bacterial biofilms, in addition to other biological systems of interest, and can eventually result in a library of relevant biological models that can be used across disciplines in order to enable optimized studies of biological systems, the prediction of biological system development to enable enhanced insight into systems, or, with respect to the application presented here, further optimization of biomedical devices designed with a detailed biological system in mind.

In order to fully enable the optimized development of biomedical devices for experimental applications, models such as the high-level, qualitative bacterial biofilm model presented here must be integrated with physical models of the device system. To achieve this, future work in this area will target the interfacing of these two model types through a common medium, thus allowing both models to be accessible, viewable, and configurable through a single port. For the systems-based development of biomedical devices, as discussed throughout this thesis, a prime candidate for such integration is through an established system modeling language, such as SysML or UML. By interfacing physical system models (such as that of the Micro-BOAT device subsystems) with biological models (such as the biofilm model), a full-system view is achieved that is not currently available using present techniques. At the present, biomedical devices are designed by either (i) simulating a biological system under a set of environmental conditions and inserting characteristics or constraints related to this biological system in a functional model of a device system, or (ii) simulating the functionality of a device

system and modeling a biological system based on the environmental or other conditions the biological system is subject to, based on the operation of the device. Through an integrated approach, a truly unified model of the full experimental biomedical system is achieved. Ideally, through the successful integration of the two models in a medium such as SysML or UML, a developer from either the biological or engineering regime can access the model, adjust parameters relevant to the model, and determine the effects of such changes upon the operation of the system as a whole in terms of both its biological and device systems.

In order to achieve this final goal, future work must focus on two central areas. First, the use of various modeling mechanisms, such as the proposed Markov Modeling scheme presented here, must be explored and evaluated in further detail for efficacy, accuracy, and efficiency in modeling stochastic biological systems such as the bacterial biofilm system explored in this work. Secondly, the interfacing of a biological model, developed in a specific modeling paradigm or using a specific modeling method, with a physical system model must be addressed. While the development of individual models representing both the physical system and the biological system are critical for the unified design of biomedical devices for experimental applications, it is the integration of these two mechanisms that is required for the truly successful system engineering of device systems for experimental biomedical applications. Without such an interface, the disconnect between biological and engineering regimes is not truly addressed, thus leaving the development of biomedical devices to choose a stronghold in one regime or the other, without a truly integrated approach to optimized system design. By developing such an interface, or set of interfaces, however, the bridge between biological and system

domains is fully completed, and a new generation of biomedical devices optimized for their specific application can be pursued concurrently by both biologists and engineers.

5.5.2 Micro-BOAT System

Here we have demonstrated biofilm monitoring via CCD components to provide insight into both average and localized changes in biofilm optical density. Physical changes in biofilm structure, such as localized growth, detachment, or the aggregation of free-flowing biofilm particulates over an established biofilm structure are detectable using the microsystem, a principle advantage of this tool over currently available technologies. While other methods such as confocal microscopy may provide higher resolution of biofilm structure and morphology in comparison to the optical density approach presented here, biofilm measurements using these systems are limited strictly to end-point measurements in which the samples must be labeled and imaged after experiment completion. In comparison, the OD measurement demonstrated in this work through the integrated Micro-BOAT system is capable of performing label-free *in situ* biofilm measurement in order to provide additional information with respect to time-variant biofilm characteristics. Additionally, the Micro-BOAT system is capable of providing similar measurements as those achieved using other optical density tools, including commercially available spectrophotometers, and at a fraction of the cost of these systems [100]. While the device detection limit of the Micro-BOAT system (DL = 0.0019 AU_{CCD}) is less than that of commercially available systems, which typically have detection limits on the order of 0.01 AU_{SOD}, the low cost and ability of the Micro-BOAT to determine real-time net changes in optical density as opposed to end-point values

remains an advantage of this system. This method also enables the correlation of optical density measurements using the Micro-BOAT tool (OD_{CCD}) to other common methods, such as optical absorbance at 600 nm (OD_{SOD}), with limited calibration. As mentioned, a principle advantage of this tool lies in the capabilities of the system to monitor these changes spatially and in real-time. As shown in Figure 4.10, the Micro-BOAT is capable of performing full-channel imaging of the biofilm structures continuously in order to determine both average changes in the naturally variant biofilms, as well as changes with respect to biofilm morphology and surface coverage. The non-specific detection achieved through broad-spectrum optical density analysis makes this an ideal method for evaluating the efficacy of treatments, including the superpositioned bioelectric effect presented here, on a number of clinically relevant bacterial strains without the need for specialized labeling. The additional advantages enabled by the use of microfluidics in the Micro-BOAT system to reduce reagent volumes, increase testing rates and environmental control, and enable high-throughput testing substantiate this system as an advancement of current methods. Based on the advantages of optical density measurement using the Micro-BOAT system and the advantages of detecting biofilms grown and treated in microfluidic environments, the system can advance fundamental and drug discovery research efforts, including those aimed at the development of new biofilm treatment methods.

5.5.3 Superpositioned Bioelectric Effect Biofilm Treatment

Using the Micro-BOAT system as a testing instrument, this work has demonstrated improved efficacy of biofilm treatment at the microscale through the use of

an enhanced bioelectric effect that combines traditional antibiotic treatments with externally applied, SP electric fields. Using a superpositioned electric field characterized to be well within biocompatible limits and below the media electrolysis potential, this treatment produced repeatable results averaging a 167% greater reduction in bacterial biomass compared to traditional antibiotics as measured by the average change in biofilm OD for each treatment. Affirmation of these results using microscopy and image analysis reveals that this method not only reduces total biofilm mass, but also the ratio of live to dead cells within the remaining biofilms. Compared to standard antibiotic therapy using gentamicin, biofilms treated with the SP BE demonstrated a 56% increase in dead bacterial cell density. Such a metric is vital to quantifying the enhanced biofilm treatment of gentamicin in conjunction with the SP electric fields, as it enables the determination of a new MIC value for this specific treatment. While this value has not yet been determined, it is clear that the MIC of gentamicin for the SP BE is below both the current MIC of ~32 μg/mL and the gentamicin concentration utilized in this work of 10 μg/mL [101, 102]. The cumulative effect of biomass reduction and cell viability reduction using this enhanced treatment method suggests it is a strong candidate for future biofilm treatments, both clinical and non-clinical in nature.

While enhanced biofilm treatment using the SP BE has been demonstrated previously within our group at the macroscale using milliliter reagent volumes, the demonstration of this method at the microscale using a device featuring planar, thin-film electrodes encourages the prospective use of this technique for various clinical applications including the *in vivo* treatment of bacterial infections. The size reduction of the SP BE was a necessary transition in the realization of this method for these clinical

uses, since a microscale device is required for any implantable applications that arise. Additionally, scaling of the device dimensions to micrometer ranges was necessary in order to achieve the electric fields required for effective biofilm treatment while maintaining voltage potentials within biocompatible limits and below that of media electrolysis. By applying biocompatible electric fields in the presence of lower, sustainable doses of antibiotics, infection treatment efficacies are achievable that are traditionally realized only through the use of much higher antibiotic concentrations or invasive surgery. Additionally, current results suggest that the use of the SP BE can not only increase the efficacy of such treatments, but also the rate at which biofilm reduction takes place. As seen in Figure 8, treatment using the SP BE has a near immediate effect on biofilm mass, causing reductions within the first few hours of treatment, while therapy using antibiotics exclusively requires a longer period for treatment to commence, typically on the order of five to ten hours. The rapid onset of treatment using this new method can aid in early treatment of biofilm infections once detected, thereby mitigating the risks associated with such infections. Forward-looking applications of this treatment for *in vivo* applications can utilize micro-devices with integrated planar electrodes such as those featured in the Micro-BOAT system in order to achieve localized biofilm treatment in areas at high threat of bacterial biofilm development, such as medical implants, catheters, urinary tracts, dental cavities, and others. By applying localized treatment through the SP BE, antibiotic concentrations can be adjusted to sustainable levels by creating highly lethal concentrations of antibiotics in areas that have succumb to bacterial infections, thereby reducing the proliferation of antibiotic resistance, while limiting the

concentrations of these antibiotics in other areas within the body to much lower levels [103-105].

While the superpositioned bioelectric effect has demonstrated improved biofilm treatment efficacy in both macro- and micro-scaled applications, understanding of the fundamental mechanisms of this treatment method remains in preliminary stages. Recent work with respect to the bioelectric effect utilizing only DC electric fields suggests that the electrophoretic force induced by this electric field can create a gradient of the charged antibiotic molecules, thereby effectively forcing greater amounts of antibiotics into the biofilm structure [106-108]. Similarly, the application of an AC bioelectric effect is believed to increase the permeability of individual bacterial cells by inducing molecular vibrations in the cell membranes, thus enabling antibiotics to infiltrate and affect bacteria more readily [109, 110]. Building upon these suggestions from the literature, by combining these two mechanisms one can both increase the concentration of antibiotics within the targeted biofilm (DC component) as well as the effectiveness of these antibiotics by enabling them to more readily affect bacteria comprising the biofilm (AC component). This notion supports future work to improve the efficacy of the SP BE to achieve treatment levels on par with the biofilm reduction observed in macroscale applications, which demonstrated efficacy on the order of two orders of magnitude reduction in biofilm mass [45]. While these macroscale applications utilized uniformly distributed electric fields perpendicular to the biofilm growth substrate, the Micro-BOAT features 0.2 µm planar thin-film gold electrodes in a 100 µm deep microfluidic channel, thereby inducing a non-uniform electric field within the microchannel [111]. The applied electric field decreases in intensity from the channel substrate towards the top of the

channel due to the inversely proportional relationship between field intensity and distance from the electrodes. Although the induction of a non-uniform electric field toward the top area of the channel reduces the biocidal effects of the SP BE compared to the uniformly applied field utilized in macroscale experiments, the thin-film electrodes utilized by this system enable a reduction in device dimensions that is critical for future implantable treatment system development [94]. Therefore, the future implementation of electrodes capable of uniform electric field induction may further enhance the efficacy of this treatment method at the microscale, in turn allowing the further reduction of antibiotic concentrations required for effective localized biofilm treatment.

Chapter 6: Summary and Future Direction

6.1 Research Summary

Two principle thrusts were pursued through this research work: (1) the development of a Micro-BOAT system for biofilm investigations including those for drug discovery, and (2) the adaptation of a novel SP BE to the microscale to enable future applications of this method for bacterial infection treatment. Overall, both of these goals have been demonstrated through this work and provide a strong basis for the future development of microsystems for drug discovery applications and the continued investigation of the SP BE for antimicrobial infection treatments in clinical applications.

The developed Micro-BOAT device is an integrated system that provides a microfluidic environment for bacterial biofilm growth offering added control of experimental growth conditions, of expediting drug screening processes through parallel testing and reduced assay times, and of decreasing the cost of drug screening efforts by reducing necessary reagent volumes. Through the use of one-dimensional linear array charge-coupled devices integrated with the microfluidic biofilm growth chambers, optical density monitoring of biofilm growth and treatment is achieved that enables the non-invasive, real-time, label-free measurement of biofilms *in situ*. This capacity constitutes a novel capability of this technique providing critical advancements over established methods including confocal microscopy and spectroscopy by commercially available systems. By integrating these devices with external software, six parallel experiments contained on a single chip can be monitored and measured simultaneously. The system demonstrated an OD detection limit of 0.0019 AU_{CCD}, which enables the spatiotemporal tracking of average changes in bacterial growth and correlates to an OD_{600} detection limit

of 0.095 AU_{SOD}. The capability of the Micro-BOAT system to monitor these spatiotemporal changes in biofilm optical density provides further insight into the stochastic nature of bacterial biofilms during growth and treatment that is currently unavailable using established monitoring methods. The ability of the system to perform such measurements continuously and in real-time is a principle advantage of the Micro-BOAT system over current methods, which are typically limited to end-point biofilm measurements. Overall, the Micro-BOAT represents a stand-alone system capable of the parallel growth and treatment of bacterial biofilms and temporal, spatially realized monitoring of biofilms through an optical density approach providing added capabilities over currently available technologies.

By integrating planar, thin-film gold electrodes with the microfluidic channels of the Micro-BOAT system, an enhanced biofilm treatment method utilizing superpositioned AC and DC electric fields in the presence of antibiotics was demonstrated showing significantly improved efficacy over traditional antibiotic treatments. On average, biofilms treated using the SP BE showed a 167% reduction in overall biomass compared to traditional antibiotic therapies, as measured by the change in biofilm optical density during experimental treatments. In addition to the improved biomass reduction realized through this method, biofilms treated with the SP BE also display a reduction in cell viability following treatment. Fluorescence microscopy studies performed at the conclusion of biofilm experiments display that those samples treated by the SP BE average a 56% increase in dead cell density compared to traditional antibiotic therapies using only gentamicin. The on-chip validation of this method in a microscale device has far-reaching impacts by enabling its use for future clinical

applications, including the treatment of bacterial infections. Reduction of electrode geometries to the micrometer regime enables the treatment mechanism for implantable devices, while the small size of these structures allows the potentials required for the SP BE to be reduced to levels within biocompatible limits and below media electrolysis. Overall, the demonstration of the SP BE utilizing thin-film electrodes in a microsystem directs the further development of an implantable device for *in vivo* biofilm infection treatment, while the Micro-BOAT as a whole represents a new research tool for scientific biofilm studies including drug discovery and antimicrobial mechanism investigations.

Throughout the development phase of this work, systems engineering analyses played a vital role in the design and characterization of system components and their integration. Thorough requirements analysis of the proposed system resulted in a modular architecture comprised of: (1) a PCB base to house parallel CCD components and supporting electronics, (2) a transparent substrate with micropatterned gold electrodes to limit light extraneous to the OD measurement and apply the SP electric fields, and (3) a PDMS-based microfluidic module to provide biofilm growth chambers. Low-level modeling of optical, fluidic, electromagnetic, and electronic components verified proper system operation and enabled optimization of component design parameters. The top-down approach utilized in this work achieved full system integration of the various modules and software resulting in a novel tool for the spatiotemporal monitoring of bacterial biofilms. As discussed in the following section, this architecture is adaptable to future generations of the device system to enable expanded capabilities of the Micro-BOAT without complete system redesign, a critical advantage of the system-level development performed in this work.

6.2 Future Research Directions

The work presented here provides a foundation for the future advancement of technologies relating to both biofilm optical density measurement in devices such as the Micro-BOAT, as well as those relating to enhanced biofilm treatment using the SP BE. By advancing these two areas through short- and long-term goals, the benefits of this engineering research can have far reaching impacts on the biomedical field with respect to scientific studies of bacterial biofilms, including antibiotic development applications, and the emergence of new treatment methods for bacterial infections.

With respect to the Micro-BOAT system and similar devices utilizing CCD components in microsystems to perform optical density monitoring of bacterial biofilms, short-term research directions primarily concern increasing the reliability and precision of the system, as well as the expansion of detection capabilities to two dimensions. While the theoretical noise limits of many CCD ICs lies in the sub-millivolt range, the current system is subject to slightly higher noise levels on the order of several millivolts due to the circuitry and external wiring required to support the Micro-BOAT system. By lowering these noise levels, optical density detection limits can be reduced, thereby increasing the sensitivity of the biofilm monitoring system. Similarly, improvements in the methodology used to drive the CCD system and sample optical density measurements can improve device performance and overall system reliability. To achieve these improvements, several key areas should be addressed including: (1) synchronization of the LED light source and CCD activation to produce a discrete light pulse as opposed to the currently used continuous lighting, (2) synchronization of CCD drive clock, serial input, and sampling, and (3) integration of an improved data acquisition card capable of

parallel channel sampling (as opposed to the single channel sampling capability of the current DAQ) and of sampling rates well above the Nyquist rate of the CCD output. Additional studies may also investigate variations in the geometry of the microfluidic biofilm growth chambers in order to optimize the system for biofilm growth. In doing so, treatment efficacies can be more readily detected by the system, since thicker, more developed biofilms will display a greater change in optical density if effectively treated. In order to increase the precision of the system, light filters or gratings may be useful in reducing the effects of light scattering, which provides a current limitation in the ability of the device to detect changes in OD of biofilm located directly above a particular CCD pixel. Finally, the short-term adaptation of the current system to accommodate a two-dimensional CCD component is also of immediate interest, since the use of such a device to perform biofilm monitoring can provide additional data, including such metrics as average biofilm surface coverage, not achievable using the current linear array device.

In the long-term, microsystems such as the integrated Micro-BOAT system presented here should be fully enclosed systems requiring minimal user interaction to perform precisely guided experiments. On-chip fluidic reservoirs and lighting will eliminate the current needs for external equipment, thereby enabling a fully autonomous lab-on-a-chip device. Additionally, the integration of microfabricated photopixels on the device substrate can enable improved biofilm optical density monitoring by providing precise sensor alignment, higher sensitivity, and reduced reliance on external components.

Future work in the development of the superpositioned bioelectric effect concerns, in the near term, investigation of the mechanism of this method that leads to

enhanced biofilm treatment and further confirmation of its biocompatibility for clinical applications. While the results presented here provide strong support of this method for the prevention and treatment of bacterial infections, the precise mechanism leading to the increased efficacy of antibiotics when in the presence of AC and DC electric fields is not yet fully understood. Before clinical applications of this method can be pursued in earnest, the mechanism of treatment enhancement must be investigated and its origins fully understood. Building upon this immediate need, other future work must investigate the biocompatibility and possible side effects of this treatment method as applicable to clinical applications.

With these areas satisfied, the long-term research focus of the SP BE concerns the integration of this method in medical devices for the localized treatment of bacterial infections *in vivo*. By implementing this treatment method for clinical applications, such as on medical implants or catheters, a new era of biofilm treatment may be realized that can reduce the health risks of surgery and of bacterial infections, limit the required intake of antibiotics in infected patients, and stunt the proliferation of antibiotic resistive bacteria in the clinical realm. Towards this goal, preliminary work in the verification of this treatment method can pursue the integration of thin-film surface electrodes on microscale devices, followed by testing in both *in vitro* and *in vivo* environments in order to determine the feasibility of this method for future clinical patient treatment.

Appendix A – TAOS TSL202R Specification

Device Functionality:

Functional Block Diagram (each section — pin numbers apply to section 1)

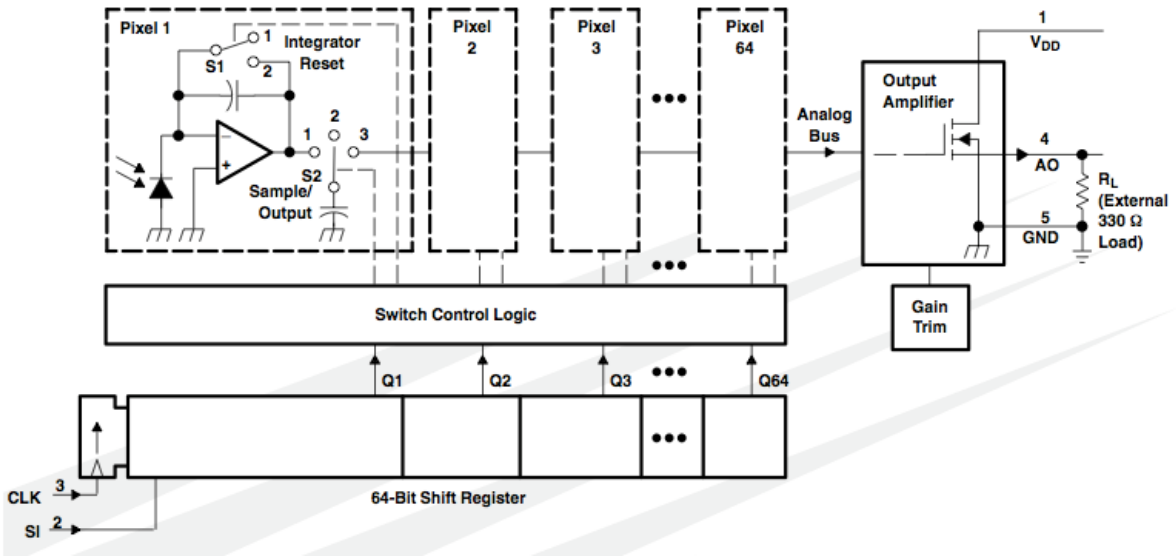

Device Terminal Functions and Wiring Diagram

TERMINAL NAME	TERMINAL NO.	DESCRIPTION
AO1	4	Analog output of section 1
AO2	8	Analog output of section 2
CLK	3	Clock. Clk controls charge transfer, pixel output, and reset.
GND	5,12	Ground (substrate). All voltages are referenced to GND.
NC	7, 9, 11, 14	No internal connection
SI1	2	Serial input (section 1). SI1 defines the start of the data-out sequence.
SI2	10	Serial input (section 2). SI2 defines the start of the data-out sequence.
SO1	13	Serial output (section 1). SO1 provides a signal to drive the SI2 input.
SO2	6	Serial output (section 2). SO2 provides a signal to drive the SI input of another device for cascading or as an end-of-data indication.
V_{DD}	1	Supply voltage. Supply voltage for both analog and digital circuitry.

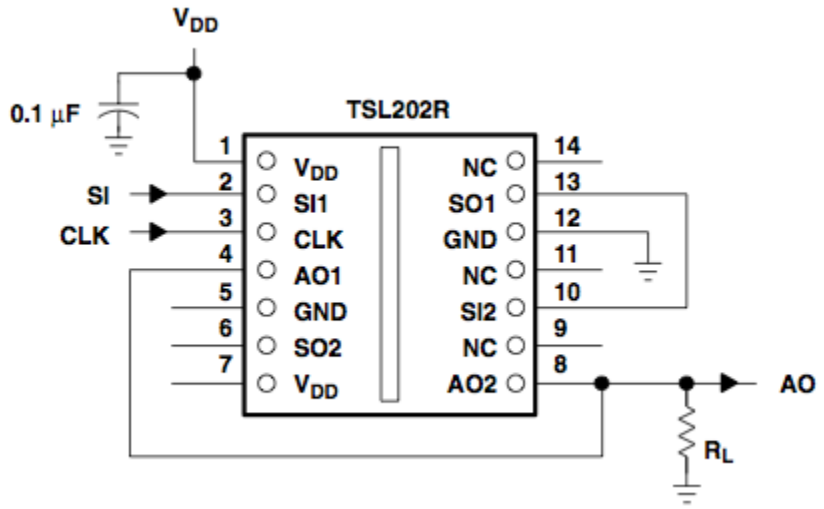

Device Timing and Actuation

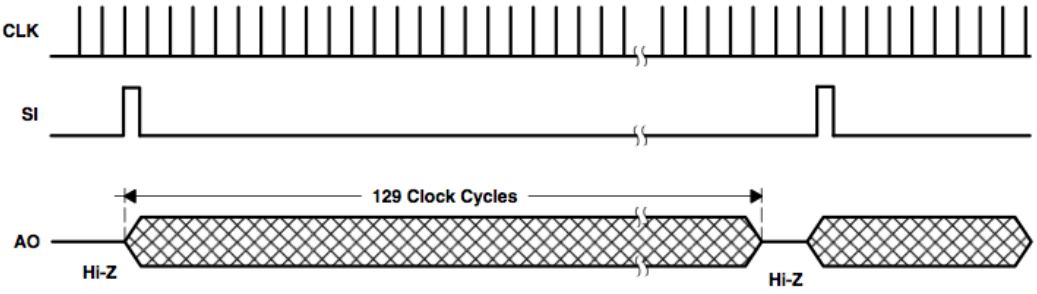

Figure 1. Timing Waveforms

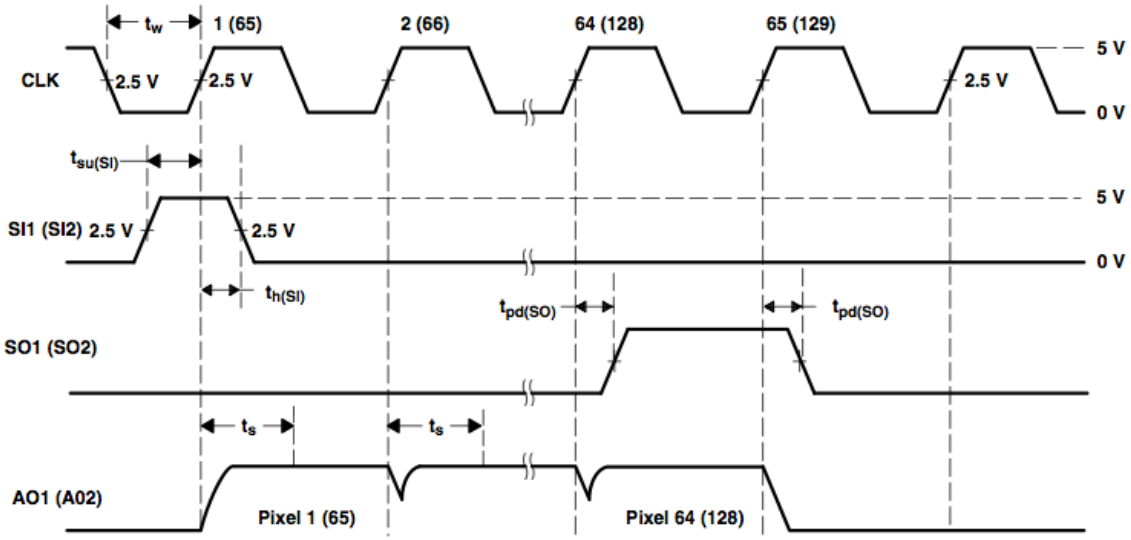

Figure 2. Operational Waveforms (each section)

Device Sensitivity and Output Settling Times

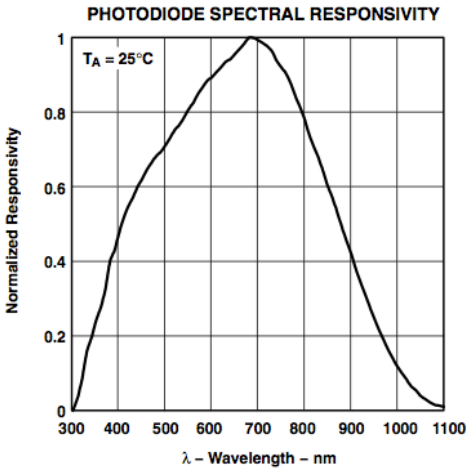

Figure 3

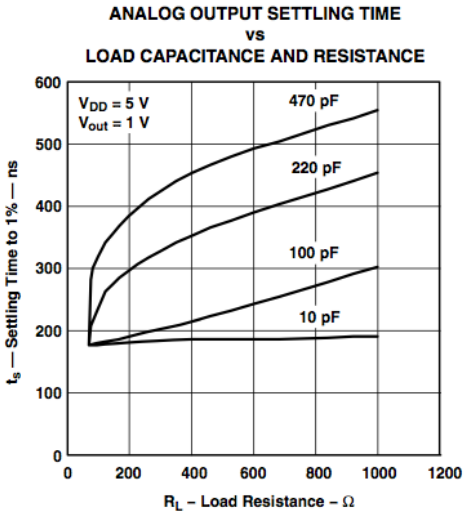

Figure 4

Device Dimensions

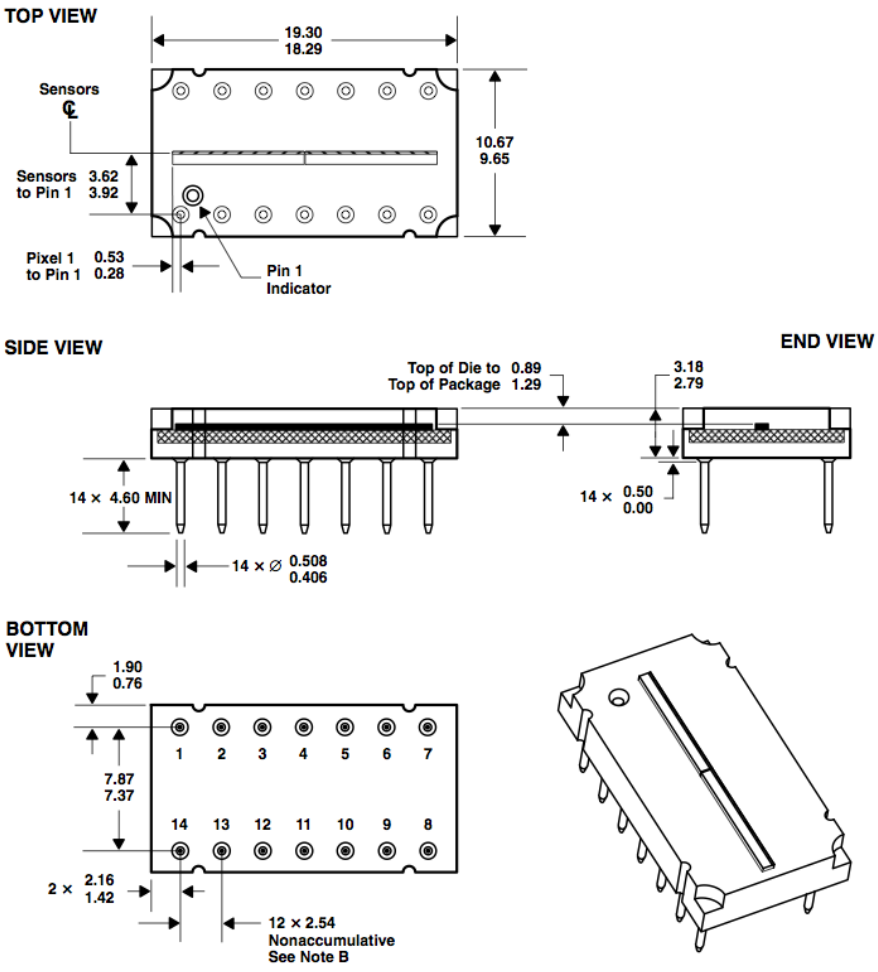

Appendix B – Biofilm Simulation using the Markov Chain Modeling Tool

```
Machine: Nutrient
  State: low labels: level=low
    p[low] = 1/2, p[high]=1/2
  State: high labels: level=high
    p[low] = 1/2, p[high]=1/2

Machine: ShearStress
  State: low labels: level=low
    p[low] = 1/2, p[high]=1/2
  State: high labels: level=high
    p[low] = 1/2, p[high]=1/2

Machine: Film0
  State: little labels: level=little
    if (Nutrient::level=low /\ ShearStress::level=low) \/ (Nutrient::level=high /\
ShearStress::level=high)
      if   Film1::level=little       p[little] = 4/5, p[moderate] = 1/5
      else if Film1::level=moderate  p[little] = 1/2, p[moderate] = 1/2
      else                           p[little] = 1/5, p[moderate] = 4/5
    else if Nutrient::level=high /\ ShearStress::level=low  // growth
      if      Film1::level=little    p[little] = 1/2, p[moderate] = 1/2
      else if Film1::level=moderate  p[little] = 1/5, p[moderate] = 4/5
      else                           p[little] = 1/10, p[moderate] = 9/10
    else  // nutrient low shear high // inhibit
      if      Film1::level=little    p[little] = 9/10, p[moderate] = 1/10
      else if Film1::level=moderate  p[little] = 4/5, p[moderate] = 1/5
      else                           p[little] = 7/10, p[moderate] = 3/10
  State: moderate labels: level=moderate
    if (Nutrient::level=low /\ ShearStress::level=low) \/ (Nutrient::level=high /\
ShearStress::level=high)
      if   Film1::level=little       p[little] = 3/5, p[moderate] = 3/10, p[large] = 1/10
      else if Film1::level=moderate  p[little] = 3/10, p[moderate] = 2/5, p[large] = 3/10
      else                           p[little] = 1/5, p[moderate] = 3/10, p[large] = 1/2
    else if Nutrient::level=high /\ ShearStress::level=low  // growth
      if   Film1::level=little       p[little] = 3/10, p[moderate] = 2/5, p[large] = 3/10
      else if Film1::level=moderate  p[little] = 1/5, p[moderate] = 2/5, p[large] = 2/5
      else                           p[little] = 1/10, p[moderate] = 3/10, p[large] = 3/5
    else  // nutrient low shear high // inhibit
      if   Film1::level=little       p[little] = 1/2, p[moderate] = 2/5, p[large] = 1/10
      else if Film1::level=moderate  p[little] = 3/10, p[moderate] = 1/2, p[large] = 1/5
      else                           p[little] = 1/5, p[moderate] = 1/2, p[large] = 3/10
  State: large labels: level=large
    if (Nutrient::level=low /\ ShearStress::level=low) \/ (Nutrient::level=high /\
ShearStress::level=high)
      if   Film1::level=little       p[moderate] = 4/5, p[large] = 1/5
      else if Film1::level=moderate  p[moderate] = 3/5, p[large] = 2/5
      else                           p[moderate] = 3/10, p[large] = 7/10
    else if Nutrient::level=high /\ ShearStress::level=low  // growth
      if   Film1::level=little       p[moderate] = 3/5, p[large] = 2/5
      else if Film1::level=moderate  p[moderate] = 3/10, p[large] = 7/10
      else                           p[moderate] = 1/10, p[large] = 9/10
```

```
    else  // nutrient low shear high // inhibit
      if   Film1::level=little       p[moderate] = 9/10, p[large] = 1/10
      else if Film1::level=moderate  p[moderate] = 3/5, p[large] = 2/5
      else                           p[moderate] = 1/2, p[large] = 1/2

Machine: Film1
  State: little labels: level=little
    if (Nutrient::level=low /\ ShearStress::level=low) \/ (Nutrient::level=high /\
ShearStress::level=high)
      if   Film2::level=little       p[little] = 4/5, p[moderate] = 1/5
      else if Film2::level=moderate  p[little] = 1/2, p[moderate] = 1/2
      else                           p[little] = 1/5, p[moderate] = 4/5
    else if Nutrient::level=high /\ ShearStress::level=low  // growth
      if      Film2::level=little    p[little] = 1/2, p[moderate] = 1/2
      else if Film2::level=moderate  p[little] = 1/5, p[moderate] = 4/5
      else                           p[little] = 1/10, p[moderate] = 9/10
    else  // nutrient low shear high // inhibit
      if      Film2::level=little    p[little] = 9/10, p[moderate] = 1/10
      else if Film2::level=moderate  p[little] = 4/5, p[moderate] = 1/5
      else                           p[little] = 7/10, p[moderate] = 3/10
  State: moderate labels: level=moderate
    if (Nutrient::level=low /\ ShearStress::level=low) \/ (Nutrient::level=high /\
ShearStress::level=high)
      if   Film2::level=little       p[little] = 3/5, p[moderate] = 3/10, p[large] = 1/10
      else if Film2::level=moderate  p[little] = 3/10, p[moderate] = 2/5, p[large] = 3/10
      else                           p[little] = 1/5, p[moderate] = 3/10, p[large] = 1/2
    else if Nutrient::level=high /\ ShearStress::level=low  // growth
      if   Film2::level=little       p[little] = 3/10, p[moderate] = 2/5, p[large] = 3/10
      else if Film2::level=moderate  p[little] = 1/5, p[moderate] = 2/5, p[large] = 2/5
      else                           p[little] = 1/10, p[moderate] = 3/10, p[large] = 3/5
    else  // nutrient low shear high // inhibit
      if   Film2::level=little       p[little] = 1/2, p[moderate] = 2/5, p[large] = 1/10
      else if Film2::level=moderate  p[little] = 3/10, p[moderate] = 1/2, p[large] = 1/5
      else                           p[little] = 1/5, p[moderate] = 1/2, p[large] = 3/10
  State: large labels: level=large
    if (Nutrient::level=low /\ ShearStress::level=low) \/ (Nutrient::level=high /\
ShearStress::level=high)
      if   Film2::level=little       p[moderate] = 4/5, p[large] = 1/5
      else if Film2::level=moderate  p[moderate] = 3/5, p[large] = 2/5
      else                           p[moderate] = 3/10, p[large] = 7/10
    else if Nutrient::level=high /\ ShearStress::level=low  // growth
      if   Film2::level=little       p[moderate] = 3/5, p[large] = 2/5
      else if Film2::level=moderate  p[moderate] = 3/10, p[large] = 7/10
      else                           p[moderate] = 1/10, p[large] = 9/10
    else  // nutrient low shear high // inhibit
      if   Film2::level=little       p[moderate] = 9/10, p[large] = 1/10
      else if Film2::level=moderate  p[moderate] = 3/5, p[large] = 2/5
      else                           p[moderate] = 1/2, p[large] = 1/2

Machine: Film2
  State: little labels: level=little
    if (Nutrient::level=low /\ ShearStress::level=low) \/ (Nutrient::level=high /\
ShearStress::level=high)
      if   Film3::level=little       p[little] = 4/5, p[moderate] = 1/5
```

```
      else if Film3::level=moderate  p[little] = 1/2, p[moderate] = 1/2
      else                           p[little] = 1/5, p[moderate] = 4/5
    else if Nutrient::level=high /\ ShearStress::level=low  // growth
      if      Film3::level=little    p[little] = 1/2, p[moderate] = 1/2
      else if Film3::level=moderate  p[little] = 1/5, p[moderate] = 4/5
      else                           p[little] = 1/10, p[moderate] = 9/10
    else  // nutrient low shear high // inhibit
      if      Film3::level=little    p[little] = 9/10, p[moderate] = 1/10
      else if Film3::level=moderate  p[little] = 4/5, p[moderate] = 1/5
      else                           p[little] = 7/10, p[moderate] = 3/10
  State: moderate labels: level=moderate
    if (Nutrient::level=low /\ ShearStress::level=low) \/ (Nutrient::level=high /\
ShearStress::level=high)
      if   Film3::level=little       p[little] = 3/5, p[moderate] = 3/10, p[large] = 1/10
      else if Film3::level=moderate  p[little] = 3/10, p[moderate] = 2/5, p[large] = 3/10
      else                           p[little] = 1/5, p[moderate] = 3/10, p[large] = 1/2
    else if Nutrient::level=high /\ ShearStress::level=low  // growth
      if   Film3::level=little       p[little] = 3/10, p[moderate] = 2/5, p[large] = 3/10
      else if Film3::level=moderate  p[little] = 1/5, p[moderate] = 2/5, p[large] = 2/5
      else                           p[little] = 1/10, p[moderate] = 3/10, p[large] = 3/5
    else  // nutrient low shear high // inhibit
      if   Film3::level=little       p[little] = 1/2, p[moderate] = 2/5, p[large] = 1/10
      else if Film3::level=moderate  p[little] = 3/10, p[moderate] = 1/2, p[large] = 1/5
      else                           p[little] = 1/5, p[moderate] = 1/2, p[large] = 3/10
  State: large labels: level=large
    if (Nutrient::level=low /\ ShearStress::level=low) \/ (Nutrient::level=high /\
ShearStress::level=high)
      if   Film3::level=little       p[moderate] = 4/5, p[large] = 1/5
      else if Film3::level=moderate  p[moderate] = 3/5, p[large] = 2/5
      else                           p[moderate] = 3/10, p[large] = 7/10
    else if Nutrient::level=high /\ ShearStress::level=low  // growth
      if   Film3::level=little       p[moderate] = 3/5, p[large] = 2/5
      else if Film3::level=moderate  p[moderate] = 3/10, p[large] = 7/10
      else                           p[moderate] = 1/10, p[large] = 9/10
    else  // nutrient low shear high // inhibit
      if   Film3::level=little       p[moderate] = 9/10, p[large] = 1/10
      else if Film3::level=moderate  p[moderate] = 3/5, p[large] = 2/5
      else                           p[moderate] = 1/2, p[large] = 1/2

Machine: Film3
  State: little labels: level=little
    if (Nutrient::level=low /\ ShearStress::level=low) \/ (Nutrient::level=high /\
ShearStress::level=high)
      if   Film4::level=little       p[little] = 4/5, p[moderate] = 1/5
      else if Film4::level=moderate  p[little] = 1/2, p[moderate] = 1/2
      else                           p[little] = 1/5, p[moderate] = 4/5
    else if Nutrient::level=high /\ ShearStress::level=low  // growth
      if      Film4::level=little    p[little] = 1/2, p[moderate] = 1/2
      else if Film4::level=moderate  p[little] = 1/5, p[moderate] = 4/5
      else                           p[little] = 1/10, p[moderate] = 9/10
    else  // nutrient low shear high // inhibit
      if      Film4::level=little    p[little] = 9/10, p[moderate] = 1/10
      else if Film4::level=moderate  p[little] = 4/5, p[moderate] = 1/5
      else                           p[little] = 7/10, p[moderate] = 3/10
```

```
  State: moderate labels: level=moderate
    if (Nutrient::level=low /\ ShearStress::level=low) \/ (Nutrient::level=high /\
ShearStress::level=high)
      if   Film4::level=little       p[little] = 3/5, p[moderate] = 3/10, p[large] = 1/10
      else if Film4::level=moderate  p[little] = 3/10, p[moderate] = 2/5, p[large] = 3/10
      else                           p[little] = 1/5, p[moderate] = 3/10, p[large] = 1/2
    else if Nutrient::level=high /\ ShearStress::level=low  // growth
      if   Film4::level=little       p[little] = 3/10, p[moderate] = 2/5, p[large] = 3/10
      else if Film4::level=moderate  p[little] = 1/5, p[moderate] = 2/5, p[large] = 2/5
      else                           p[little] = 1/10, p[moderate] = 3/10, p[large] = 3/5
    else  // nutrient low shear high // inhibit
      if   Film4::level=little       p[little] = 1/2, p[moderate] = 2/5, p[large] = 1/10
      else if Film4::level=moderate  p[little] = 3/10, p[moderate] = 1/2, p[large] = 1/5
      else                           p[little] = 1/5, p[moderate] = 1/2, p[large] = 3/10
  State: large labels: level=large
    if (Nutrient::level=low /\ ShearStress::level=low) \/ (Nutrient::level=high /\
ShearStress::level=high)
      if   Film4::level=little       p[moderate] = 4/5, p[large] = 1/5
      else if Film4::level=moderate  p[moderate] = 3/5, p[large] = 2/5
      else                           p[moderate] = 3/10, p[large] = 7/10
    else if Nutrient::level=high /\ ShearStress::level=low  // growth
      if   Film4::level=little       p[moderate] = 3/5, p[large] = 2/5
      else if Film4::level=moderate  p[moderate] = 3/10, p[large] = 7/10
      else                           p[moderate] = 1/10, p[large] = 9/10
    else  // nutrient low shear high // inhibit
      if   Film4::level=little       p[moderate] = 9/10, p[large] = 1/10
      else if Film4::level=moderate  p[moderate] = 3/5, p[large] = 2/5
      else                           p[moderate] = 1/2, p[large] = 1/2

Machine: Film4
  State: little labels: level=little
    if (Nutrient::level=low /\ ShearStress::level=low) \/ (Nutrient::level=high /\
ShearStress::level=high)
      if   Film0::level=little       p[little] = 4/5, p[moderate] = 1/5
      else if Film0::level=moderate  p[little] = 1/2, p[moderate] = 1/2
      else                           p[little] = 1/5, p[moderate] = 4/5
    else if Nutrient::level=high /\ ShearStress::level=low  // growth
      if      Film0::level=little    p[little] = 1/2, p[moderate] = 1/2
      else if Film0::level=moderate  p[little] = 1/5, p[moderate] = 4/5
      else                           p[little] = 1/10, p[moderate] = 9/10
    else  // nutrient low shear high // inhibit
      if      Film0::level=little    p[little] = 9/10, p[moderate] = 1/10
      else if Film0::level=moderate  p[little] = 4/5, p[moderate] = 1/5
      else                           p[little] = 7/10, p[moderate] = 3/10
  State: moderate labels: level=moderate
    if (Nutrient::level=low /\ ShearStress::level=low) \/ (Nutrient::level=high /\
ShearStress::level=high)
      if   Film0::level=little       p[little] = 3/5, p[moderate] = 3/10, p[large] = 1/10
      else if Film0::level=moderate  p[little] = 3/10, p[moderate] = 2/5, p[large] = 3/10
      else                           p[little] = 1/5, p[moderate] = 3/10, p[large] = 1/2
    else if Nutrient::level=high /\ ShearStress::level=low  // growth
      if   Film0::level=little       p[little] = 3/10, p[moderate] = 2/5, p[large] = 3/10
      else if Film0::level=moderate  p[little] = 1/5, p[moderate] = 2/5, p[large] = 2/5
      else                           p[little] = 1/10, p[moderate] = 3/10, p[large] = 3/5
```

```
    else  // nutrient low shear high // inhibit
      if   Film0::level=little       p[little] = 1/2, p[moderate] = 2/5, p[large] = 1/10
      else if Film0::level=moderate  p[little] = 3/10, p[moderate] = 1/2, p[large] = 1/5
      else                           p[little] = 1/5, p[moderate] = 1/2, p[large] = 3/10
  State: large labels: level=large
    if (Nutrient::level=low /\ ShearStress::level=low) \/ (Nutrient::level=high /\
ShearStress::level=high)
      if   Film0::level=little       p[moderate] = 4/5, p[large] = 1/5
      else if Film0::level=moderate  p[moderate] = 3/5, p[large] = 2/5
      else                           p[moderate] = 3/10, p[large] = 7/10
    else if Nutrient::level=high /\ ShearStress::level=low  // growth
      if   Film0::level=little       p[moderate] = 3/5, p[large] = 2/5
      else if Film0::level=moderate  p[moderate] = 3/10, p[large] = 7/10
      else                           p[moderate] = 1/10, p[large] = 9/10
    else  // nutrient low shear high // inhibit
      if   Film0::level=little       p[moderate] = 9/10, p[large] = 1/10
      else if Film0::level=moderate  p[moderate] = 3/5, p[large] = 2/5
      else                           p[moderate] = 1/2, p[large] = 1/2
```

Appendix C – Optical Density Measurement MATLAB Analysis Scripts

```
%MATLAB SCRIPT TO CREATE 3D WATERFALL IMAGE OF TREATMENT O.D. DATA

%Grab file data and set variables
close all;
data = DLMREAD('File_Name.csv', ',');     %read in the .CSV file

x=186;      %SET X TO BE THE NUMBER OF SAMPLES PER GRAB!
y=8;        %SET Y TO BE THE NUMBER OF MINUTES BETWEEN EACH SAMPLE GRAB!

%1st Task: Organize data into matrix that MATLAB can work with
[A, B]=size(data);            %create 2x1 matrix with A= # rows, B= #
columns voltage=zeros(x, A/x);
                              %voltage is 2D array with x rows and
                              (A/x) columns, which is the number of
                              times I have grabbed data (x = number of
                              samples per grab).  'zeros' initializes
                              the array to all 0s
timestamp=0;                  %initialize time = 0 as a starting point

values = zeros(A,3);

c=1; d=1;                     %counters
j=1;

timestamp=0:(y/60):((((A/x)-1)*y)/60);
                              %first value is that the experiment
                              starts at t=0.  middle value (increment)
                              is the fraction of an hour between each
                              grab.  Last value is the final grab time
                              in hours.
Position=(0:1:(x-1))*84.9/1000;
                              %first term divides the data points into
                              a   physical location. second term
                              multiplies each location by a distance
                              along the channel


p=1;
q=1;
t=1;                          %counters

%2nd Task: Perform data analysis on the formatted matrix
for S = 1:A                   %start at top of the csv file, parse down
    values(S,2) = (x*(84.9/1000))-(p*(84.9/1000));
                              %write the position value (x-axis) as a
                              multiple of (p*length of each pixel)
    values(S,1) = (q*(y/60));
                              %write the time value (y-axis)as a
                              multiple of (q*hours between grabs)
    values(S,3)=abs(log10(data(S,3)/data(p,3)));
```

```
                                %calculate change in OD for the z-axis
                                (data) || value next to data(S,#) is the
                                column with the needed data
    p=p+1;
        if p==(x+1)
            p=1;
            q=q+1;
        end
end

%3rd Task: Plot the O.D. data using MATLAB and the GridFit Plug-In
pos=values(:,2);
time=values(:,1);
od=values(:,3);

gx=(0:2:(x-1))*84.9/1000;
gy=0:(y/30):((((A/x)-1)*y)/60);

g=gridfit(time,pos,od,gy,gx,'smoothness',[25 3]);
figure
colormap(jet(256));
surf(gy,gx,g);
camlight right;
lighting phong;
shading interp

xlabel('Time (hr)')
ylabel('Position (mm)')
zlabel('Change in Optical Density (AU)')
title('Test_Title')

%4th Task: Save the output data for future use and analysis
output=[0 timestamp; Position' voltage];

dlmwrite('dataoutput.csv',output,',')
```

```
%MATLAB SCRIPT TO CREATE TIMELAPSE IMAGES FOR GIF ANIMATION

%Grab file data and set variables
close all;
data = DLMREAD('File_Name.csv', ',');     %Read in the .CSV data file

x=186;          %SET X TO BE THE NUMBER OF SAMPLES PER GRAB!
y=0.016;        %SET Y TO BE THE NUMBER OF MINUTES BETWEEN EACH SAMPLE
GRAB!
device=2;       %SET TO THE COLUMN OF THE CSV WITH THE DEVICE DATA

%1st Task: Organize data into a matrix that MATLAB can work with
[A, B]=size(data);            %create 2x1 matrix with A= # rows, B= #
columns
voltage=zeros(x, A/x);
                              %voltage is 2D array with x rows and
                              (A/x) columns which is the number of
                              times I have grabbed data (x = number of
                              samples per grab).  'zeros' initializes
                              the array to all 0s
averageold = [];
timestamp=0;                  %initialize time = 0 as a starting point

c=1;
d=1;
j=1;                          %counters


timestamp=0:(y/60):((((A/x)-1)*y)/60);
                              %first value is that the experiment
                              starts at t=0.  Middle value (increment)
                              is the fraction of an hour between each
                              grab.  Last value is the final grab time
                              in hours.
Position=(0:1:(x-1))*84.9/1000;
                              %First term is divides the data points
                              into a physical location. Second term
                              multiplies each location by a distance
                              along the channel

%2nd Task: Perform data analysis and plot each O.D. image
for R = 1:A
voltage((x+1)-j,c)=abs(log10(data(R,device)/data(j,device)));
                              %voltage((x+1)-j,c) flips the order of
                              the pixels so they are in their real
                              locations (data reads out in reverse
                              order)
    j=j+1;
        if j==(x+1)

            yy = smooth(voltage(:,c), 101, 'sgolay', 2);

            %Plot and store each O.D. image
            area(Position, yy, 'FaceColor', [1 0 0]);
            axis([ 0 15.73 0 0.2]);
```

```
            xlabel('Position (mm)', 'FontSize', 14);
            ylabel('Change in Optical Density (AU)', 'FontSize', 14);
            title('Spatiotemporal Detection via Micro-BOAT',
            'FontSize', 14);
            set(gcf, 'color', 'white');
            set(gcf, 'PaperSize', [10 6]);
            set(gca, 'color', [.99 .99 .985]);
                  %This color code creates a white background!!!
            drawnow;
            pause(0.0)
            j=1;
            c=c+1;

            %Store the generated image
            frame = getframe(gcf);
            frameasimg = frame2im(frame);
            imwrite(frameasimg, sprintf('spatialtest%d.tif', (c-1)),
            'tiff');


            %3rd Task: Plot and store average OD at each time point
            avgod = mean(voltage(:,(c-1)));
            timestep = (c-1)*y;
            averagenew = [averageold ; timestep avgod];
            averageold = averagenew;
            avgavg = smooth(averagenew(:,2), 11, 'sgolay', 2);

            plot((averagenew(:,1)), avgavg,'r', 'LineWidth', [2.0]);
            axis([0 3 0 .1]);
            xlabel('Time (min)', 'FontSize', 14);
            ylabel('Averaged Change in O.D. (AU)', 'FontSize', 14);
            title('Average Change in OD with Time', 'FontSize', 14);
            set(gcf, 'color', 'white');
            set(gcf, 'PaperSize', [10 6]);
            set(gca, 'color', [.99 .99 .985]);
                  %This color code creates a white background!!!
            drawnow;

            %Store the generated image
            frameavg = getframe(gcf);
            frameavgimg = frame2im(frameavg);
            imwrite(frameavgimg, sprintf('avgtest%d.tif', (c-1)),
            'tiff');

      end

end
```

Appendix D – LabVIEW Control Program

Note: This appendix supplies low-level coding of the various LabVIEW functions required to perform data acquisition and analysis. High-level LabVIEW operation is provided in Figure X.X of this thesis.

Section A: Data Storage File Initialization

1 of 2: File Initialization

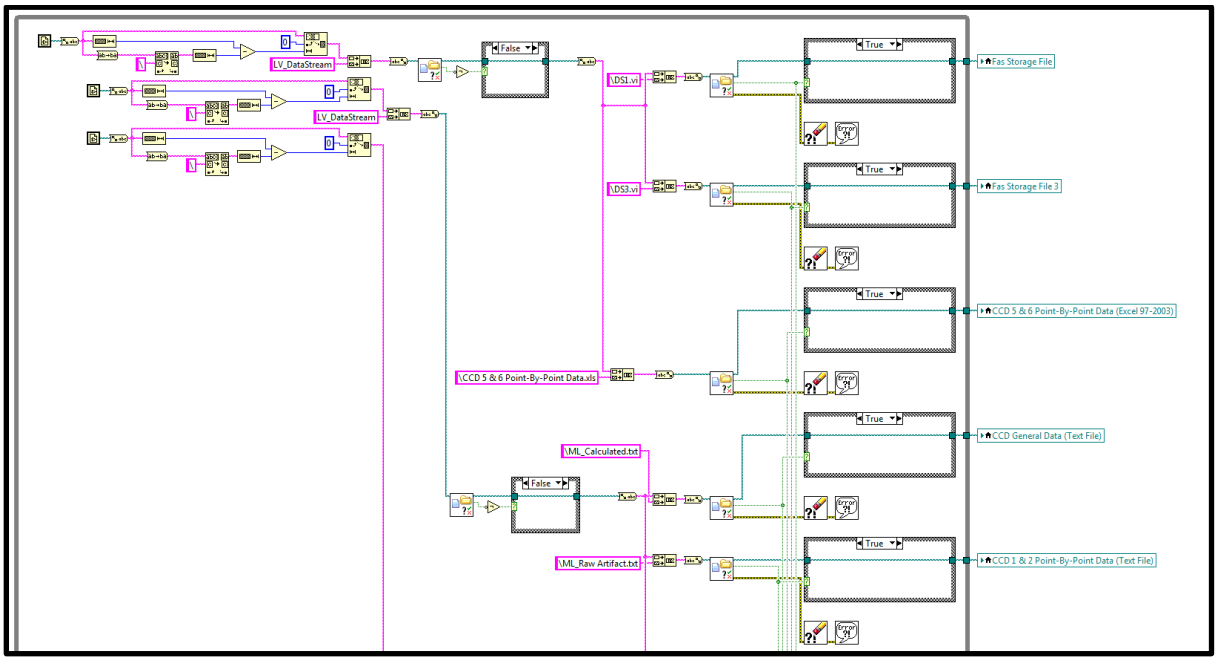

2 of 2: File Initialization

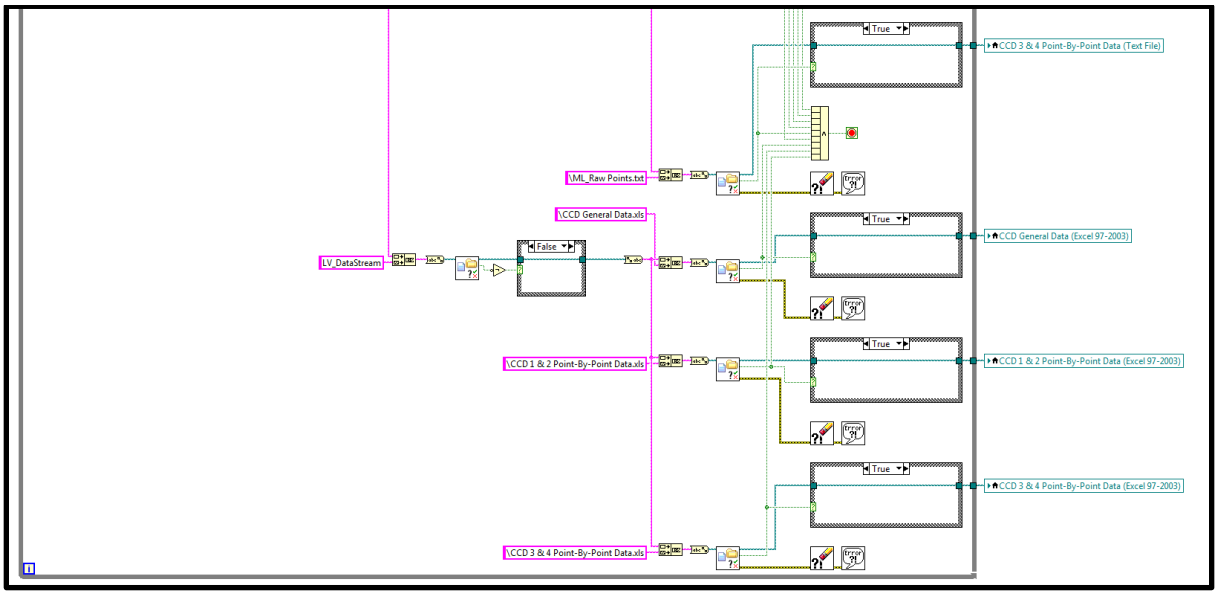

Section B: Data Acquisition Method

First CCD shown here. Same code duplicated in series for 6 devices.

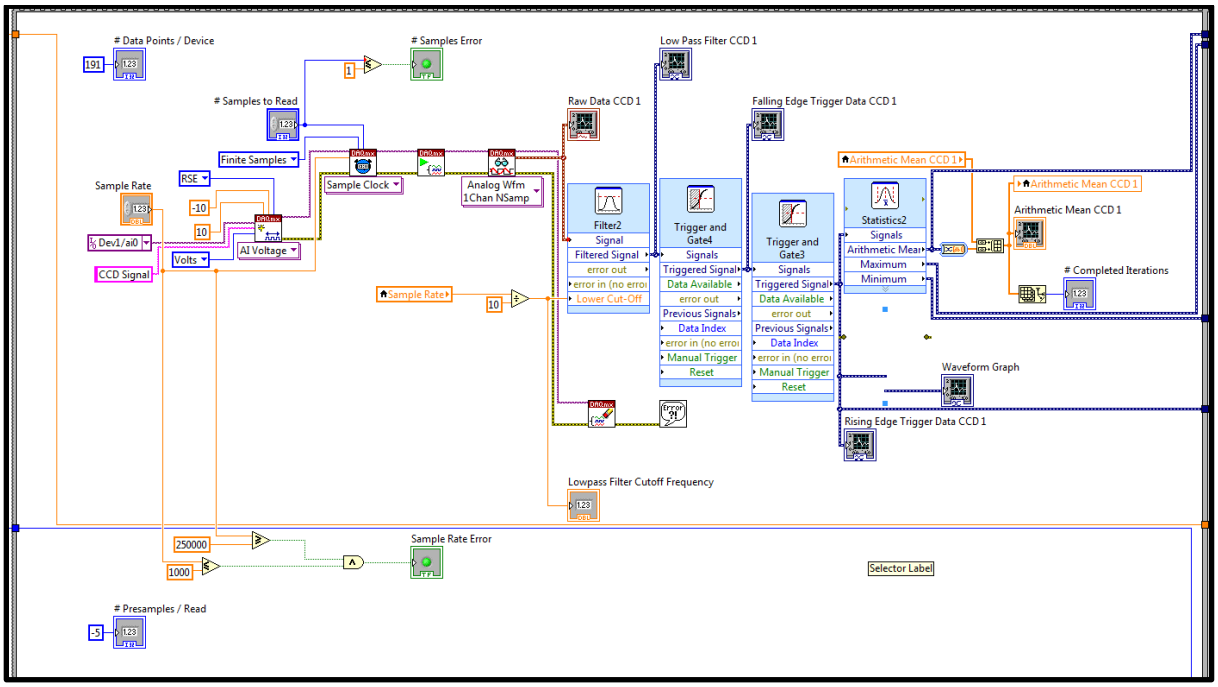

CCD Data Acquisition for subsequent CCDs (2-6) follow the protocol below.

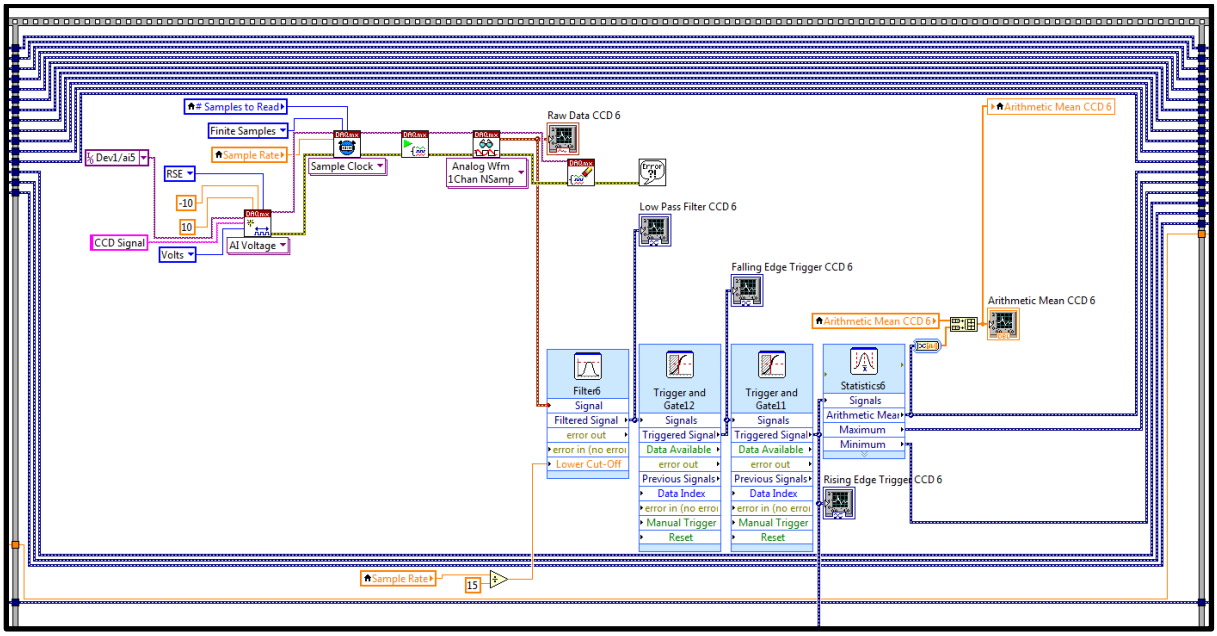

Section C: Data Storage Mechanisms

Average Optical Density data storage in a single table.

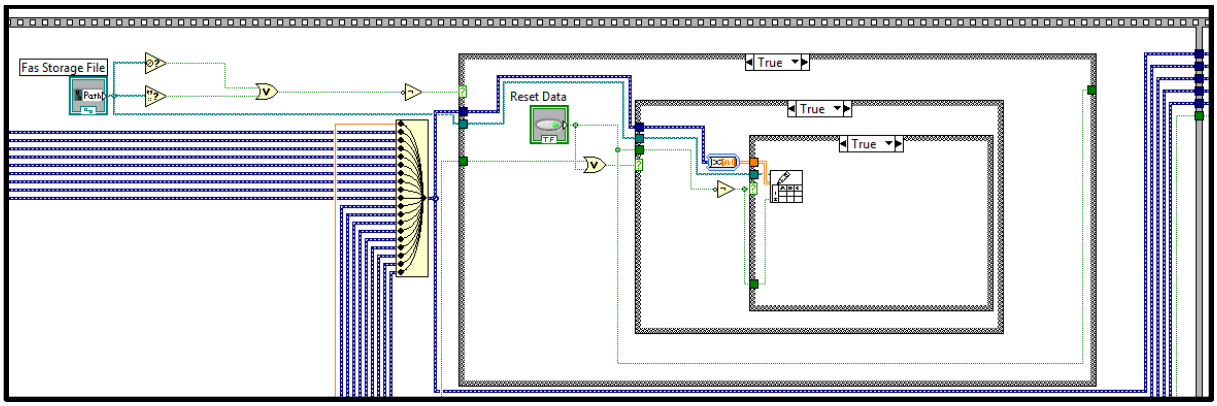

1 of 2: Average Optical Density data from 6 CCD devices stored in a single file.

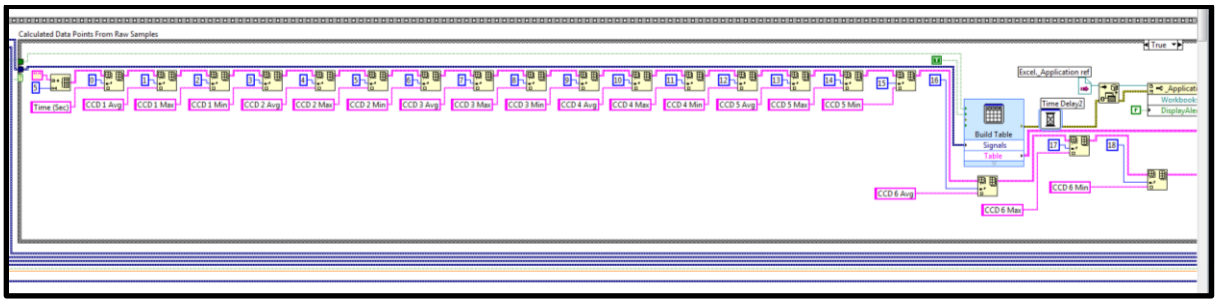

2 of 2: Average Optical Density data from 6 CCD devices stored in a single file

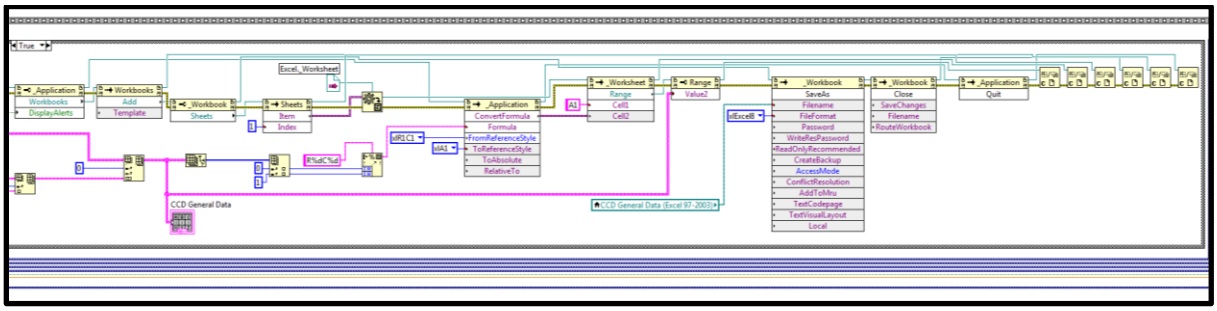

1 of 2: Storage of Spatiotemporal CCD Data. Data from 2 devices is stored in a single file.

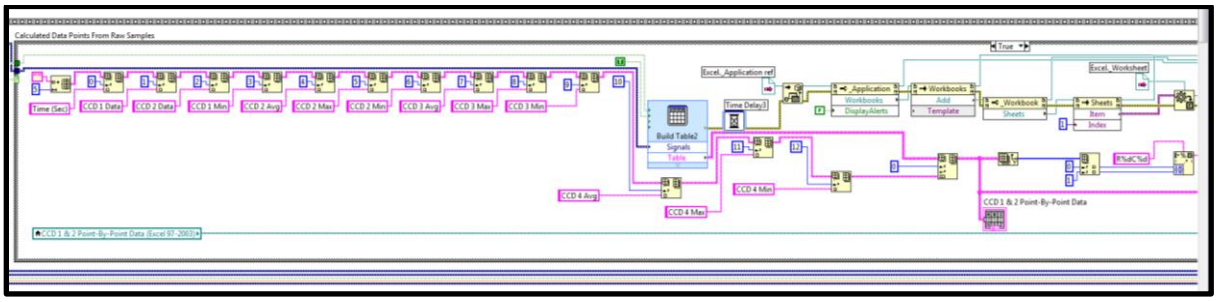

2 of 2: Storage of Spatiotemporal CCD Data. Data from 2 devices is stored in a single file.

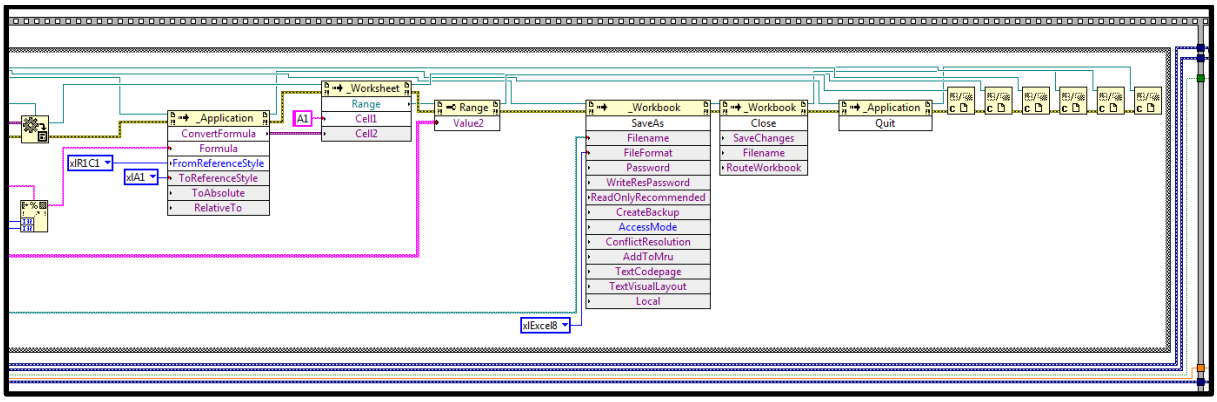

Section D: Timing Mechanisms

System experiment clock.

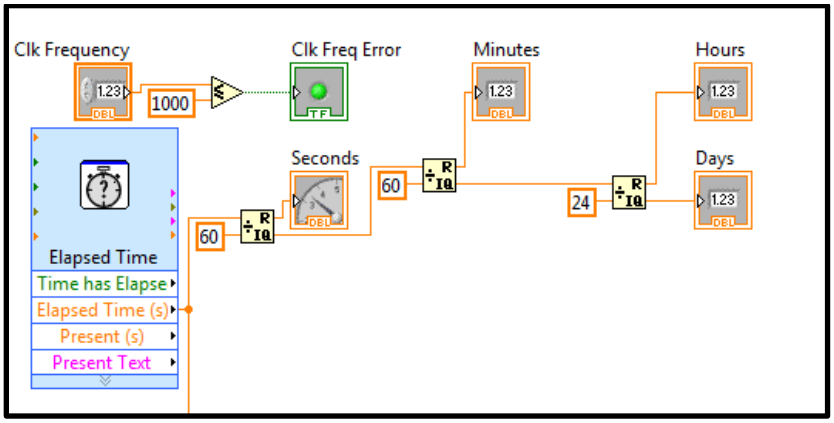

Timer used to guide acquisition of data signals in user-specified increments.

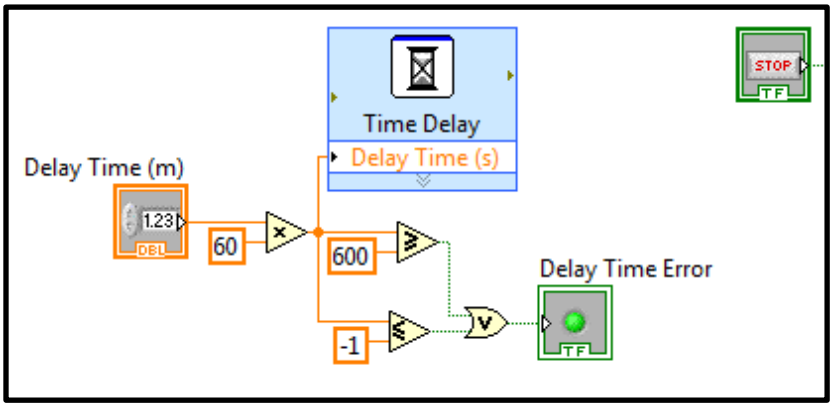

References

[1] J. W. Costerton, P. S. Stewart, and E. P. Greenberg, "Bacterial biofilms: a common cause of persistent infections," *Science,* vol. 284, pp. 1318-22, May 21 1999.

[2] C. Potera, "Forging a link between biofilms and disease," *Science,* vol. 283, pp. 1837, 1839, Mar 19 1999.

[3] J. W. Costerton, B. Ellis, K. Lam, F. Johnson, and A. E. Khoury, "Mechanism of electrical enhancement of efficacy of antibiotics in killing biofilm bacteria," *Antimicrobial Agents and Chemotherapy,* vol. 38, pp. 2803-9, Dec 1994.

[4] R. M. Donlan, "Biofilms and device-associated infections," *Emerging Infectious Diseases,* vol. 7, pp. 277-81, Mar-Apr 2001.

[5] A. Coates, Y. Hu, R. Bax, and C. Page, "The future challenges facing the development of new antimicrobial drugs," *Nature Reviews: Drug Discovery,* vol. 1, pp. 895-910, Nov 2002.

[6] M. T. Meyer, V. Roy, W. E. Bentley, and R. Ghodssi, "Development and validation of a microfluidic reactor for biofilm monitoring via optical methods," *Journal of Micromechanics and Microengineering,* vol. 21, May 2011.

[7] K. L. Swope and M. C. Flickinger, "The use of confocal scanning laser microscopy and other tools to characterize Escherichia coli in a high-cell-density synthetic biofilm," *Biotechnology and Bioengineering,* vol. 52, pp. 340-56, Oct 20 1996.

[8] D. Endy, "Foundations for engineering biology," *Nature,* vol. 438, pp. 449-53, Nov 24 2005.

[9] Z. N. Oltvai and A. L. Barabasi, "Systems biology: life's complexity pyramid," *Science,* vol. 298, pp. 763-4, Oct 25 2002.

[10] M. E. Csete and J. C. Doyle, "Reverse engineering of biological complexity," *Science,* vol. 295, pp. 1664-9, Mar 1 2002.

[11] D. B. Weibel, W. R. DiLuzio, and G. M. Whitesides, "Microfabrication meets microbiology," *Nature Reviews: Microbiology,* vol. 5, pp. 209-218, Mar 2007.

[12] G. M. Whitesides, E. Ostuni, S. Takayama, X. Jiang, and D. E. Ingber, "Soft lithography in biology and biochemistry," *Annual Review of Biomedical Engineering,* vol. 3, pp. 335-73, 2001.

[13] G. M. Whitesides, "The origins and the future of microfluidics," *Nature,* vol. 442, pp. 368-73, Jul 27 2006.

[14] R. Bakke, R. Kommedal, and S. Kalvenes, "Quantification of biofilm accumulation by an optical approach," *Journal of Microbiological Methods,* vol. 44, pp. 13-26, Feb 1 2001.

[15] M. Mosteller, M. Austin, S. Yang, and R. Ghodssi, "Platforms for engineering experimental biomedical systems," presented at the 22nd Annual INCOSE International Symposium, Rome, Italy, 2012.

[16] L. Hall-Stoodley, J. W. Costerton, and P. Stoodley, "Bacterial biofilms: from the natural environment to infectious diseases," *Nature Reviews: Microbiology,* vol. 2, pp. 95-108, Feb 2004.

[17] W. G. Characklis, "Fouling biofilm development: a process analysis," *Biotechnology and Bioengineering,* vol. 23, pp. 1923-1960, 1981.

[18] S. H. Hong, M. Hegde, J. Kim, X. Wang, A. Jayaraman, and T. K. Wood, "Synthetic quorum-sensing circuit to control consortial biofilm formation and dispersal in a microfluidic device," *Nature Communications,* vol. 3, p. 613, 2012.

[19] G. D. Ehrlich, Hu, F.Z., Lin, Q., Costerton, J.W., Post, J.C., "Intelligent implants to battle biofilms," *American Society for Microbiology News,* vol. 70, pp. 127-133, 2004.

[20] C. A. Fux, P. Stoodley, L. Hall-Stoodley, and J. W. Costerton, "Bacterial biofilms: a diagnostic and therapeutic challenge," *Expert Review of Anti-Infective Therapy,* vol. 1, pp. 667-83, Dec 2003.

[21] R. O. Darouiche, "Treatment of infections associated with surgical implants," *The New England Journal of Medicine,* vol. 350, pp. 1422-9, Apr 1 2004.

[22] W. Zimmerli, "Prosthetic-joint-associated infections," *Best Practice and Research: Clinical Rheumatology,* vol. 20, pp. 1045-1063, 2006.

[23] J. W. Costerton, Z. Lewandowski, D. E. Caldwell, D. R. Korber, and H. M. Lappin-Scott, "Microbial biofilms," *Annual Review of Microbiology,* vol. 49, pp. 711-45, 1995.

[24] D. Whitters and R. Stockley, "Immunity and bacterial colonisation in bronchiectasis," *Thorax,* Sep 20 2011.

[25] J. D. Shrout, T. Tolker-Nielsen, M. Givskov, and M. R. Parsek, "The contribution of cell-cell signaling and motility to bacterial biofilm formation," *Materials Research Society Bulletin,* vol. 36, pp. 367-373, May 1 2011.

[26] I. W. Sutherland, "Exopolysaccharides in biofilms, flocs and related structures," *Water Science and Technology,* vol. 43, pp. 77-86, 2001.

[27] D. G. Davies, A. M. Chakrabarty, and G. G. Geesey, "Exopolysaccharide production in biofilms: substratum activation of alginate gene expression by Pseudomonas aeruginosa," *Applied and Environmental Microbiology,* vol. 59, pp. 1181-6, Apr 1993.

[28] T. R. De Kievit, R. Gillis, S. Marx, C. Brown, and B. H. Iglewski, "Quorum-sensing genes in Pseudomonas aeruginosa biofilms: their role and expression patterns," *Applied and Environmental Microbiology,* vol. 67, pp. 1865-73, Apr 2001.

[29] P. Stoodley, K. Sauer, D. G. Davies, and J. W. Costerton, "Biofilms as complex differentiated communities," *Annual Review of Microbiology,* vol. 56, pp. 187-209, 2002.

[30] O. Wanner and P. Reichert, "Mathematical modeling of mixed-culture biofilms," *Biotechnology and Bioengineering,* vol. 49, pp. 172-184, Jan 20 1996.

[31] R. W. Finberg, R. C. Moellering, F. P. Tally, W. A. Craig, G. A. Pankey, E. P. Dellinger, M. A. West, M. Joshi, P. K. Linden, K. V. Rolston, J. C. Rotschafer, and M. J. Rybak, "The importance of bactericidal drugs: future directions in infectious disease," *Clinical Infectious Diseases,* vol. 39, pp. 1314-20, Nov 1 2004.

[32] W. Costerton, R. Veeh, M. Shirtliff, M. Pasmore, C. Post, and G. Ehrlich, "The application of biofilm science to the study and control of chronic bacterial infections," *The Journal of Clinical Investigation,* vol. 112, pp. 1466-77, Nov 2003.

[33] J. L. del Pozo and R. Patel, "The challenge of treating biofilm-associated bacterial infections," *Clinical Pharmacology and Therapeutics,* vol. 82, pp. 204-209, 2007.

[34] P. S. Stewart, "Mechanisms of antibiotic resistance in bacterial biofilms," *International Journal of Medical Microbiology,* vol. 292, pp. 107-13, Jul 2002.

[35] A. E. Khoury, K. Lam, B. Ellis, and J. W. Costerton, "Prevention and control of bacterial infections associated with medical devices," *American Society for Artificial Internal Organs,* vol. 38, pp. M174-8, Jul-Sep 1992.

[36] X. Khoo and M. W. Grinstaff, "Novel infection-resistant surface coatings: a bioengineering approach," *Materials Research Society Bulletin,* vol. 36, pp. 357-366, May 2011.

[37] A. Pareilleux and N. Sicard, "Lethal effects of electric current on Escherichia coli," *Applied Microbiology,* vol. 19, pp. 421-4, Mar 1970.

[38] S. D. Barranco, J. A. Spadaro, T. J. Berger, and R. O. Becker, "In vitro effect of weak direct current on Staphylococcus aureus," *Clinical Orthopaedics and Related Research,* pp. 250-5, May 1974.

[39] L. Bolton, B. Foleno, B. Means, and S. Petrucelli, "Direct-current bactericidal effect on intact skin," *Antimicrobial Agents and Chemotherapy,* vol. 18, pp. 137-41, Jul 1980.

[40] C. P. Davis, N. Wagle, M. D. Anderson, and M. M. Warren, "Iontophoresis generates an antimicrobial effect that remains after iontophoresis ceases," *Antimicrobial Agents and Chemotherapy*, vol. 35, pp. 2131-2134, 1991.

[41] T. Matsunaga, S. Nakasono, T. Takamuku, J. G. Burgess, N. Nakamura, and K. Sode, "Disinfection of drinking water by using a novel electrochemical reactor employing carbon-cloth electrodes," *Applied and Environmental Microbiology,* vol. 58, pp. 686-9, Feb 1992.

[42] S. A. Blenkinsopp, A. E. Khoury, and J. W. Costerton, "The electricidal effect: reduction of Staphylococcus and Pseudomonas biofilms by prolonged exposure to low-intensity electrical current," *Applied and Environmental Microbiology,* vol. 58, pp. 3770-3773, 1992.

[43] P. Stoodley, D. deBeer, and H. M. Lappin-Scott, "Influence of electric fields and pH on biofilm structure as related to the bioelectric effect," *Antimicrobial Agents and Chemotherapy,* vol. 41, pp. 1876-9, Sep 1997.

[44] J. L. Del Pozo, M. S. Rouse, and R. Patel, "Bioelectric effect and bacterial biofilms: a systematic review," *The International Journal of Artificial Organs,* vol. 31, pp. 786-95, Sep 2008.

[45] Y. W. Kim, H. Ben-Yoav, H. C. Wu, D. Quan, K. Carte, M. T. Meyer, K. Gerasopoulos, W. E. Bentley, and R. Ghodssi, "Bacterial biofilm treatment via the superpositioned bioelectric effect," *[Submitted],* 2012.

[46] W. W. Judy, "Microelectromechanical systems (MEMS): fabrication, design, and applications," in *Smart Materials and Structures*. vol. 10, ed, 2000, pp. 1115-1134.

[47] K. E. Petersen, "Silicon as a mechanical material," *Proceedings of the IEEE*, vol. 70, pp. 420-457, 1982.

[48] R. Ghodssi and P. Lin, *MEMS Materials And Processes Handbook*. New York: Springer, 2011.

[49] R. S. Muller, "MEMS: quo vadis in century XXI," in *Microelectronic Engineering*. vol. 53, ed, 2002, pp. 47-54.

[50] D. M. Citron, Y. A. Warren, H. T. Fernandez, M. A. Goldstein, K. L. Tyrrell, and E. J. Goldstein, "Broth microdilution and disk diffusion tests for susceptibility testing of Pasteurella species isolated from human clinical specimens," *Journal of Clinical Microbiology*, vol. 43, pp. 2485-8, May 2005.

[51] J. H. Jorgensen and M. J. Ferraro, "Antimicrobial susceptibility testing: a review of general principles and contemporary practices," *Clinical Infectious Diseases*, vol. 49, pp. 1749-55, Dec 1 2009.

[52] C. Cháfer-Pericás, A. Maquieira, and R. Puchades, "Screening methods for antibiotic determination in food samples," presented at the International Conference on Food Innovation, Valencia, Spain, 2010.

[53] J. M. Song, M. Culha, P. A. Kasili, G. D. Griffin, and T. Vo-Dinh, "A compact CMOS biochip immunosensor towards the detection of a single bacteria," *Biosensors and Bioelectronics*, vol. 20, pp. 2203-2209, May 15 2005.

[54] E. Leoni and P. P. Legnani, "Comparison of selective procedures for isolation and enumeration of Legionella species from hot water systems," *Journal of Applied Microbiology*, vol. 90, pp. 27-33, Jan 2001.

[55] A. K. Bej, M. H. Mahbubani, J. L. Dicesare, and R. M. Atlas, "Polymerase chain reaction-gene probe detection of microorganisms by using filter-concentrated samples," *Applied and Environmental Microbiology*, vol. 57, pp. 3529-34, Dec 1991.

[56] J. T. Trevors, "Fluorescent probes for bacterial cytoplasmic membrane research," *Journal of bBochemical and Biophysical Methods*, vol. 57, pp. 87-103, Aug 29 2003.

[57] E. Heyduk and T. Heyduk, "Fluorescent homogeneous immunosensors for detecting pathogenic bacteria," *Analytical Biochemistry*, vol. 396, pp. 298-303, Jan 15 2010.

[58] G. H. Patterson, S. M. Knobel, W. D. Sharif, S. R. Kain, and D. W. Piston, "Use of the green fluorescent protein and its mutants in quantitative fluorescence microscopy," *Biophysical Journal,* vol. 73, pp. 2782-90, Nov 1997.

[59] S. A. Soper, K. Brown, A. Ellington, B. Frazier, G. Garcia-Manero, V. Gau, S. I. Gutman, D. F. Hayes, B. Korte, J. L. Landers, D. Larson, F. Ligler, A. Majumdar, M. Mascini, D. Nolte, Z. Rosenzweig, J. Wang, and D. Wilson, "Point-of-care biosensor systems for cancer diagnostics/prognostics," *Biosensors and Bioelectronics,* vol. 21, pp. 1932-42, Apr 15 2006.

[60] Leinco Technologies Inc. (2006). *Sandwich ELISA protocol*. Available: http://www.leinco.com/sandwich_elisa

[61] J. H. Lee, J. B. Kaplan, and W. Y. Lee, "Microfluidic devices for studying growth and detachment of Staphylococcus epidermidis biofilms," *Biomedical Microdevices,* vol. 10, pp. 489-498, Aug 2008.

[62] J. Kim, M. Hegde, and A. Jayaraman, "Co-culture of epithelial cells and bacteria for investigating host-pathogen interactions," *Lab On A Chip,* vol. 10, pp. 43-50, 2010.

[63] J. Kim, M. Hegde, S. H. Kim, T. K. Wood, and A. Jayaraman, "A microfluidic device for high throughput bacterial biofilm studies," *Lab On A Chip,* vol. 12, pp. 1157-63, Mar 21 2012.

[64] S. B. Prakash and P. Abshire, "On-chip capacitance sensing for cell monitoring applications," *IEEE Sensors,* vol. 7, pp. 440-447, Mar-Apr 2007.

[65] L. Richter, C. Stepper, A. Mak, A. Reinthaler, R. Heer, M. Kast, H. Bruckl, and P. Ertl, "Development of a microfluidic biochip for online monitoring of fungal biofilm dynamics," *Lab On A Chip,* vol. 7, pp. 1723-1731, 2007.

[66] J. J. Yu, Z. B. Liu, Q. J. Liu, K. T. Yuen, A. F. T. Mak, M. Yang, and P. Leung, "A polyethylene glycol (PEG) microfluidic chip with nanostructures for bacteria rapid patterning and detection," *Sensors and Actuators A,* vol. 154, pp. 288-294, Sep 24 2009.

[67] M. S. Mannoor, S. Y. Zhang, A. J. Link, and M. C. McAlpine, "Electrical detection of pathogenic bacteria via immobilized antimicrobial peptides," *Proceedings of the National Academy of Sciences,* vol. 107, pp. 19207-19212, Nov 9 2010.

[68] L. J. Yang, Y. B. Li, C. L. Griffis, and M. G. Johnson, "Interdigitated microelectrode (IME) impedance sensor for the detection of viable Salmonella typhimurium," *Biosensors and Bioelectronics,* vol. 19, pp. 1139-1147, May 15 2004.

[69] Y. W. Kim, S. E. Sardari, M. T. Meyer, A. A. Iliadis, H. C. Wu, W. E. Bentley, and R. Ghodssi, "An ALD aluminum oxide passivated surface acoustic wave sensor for early biofilm detection," *Sensors and Actuators B,* vol. 163, pp. 136-145, Mar 1 2012.

[70] E. Berkenpas, P. Millard, and M. Pereira da Cunha, "Detection of Escherichia coli O157:H7 with langasite pure shear horizontal surface acoustic wave sensors," *Biosensors and Bioelectronics,* vol. 21, pp. 2255-62, Jun 15 2006.

[71] F. L. Dickert, P. Lieberzeit, and O. Hayden, "Sensor strategies for microorganism detection - from physical principles to imprinting procedures," *Analytical and Bioanalytical Chemistry,* vol. 377, pp. 540-9, Oct 2003.

[72] R. D. Hamelin, R. D. Kingler, and C. Dieckmann, "Adaptive systems engineering: a medical paradigm for practicing systems engineering," presented at the 21st Annual INCOSE International Symposium, Denver, CO, 2011.

[73] G. C. L. Wong and G. A. O'Toole, "All together now: integrating biofilm research across disciplines," *Materials Research Society Bulletin,* vol. 36, pp. 339-345, May 2011.

[74] F. Eubanks and M. Masters, "Assurance cases: a new form of requirements traceability matrix for medical devices," presented at the 21st Annual INCOSE International Symposium, Denver, CO, 2011.

[75] S. Yang, Y. Zhou, and J. Baras, "Compositional analysis of dynamic bayesian networks and applications to CPS," presented at the Third International Conference on Cyber-Physical Systems, Beijing, China, 2012.

[76] C. J. Tomlin and J. D. Axelrod, "Understanding biology by reverse engineering the control," *Proceedings of the National Academy of Sciences,* vol. 102, pp. 4219-4220, Mar 22 2005.

[77] N. Maluf and K. Williams, *Introduction to Microelectromechanical Systems Engineering*, 2nd ed. Boston: Artech House, 2004.

[78] M. Austin, "ENSE 621 systems engineering concepts, issues, and processes," ed. University of Maryland, 2010.

[79] M. Austin, "ENSE 622 information-centric systems engineering," ed. University of Maryland, 2011.

[80] M. Austin, "ENSE 623 systems engineering validation and verification," ed. University of Maryland, 2011.

[81] C. J. Tomlin and J. D. Axelrod, "Biology by numbers: mathematical modelling in developmental biology," *Nature reviews. Genetics,* vol. 8, pp. 331-40, May 2007.

[82] L. R. Rabiner and B. H. Juang, "An introduction to hidden markov models," *IEEE Acoustics, Speech, and Signal Processing,* vol. 3, pp. 4-16, 1986.

[83] S. Kim, H. Li, E. R. Dougherty, N. Cao, Y. Chen, M. Bittner, and E. B. Suh, "Can markov chains mimic biological regulation?," *Journal of Biological Systems,* vol. 10, pp. 337-357, 2002.

[84] M. C. Belanger and Y. Marois, "Hemocompatibility, biocompatibility, inflammatory and in vivo studies of primary reference materials low-density polyethylene and polydimethylsiloxane: a review," *Journal of Biomedical Materials Research,* vol. 58, pp. 467-77, 2001.

[85] A. B. Mathur, T. O. Collier, W. J. Kao, M. Wiggins, M. A. Schubert, A. Hiltner, and J. M. Anderson, "In vivo biocompatibility and biostability of modified polyurethanes," *Journal of Biomedical Materials Research,* vol. 36, pp. 246-57, Aug 1997.

[86] K. P. Kim, Y. G. Kim, C. H. Choi, H. E. Kim, S. H. Lee, W. S. Chang, and C. S. Lee, "In situ monitoring of antibiotic susceptibility of bacterial biofilms in a microfluidic device," *Lab On A Chip,* vol. 10, pp. 3296-9, Dec 7 2010.

[87] V. Janakiraman, D. Englert, A. Jayaraman, and H. Baskaran, "Modeling growth and quorum sensing in biofilms grown in microfluidic chambers," *Annals of Biomedical Engineering,* vol. 37, pp. 1206-1216, Jun 2009.

[88] R. Bakke and P. Q. Olsson, "Biofilm thickness measurements by light-microscopy," *Journal of Microbiological Methods,* vol. 5, pp. 93-98, Jul 1986.

[89] A. L. Koch, "Turbidity measurements of bacterial cultures in some available commercial instruments," *Analytical Biochemistry,* vol. 38, pp. 252-&, 1970.

[90] "TSL202R 128x1 Linear Sensor Array," Texas Advanced Optoelectronic Solutions, Ed., ed. Plano, TX, 2009.

[91] D. N. Hohne, J. G. Younger, and M. J. Solomon, "Flexible microfluidic device for mechanical property characterization of soft viscoelastic solids such as bacterial biofilms," *The ACS Journal of Surfaces and Colloids,* vol. 25, pp. 7743-51, Jul 7 2009.

[92] Y. Yawata, K. Toda, E. Setoyama, J. Fukuda, H. Suzuki, H. Uchiyama, and N. Nomura, "Monitoring biofilm development in a microfluidic device using modified

confocal reflection microscopy," *Journal of Bioscience and Bioengineering*, vol. 110, pp. 377-80, Sep 2010.

[93] S. D. Senturia, "Fluids," in *Microsystem Design*, S. D. Senturia, Ed., 2nd ed: Kluwer Academic Publishers, 1999, pp. 317-350.

[94] Y. W. Kim, H. Ben-Yoav, H. C. Wu, W. E. Bentley, and R. Ghodssi, "An Enhanced Superpositioned Bioelectric Effect for Biofilm Treatment," United States of America Patent, 2011.

[95] J. O'M Bockris and K. N. Reddy, *Modern Electrochemistry*, 2nd ed. New York: Kluwer Academic / Plenum Publishers, 2000.

[96] L. L. Munn and A. Jain, "Design and fabrication of microfluidic devices for flow-based separation of blood cells," in *Lab on a Chip Technology: Biomolecular Separation and Analysis*. vol. 2, K. E. Herold, Rasooly, A., Ed., ed: Caister Academic Press, 2009, pp. 29-45.

[97] M. A. Eddings, M. A. Johnson, and B. K. Gale, "Determining the optimal PDMS-PDMS bonding technique for microfluidic devices," *Journal of Micromechanics and Microengineering*, vol. 18, Jun 2008.

[98] J. G. Proakis and M. Salehi, "Introduction," in *Communication Systems Engineering*, 2nd ed Upper Saddle River, NJ: Prentice-Hall, Inc, 2002, pp. 1-23.

[99] O. Paliy and T. S. Gunasekera, "Growth of E. coli BL21 in minimal media with different gluconeogenic carbon sources and salt contents," *Applied Microbiology and Biotechnology*, vol. 73, pp. 1169-72, Jan 2007.

[100] "DU Series 700 User's Guide," Beckamn Coulter Inc, Ed., ed, 2010, pp. 49-60.

[101] A. P. Johnson, L. Burns, N. Woodford, E. J. Threlfall, J. Naidoo, E. M. Cooke, and R. C. George, "Gentamicin resistance in clinical isolates of Escherichia coli encoded by genes of veterinary origin," *Journal of Medical Microbiology*, vol. 40, pp. 221-6, Mar 1994.

[102] S. A. Salmon and J. L. Watts, "Minimum inhibitory concentration determinations for various antimicrobial agents against 1570 bacterial isolates from turkey poults," *Avian Diseases*, vol. 44, pp. 85-98, Jan-Mar 2000.

[103] S. K. Olofsson and O. Cars, "Optimizing drug exposure to minimize selection of antibiotic resistance," *Clinical Infectious Diseases*, vol. 45 Suppl 2, pp. S129-36, Sep 1 2007.

[104] M. A. Kohanski, M. A. DePristo, and J. J. Collins, "Sublethal antibiotic treatment leads to multidrug resistance via radical-induced mutagenesis," *Molecular Cell,* vol. 37, pp. 311-20, Feb 12 2010.

[105] C. Costelloe, C. Metcalfe, A. Lovering, D. Mant, and A. D. Hay, "Effect of antibiotic prescribing in primary care on antimicrobial resistance in individual patients: systematic review and meta-analysis," *BMJ,* vol. 340, p. c2096, 2010.

[106] N. Wellman, S. M. Fortun, and B. R. McLeod, "Bacterial biofilms and the bioelectric effect," *Antimicrobial Agents and Chemotherapy,* vol. 40, pp. 2012-4, Sep 1996.

[107] J. L. del Pozo, M. S. Rouse, J. N. Mandrekar, M. F. Sampedro, J. M. Steckelberg, and R. Patel, "Effect of electrical curent on the activities of antimicrobial agents against Pseudomonas aeruginosa, Staphylococcus aureus, and Staphylococcus epidermidis biofilms," *Antimicrobial Agents and Chemotherapy,* vol. 53, pp. 35-40, 2009.

[108] J. L. del Pozo, M. S. Rouse, J. N. Mandrekar, J. M. Steckelberg, and R. Patel, "The electricidal effect: reduction of Staphylococcus pseudomonas biofilms by prolonged exposure to low-intensity electrical current," *Antimicrobial Agents and Chemotherapy,* vol. 53, pp. 41-45, 2009.

[109] R. Caubet, F. Pedarros-Caubet, M. Chu, E. Freye, M. de Belem Rodrigues, J. M. Moreau, and W. J. Ellison, "A radio frequency electric current enhances antibiotic efficacy against bacterial biofilms," *Antimicrobial Agents and Chemotherapy,* vol. 48, pp. 4662-4, Dec 2004.

[110] M. Giladi, Y. Porat, A. Blatt, E. Shmueli, Y. Wasserman, E. D. Kirson, and Y. Palti, "Microbial growth inhibition by alternating electric fields in mice with Pseudomonas aeruginosa lung infection," *Antimicrobial Agents and Chemotherapy,* vol. 54, pp. 3212-8, Aug 2010.

[111] D. K. Cheng, *Field and Wave Electromagnetics,* 2nd ed.: Addison-Wesley, 1989.